IRON DIAGENESIS IN THE INDIAN RIVER LAGOON SUBTERRANEAN ESTUARY, FLORIDA (USA)

By

MOUTUSI ROY

A DISSERTATION PRESENTED TO THE GRADUATE SCHOOL
OF THE UNIVERSITY OF FLORIDA IN PARTIAL FULFILLMENT
OF THE REQUIREMENTS FOR THE DEGREE OF
DOCTOR OF PHILOSOPHY

UNIVERSITY OF FLORIDA

2009

ACKNOWLEDGMENTS

First, I acknowledge the primary funding agency, National Science Foundation (grant # EAR 0403461) for funding the project (primary investigator Prof. Jon Martin). I also thank Geological Society of America for funding me from their student research grant ($4000), and Department of Geological Sciences at University of Florida for providing a $1000 match with the student research grant. My salary was covered by Alumni Fellowship and Grinter Fellowship from University of Florida.

I acknowledge the support of my advisor Jon, who agreed to guide me and funded me for last five years. Jon always had an open door to discuss several random ideas I had about Fe cycling. Jon was a perfect mentor who taught me how to enjoy the work and have fun in work.

I am thankful to my committee for guiding me through out, and helping me with the Fe model, and Fe concentration analysis. Specifically, I thank to Liz and Jim for challenging me with the model; John to guide me with the early diagenesis. I thank Phil for pushing me harder to understand the relation between chemical potential, fugacity, and activity coefficient. I thank George for helping me with Fe concentration analysis and clean lab techniques. Without Jaye, who agreed to be in my committee despite a very short notice, it won't be possible to organize the field work.

I am thankful to Olivier Rouxel, for helping me with Fe isotope analysis, and covering lab expenses at Woods Hole Oceanographic Institute. Completion of this thesis won't be possible with out the help of Jaye's student Chris Smith, who is currently a Mendenhall Fellow in USGS (ST. Petersburg). Chris helped me to develop an understanding in the numerical modeling. I also thank Jennifer Cherrier (Florida A and M University), and her student Amanda Dorsett for helping me in the field, and sharing their DOC data. I thank to Florian Fiebig for helping me with

sequential leaching. I appreciate the help of Jason Curtis for mentoring me with stable isotope analysis, and department officials Juanita, and Pamela for their help.

In addition to these people, I thank my parents and my friends from Gainesville, especially P. J Moore for poking me with pencils, so that I don’t sleep in the class.

TABLE OF CONTENTS

page

LIST OF TABLES

LIST OF FIGURES

Abstract of Dissertation Presented to the Graduate School
of the University of Florida in Partial Fulfillment of the
Requirements for the Degree of Doctor of Philosophy

IRON DIAGENESIS IN THE SUBTERRANEAN ESTUARY OF INDIAN RIVER LAGOON, FLORIDA

By

Moutusi Roy

December 2009

Chair: Jonathon B. Martin
Major: Geology

Iron (Fe) is an important element for a variety of ecological and diagenetic processes, such as the microbial reduction of Fe-oxides and associated remineralization of organic carbon (OC) and production of carbon dioxide (CO_2). This link between Fe and C makes it important to understand Fe diagenesis in the subterranean estuary, where submarine groundwater discharge (SGD) influences Fe reaction pathways. Submarine groundwater discharge consists of terrestrial freshwater from coastal aquifer (terrestrial SGD) and exchange of seawater across the sediment-water interface (marine SGD). To better understand Fe diagenesis in the subterranean estuary, dissolved and solid Fe, OC, and S concentrations were measured in the subterranean estuary of Indian River Lagoon, Florida. In this study area Fe-oxide coated terrestrial sediments are overlain by OC and S-rich marine sediments. Offshore thickening of these marine sediments reflects sealevel rise at the rate of 3 mm/year. Dissolved Fe maxima occur in the terrestrial sediments and Fe minima and sulfide maxima occur in the marine sediments near the sediment-water interface. Dissolved Fe maxima increase by three orders of magnitude from 1 µM nearshore to 300 µM the freshwater-saltwater boundary, where terrestrial SGD ceases to flow. Reactive-transport modeling shows Fe-oxide reduction rates do not change across the seepage face, thus the elevated Fe concentrations at the freshwater-saltwater boundary result from slow

flow rates. The freshwater-saltwater boundary moved landward during the three years of sampling as a result of a decrease in effective precipitation (precipitation minus potential evapotranspiration) from 40 cm/year to -10cm/year. The landward shift decreased the width of the seepage face by 5 m and annual flux of dissolved Fe and remineralized C by 20%. The δ^{56}Fe values in porewater were lighter than corresponding terrestrial sediments as a result of dissimilatory reduction of Fe-oxides, but porewater δ^{56}Fe values were heavier than corresponding marine sediments because of precipitation of Fe-sulfides. In the Indian River Lagoon study area, Fe diagenesis is controlled by the combination of hydrology of the subterranean estuary, its shoreward movement with sealevel rise, and distribution of OC.

CHAPTER 1
INTRODUCTION

Justifications of Studying Iron Diagenesis in Coastal Sediments

Iron-oxide (Fe-oxide) diagenesis in coastal sediments is an important process in coastal sediments. It provides dissolved iron (Fe), an important micro-nutrient, to coastal waters, remineralizes solid and dissolved organic carbon (OC) carbon-dioxide (CO_2), and thus is important for the global carbon (C) budget. Additionally Fe reactions can remobilize certain heavy metals and nutrients and can influence ecological conditions. Models of Fe fluxes to open oceans show there are various sources of Fe to open oceans, but benthic diagenesis of Fe in continental shelf sediments alone contributes up to 50% of the Fe flux from marine systems to open oceans. (Archer and Johnson, 2000; Fung et al., 2000; Wu et al., 2001; Elrod et al., 2004; Boyle et al., 2005). It was observed that in the high nutrient low chlorophyll (HNLC) zones of the open oceans primary productivity is low, and deficiency of Fe caused this low productivity (Martin et al., 1990b) by limiting chlorophyll production and growth of phytoplanktons (Martin and Fitzwater, 1988; Martin et al., 1990a; Martin et al., 1994; Pollard et al., 2009). Because of this link between Fe and OC, both for OC fixation and CO_2 production, it is important to study Fe geochemistry in coastal sediments. Additionally, Fe-oxide diagenesis can control availability of certain heavy metals (e.g. arsenic, cadmium, copper, lead) and nutrients (e.g. phosphate) that can occur as adsorbed phases on Fe-oxides (Lion et al., 1982; Caetano and Vale, 2002; Zhang et. al., 2002; Ler and Stanforth, 2003; Charette et al., 2005; Poulton and Canfield, 2006). These heavy metals and nutrients can be released to coastal waters during Fe-oxide reduction, suggesting study of Fe diagenesis in coastal sediments and porewater is necessary.

Iron Geochemistry in Coastal Sediments and Porewater

Iron concentrations in coastal sediments and porewaters depend on redox conditions. Iron has two oxidation states, oxidized (Fe^{3+}) and reduced (Fe^{2+}), but aqueous phases are typically enriched in reduced Fe^{2+} (99.9% of the total dissolved Fe), thus for practical purposes I will assume all dissolved Fe are reduced Fe^{2+} (Stumm and Morgan, 1996). In contrast, oxidized (Fe^{3+}) is mainly solid bound and forms 16 different types of oxides and hydroxides under natural atmospheric conditions (Schwertmann and Fitzpatrick, 1992; Stumm and Morgan, 1996). Dissolution of Fe from Fe-oxides is mainly microbially mediated by Fe-reducing bacteria, because natural solubilities of Fe-oxides are very low (Lovley, 1987, Thamdrup, 2000; Childers et al., 2002; Hyacinthe et al, 2006). In contrast, microbial precipitation of Fe^{2+} as Fe-oxides is very rare, because there are only few species of Fe-oxidizing bacteria compared to Fe-reducing bacteria (e.g. Straube et al, 2001). This microbial Fe-oxide reduction is coupled with OC remineralization, which occurs during early diagenetic reactions.

Early diagenetic reactions of OC can alter concentrations of electron acceptors, like Fe- and Mn-oxides in coastal sediments and porewater by orders of magnitude (e.g. Figure 1-1; Froelich et al. 1979; Wang and Van Cappellen, 1996; Slomp et al., 1997; Snyder et al., 2004; Tebo et al., 2004; Burdige, 2006). Microbes use electron acceptors to remineralize OC according to the order of their energy yields, and the sequence from high to low end of energy release is dissolved O_2, nitrate (NO_3^-), manganese (Mn)-oxides, Fe-oxides, sulfate (SO_4^{2-}), and carbon-dioxide (CO_2), (Froelich et al. 1979; Burdige, 2006). Therefore, presence of energetically favored electron acceptors like dissolved O_2, and NO_3^- can limit Fe-oxide reduction. Among these electron acceptors Fe- and Mn-oxides occur in the solid phases, while rests occur in dissolved phases. Reduction and subsequent dissolution of Fe- and Mn-oxides thus depend primarily on dissolved OC (DOC) concentrations and reduction of Fe-oxides is high where DOC

concentrations are high (Canfield et al., 1993; Van Cappellen and Wang, 1995; Snyder et al, 2004). Sources of DOC in coastal systems could be seawater, groundwater flow, rivers, and springs, or in situ production from coastal sediments. Coastal sediments usually contain both terrestrial and marine OC, but marine OC is more labile and a preferable substrate for OC remineralization over refractory terrestrial OC (Suess et al., 1980). The rate and amount of Fe-oxide reduction by OC thus can also vary depending on the sources and associated quality and quantity of OC.

Iron reactivity and associated kinetics also depend on the pH of the medium in general, and the same could be true for coastal sediments. For example, laboratory experiments show under oxic conditions in an acidic medium (pH 2 or less) Fe is dissolved from Fe-oxides, whereas in near neutral pH conditions (between 6.5 and 9) dissolved Fe precipitates from seawater as Fe-oxides (Garrels and Christ, 1990; Schwertmann and Fitzpatrick, 1992; Pham et al., 2006). In general, values of pH decrease during Fe-sulfide precipitation, which also removes dissolved Fe from porewater as Fe-sulfides (Burdige and Nealson, 1986; Reimers et al., 1996,; Poulton, 2004; Taylor et al., 2005). Precipitation of these Fe-sulfides depends on their equilibrium stability. Equilibrium constants for amorphous FeS, mackinawite, greigite, and pyrite are 3.0, 3.55, 12.85, and 16.40, respectively, suggesting amorphous Fe-sulfide is the energetically favored phase and will precipitate first in shallow coastal sediments, and then will gradually transform to ordered crystalline phases by step processes of Ostwald ripening (Berner, 1970; Sweeney and Kaplan, 1973; Morse et. al., 1987; Rickard, 1989, 2006; Furukawa and Barnes, 1995; Wilkin and Barnes, 1996, 1997; Davison et. al., 1999; Butler and Rickard, 2000). However, some dissolved Fe can also form hydroxy- sulfate minerals like jarosite and schwertmannite at near neutral pH and suboxic condition, which can be redissolved in the presence of SO_4^{2-} reducing bacteria, like

Geobacter metallireducens (Jones et al., 2006). Iron sulfides can also dissolve inorganically when pH is lower than 4 (e.g, Morse, 1987; Stumm and Morgan, 1996; Schippers et al, 2002). Furthermore, these Fe-sulfides can be oxidized by dissolved O_2 and Mn-oxides under near neutral pH (pH 8), but NO_3^- and Fe-oxides can not oxidize Fe-sulfides, suggesting Fe-oxides and Fe-sulfides can coexist under controlled laboratory conditions (Schippers et al, 2002). Since Fe-oxides form in oxidizing environments and Fe-sulfides form in reducing environment thus, their coexistence is unlikely under natural conditions, unless there is change in the depositional history from oxidizing to reducing or opposite.

Iron has four naturally occurring isotopes ^{54}Fe, ^{56}Fe, ^{57}Fe, ^{58}Fe, and their abundances on earth surface are 5.84% , 91.76%, 2.12%, and 0.28%, respectively (Beard et al., 2000). Fractionation between two abundant isotopes, ^{54}Fe and ^{56}Fe, with respect to a standard IRMM-14 (reported as δ^{56}Fe values, equation 1-1), is used to identify the pathway of Fe diagenesis (Beard and Johnson, 1999; Bergquist and Boyle, 2002; Rouxel et al, 2008).

$$\delta^{56}Fe = \left(\frac{(\frac{^{56}Fe}{^{54}Fe})_{sample}}{(\frac{^{56}Fe}{^{54}Fe})_{S\,\tan\,dard}} - 1 \right) x1000 \qquad (1\text{-}1)$$

Some labs also report δ^{57}Fe values, which are the ratio of ^{57}Fe and ^{54}Fe in the samples with respect to the standard IRM-014(Beard and Johnson, 2004). During microbial Fe-oxide precipitation, lighter ^{54}Fe isotopes fractionate into reduced Fe^{2+} and enrich porewater with lighter ^{54}Fe isotopes thus lower δ^{56}Fe values. The δ^{56}Fe values in porewater decrease by about 1 $^{o}/_{oo}$ during microbial Fe-oxide precipitation from groundwater in terrestrial environments (e.g. in Beard et al. 2003; Johnson et al., 2004; Teutsch et al., 2005). In estuarine sediments, fractionation was observed to be much larger than terrestrial environments. The δ^{56}Fe values decrease in the porewater up to 5.6 $^{o}/_{oo}$ during Fe-oxide precipitation (Rouxel et al, 2008). A

similar amount of fractionation is observed during Fe-oxide reduction; Severmann et al. (2006) showed porewater Fe^{2+} becomes 1 $^{o}/_{oo}$ lighter during Fe-oxide reduction. In contrast, during Fe-sulfide dissolution porewater becomes enriched in ^{56}Fe isotopes, increasing $\delta^{56}Fe$ values. This process increases the $\delta^{56}Fe$ values in porewater Fe^{2+} by about 2 $^{o}/_{oo}$ (Butler et al., 2001; Severmann et al., 2006). These properties of Fe isotopes allow their use in understanding the influence of coastal processes during burial diagenesis of Fe (Escoube et al., 2009; Rouxel et al, 2008).

Hydrology of the coastal aquifer

Iron diagenesis in coastal zones can be altered by discharge of fresh water. In the coastal areas freshwater discharges from coastal aquifers by the process known as submarine groundwater discharge (SGD), when the elevation of the water table of coastal aquifers is higher than the mean sea level (Ghyben, 1889; Herzberg, 1901; Fetter, 2002). Early models consider flow of terrestrial freshwater from coastal aquifers as the only source for SGD, thereby restricting SGD to freshwater SGD (e.g., Church, 1996). However, the modeled values of the freshwater discharge were found to be a few orders of magnitude lower than the measured (using seepage meters) and estimated values (using radioisotopes) of SGD at the sediment-water interface (Lee, 1977; Pandit and El-Khazen, 1990; Belanger, 1990; Younger, 1996; Cable et al., 2004). Additionally, the salinity of the water discharging across the sediment-water interface was close to seawater salinity, rather than low salinity expected from discharge of meteoric water in coastal aquifers (Moore and Church, 1996; Younger, 1996, Li et. al., 1999; Martin et al., 2004). Because of these differences in salinity and in the mass balance between the freshwater discharge and measured/estimated values of SGD, it has been suggested that a large fraction of SGD can originate from seawater (Burnett et al., 2003; Taniguchi et al., 2003; Martin et al., 2007) that

recirculates through the sediments by various mechanisms like bioirrigation (Meile et al., 2001; Martin et al., 2004; 2006), tidal pumping (Riedl et. al., 1972), wave set up (Shum, 1992), density driven convective circulation (Bokuniewicz et al., 2004), and seasonal pumping of the water table (Michael et al., 2005). This recognition of different sources of SGD has led to the definition of terrestrial freshwater discharge (terrestrial SGD) and recirculated seawater discharge (marine SGD). These two sources together have been defined as 'total SGD' or simply 'SGD' (Taniguchi et al., 2003; Martin et al., 2007). I will follow this concept here and will consider SGD as the flux of porewater to the water column across the sediment-water interface, regardless of the origin and composition of the water (Burnett et al., 2003).

Because of freshwater-saltwater mixing by SGD, a subsurface brackish water zone is formed at the seaward tip of the coastal aquifer, which by analogy to the surface estuaries is called 'the subterranean estuary' (Moore and Church, 1999). The upper part of the subterranean estuary is the 'seepage face', along which terrestrial SGD discharges to estuaries. The freshwater-saltwater boundary at the edge of the seepage face is known as the 'seepage-face boundary', and marks the offshore limit of terrestrial SGD (Martin et al., 2007; Smith et al., 2008a, 2008b). Marine SGD recirculates at two interfaces of the seepage face, including the sediment-water interface ('non local-exchange') and at the freshwater–saltwater boundary (Figure 1-2). Discharge of terrestrial SGD dominates flow within the seepage face and limits non-local exchange. However, outside the seepage face non-local exchange is the only hydrologic process. Dispersion across the freshwater-saltwater boundary also controls SGD but this process only occurs at the seepage face boundary (Ghyben, 1889; Herzberg, 1901; Cooper, 1959).

The amount of the SGD varies temporally at time scales ranging from days (e.g. in areas with high tidal range) to months (e.g. seasonal variations between dry and wet months) to years (annual variations in aquifer recharge), resulting in daily to annual shifts in the location of the seepage face boundary (Michael et al., 2005; Charette et al., 2005; Smith et al., 2008a). At the timescale of months to years, the shift of the seepage face boundary is associated with the amount of terrestrial SGD, which in turn is controlled by the aquifer recharge (Michael et al., 2005; Smith et al., 2008a). Aquifer recharge can vary from wet to dry seasons, thus seasonality may be observed in the SGD. The conventional Ghyben-Herzberg conceptualization suggests that SGD should be highest when aquifer recharge is highest (Ghyben, 1889; Herzberg, 1901; Moore, 1997). However, a lag of few months between highest recharge and highest SGD has been observed (Michael et al., 2005; Charette, 2007; Moore, 1996b). It has been suggested this lag is caused by residence time of groundwater in the coastal aquifer (Michael et al., 2005; Smith et al., 2008a; Kelly and Moran, 2002).

Linkage between hydrology of the coastal aquifer and Fe diagenesis

In coastal sediments where no SGD is present, Fe distributions vary mainly with depth (e.g., Figure 1-1; Froelich et al, 1979; Canfield et al., 1993; Burdige, 2006). Variations in sources of flows, flow rates and lengths of flowpaths of SGD, along with its temporal variations can influence metal cycling in the subterranean estuary (Huettel, 1998; Testa et al., 2002; Spiteri et al., 2006; Charette et al., 2007). A link between SGD and Fe diagenesis was observed in Waquoit Bay, Massachusetts where an ‘Fe curtain’ is formed at the freshwater-saltwater boundary of the subterranean estuary by precipitations of dissolved Fe as Fe-oxides (Charette et al., 2005; Spiteri et al., 2006). In contrast, DOC concentrations were found to increase from freshwater marsh sediments to the freshwater-saltwater boundary, causing higher Fe-oxide

reductions thus elevated dissolved Fe concentrations at the boundary (Snyder et al., 2004). These studies show that Fe concentrations vary both with depth in the sediments as well as laterally with offshore distance in the subterranean estuary as a result of differences in flow rates and lengths of flowpaths of SGD.

According to the Ghyben-Herzberg and Cooper (1959) flow models, terrestrial SGD at the freshwater–saltwater boundary has longer flowpaths and slower flow rates than at discharge points closer to shore (e.g., Figure 1-2; and Cooper, 1959; Fetter, 2001, Martin et. al., 2007). Flows along longer flowpaths should have longer residence times and thus more reducing conditions. In contrast, oxidizing conditions would be expected at the sediment-water interface, where non-local exchange brings dissolved oxygen to the shallow sediments (Figure 1-2). Because of this relation between SGD and redox conditions, it is expected that distributions of redox sensitive Fe will reflect the position of the freshwater–saltwater boundary at the time of sampling.

Since SGD varies temporally, the position of the freshwater–saltwater boundary and associated Fe distributions will also change temporally. However, such temporal changes in SGD may not influence the sedimentary Fe concentrations, and may be limited to porewater Fe chemistry. Change in sedimentary Fe pools requires long term changes in sediment geochemistry, for example resulting from transgressions during sea level rise. Rising sea level is expected to shift the subterranean estuary landward along with its flowpaths of SGD and related zones of Fe cycling. Estimated sea level rise is 1.96 mm/year over the past 200 years (e.g., Jevrejeva et. al., 2008). Despite this importance of sea level on Fe distributions in the subterranean estuary, no study has ever explored the linkage between these two processes.

Statement of Purpose

The main objective of this dissertation is to explore the link between hydrology and Fe diagenesis, and OC budget in a subterranean estuary. Two previous studies that linked Fe diagenesis in the subterranean estuary showed that dissolved Fe precipitates as Fe-oxides in the seepage face of the subterranean estuary, thus there is no Fe-oxide reduction and OC remineralization by Fe-oxides (Charette et al., 2005; Windom and Moore, 2006). These observations raise question about Fe diagenesis in the subterranean estuary including:

Can Fe oxides be reduced in the subterranean estuary? If so, how much OC would be remineralized during Fe-oxide reduction?

Because hydrology of the subterranean estuary changes over long term (sealevel change) and over short term (tidal to seasonal precipitation change) scale, this study will also determine temporal variations in Fe-flux from the subterranean estuary. As discussed earlier, it is already known that changes in freshwater-saltwater boundary occur at monthly time scales; however it is still unknown whether there is multiyear shift of the boundary. This study will address the multiyear shift of the boundary and associated variations to understand short term scale variations in hydrology and associated Fe flux.

To meet these main objectives, two hypotheses were formulated and tested:

A. Mixing of fresh and saltwater in the subterranean estuary will influence Fe diagenesis; i.e there will be systematic variations in the dissolved Fe distributions across the seepage face, with variations in flow rates and flowpaths of SGD.

B. Transient flow in the subterranean estuary should alter the Fe-diagenesis

The study area is Indian River Lagoon, Florida (USA) (Figure1-3), where hydrology is well studied and sea level rose by tens of centimeters in the past 300 years (e.g. Hartl, 2006;

Martin et al., 2007). In the Indian River Lagoon study area terrestrial SGD is from the Surficial Aquifer (Martin et al., 2007), thus temporal variations in recharge of the Surficial Aquifer may influence freshwater-saltwater boundary at the multiyear scale. In this area, Fe-oxide can be an important electron acceptor for OC remineralization, because dissolved O_2 and NO_3^- are already exhausted, making it an ideal place to determine the relation between Fe-oxide reduction and OC remineralization. Samples were collected from November 2004 to September 2007 to understand the temporal variations in Fe flux.

Chapters Overview

Each of these chapters is written as a stand-alone paper and is intended to be submitted for publication. The title of the Chapter 2 is "*Influence of sealevel rise on iron diagenesis in an east Florida subterranean estuary*". This Chapter 2 will be submitted to *Geochimica Cosmochimica Acta*. In this Chapter 2 I explored a qualitative relationship between the SGD and porewater Fe chemistry. Details of the spatial variations in dissolved Fe distributions across the seepage face, and how these spatial variations are related to variations in flowpaths and flow rates of terrestrial SGD are discussed. The relative influence of marine versus terrestrial SGD on Fe diagenesis is determined by comparing Fe data within and outside the seepage face. The sources and sinks of dissolved Fe are also identified by the correspondence between sediment and porewater S, OC, and Fe concentrations. After exploring influences of modern day hydrology on Fe diagenesis, I discuss how transgression of the seepage face shifted these source and sink zones of Fe, along with flowpaths of terrestrials SGD, landward.

Based on observations from the Chapter 2, the Chapter 3 presents a numerical reactive-transport model that estimates Fe flux from the seepage face. The title of the Chapter 3 is "*Reactive transport model of iron diagenesis and associated organic carbon remineralization in*

a Florida (USA) subterranean estuary". This Chapter 3 will be submitted to *Marine Chemistry*. In this Chapter 3 I give an estimate of dissolved Fe production and consumption rates across the seepage face, and discussed the link between spatial variations of rates and hydrology. Using modern dissolved Fe production and consumptions rates, I determined how much Fe had been produced from the sediments or sequestered to sediments of the seepage face during the past 300 years of sealevel rise.

The title of the Chapter 4 is "*Influence of aquifer recharge on iron and organic carbon diagenesis in the seepage face of a subterranean estuary*". In this Chapter 4 I determine the effect that average annual aquifer recharge has on the average annual Fe flux from the seepage face, using the reactive transport model developed in Chapter 3. The amount of aquifer recharge is calculated from effective precipitation (precipitation-potential evapotranspiration). This Chapter 4 will be submitted to *Marine Chemistry* along with Chapter 3.

The title of Chapter 5 is "*Identification of pathway of iron diagenesis in an east Florida (USA) subterranean estuary using iron isotopes*". In this Chapter 5 various pathways of Fe diagenesis were identified using δ^{56}Fe values. This Chapter 5 will be submitted to either *Geochimica Cosmochimica Acta* or *Earth and Planetary Science Letters*.

Results of this doctoral study will be beneficial for understanding Fe diagenesis and OC remineralization in one subterranean estuary. Considering numerous subterranean estuaries occur all over the world, this study needs to be up-scaled to understand the global impact of OC remineralization in all these subterranean estuaries toward the global C budget.

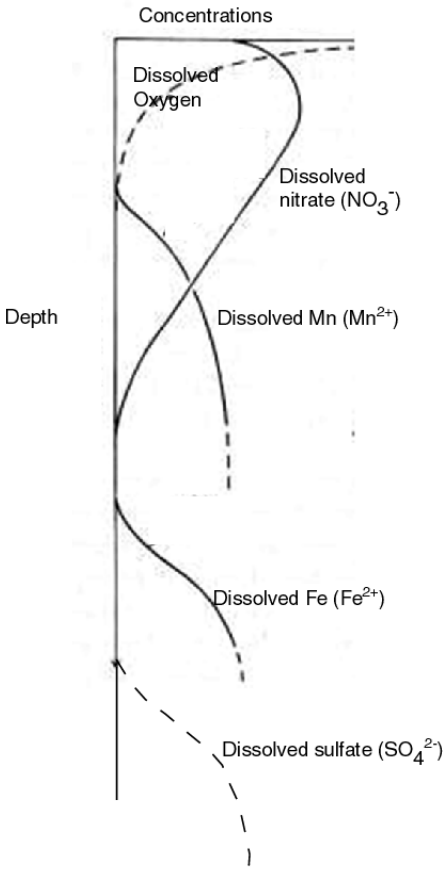

Figure 1-1. Redox zonations of electron acceptors in the coastal sediments. Note, dissolved Fe and Mn are the products of Fe- and Mn-oxide reductions, and are not the electron acceptors by themselves (source of the figure is Froelich et al, 1979).

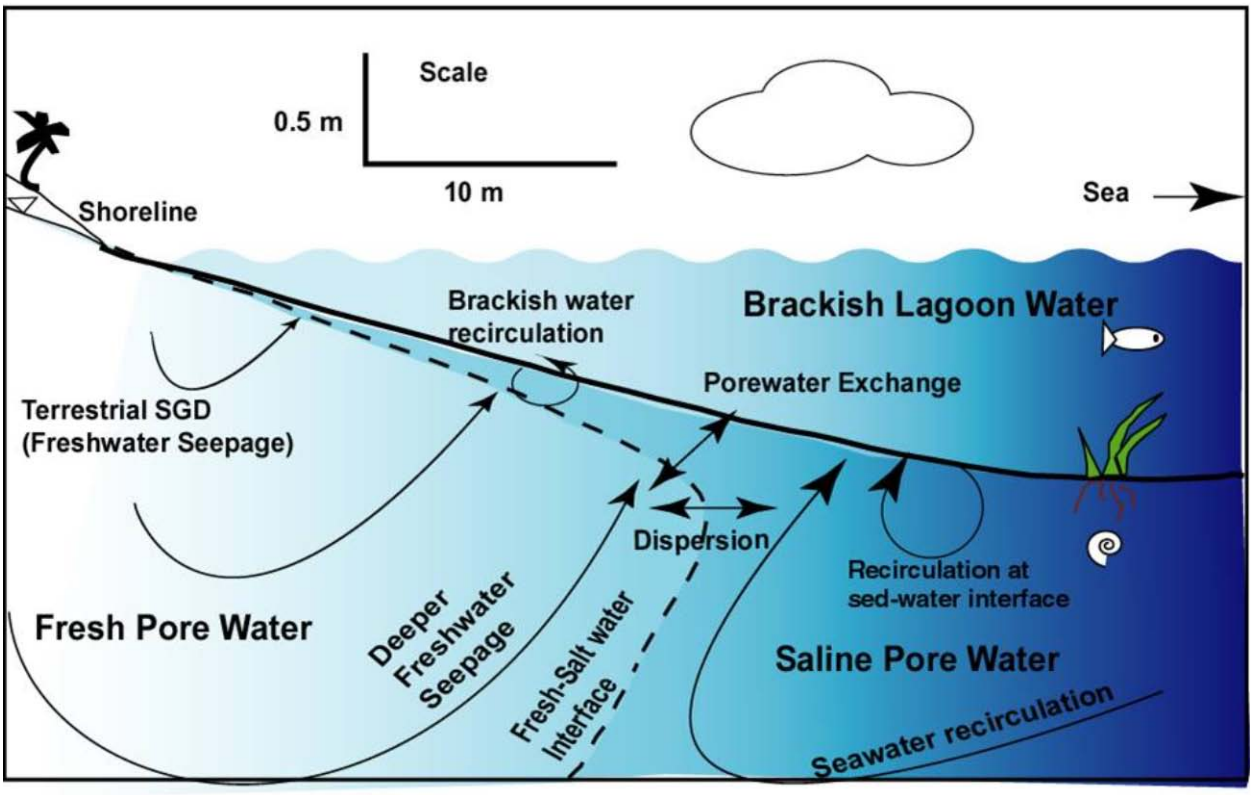

Figure 1-2. Schematic diagram of flowpaths of SGD. Terrestrial SGD has deeper flowpaths near the fresh-saltwater interface compared to flowpaths near shore. Marine SGD has shallower recirculation at the sediment-water interface and deeper seawater recirculation at the fresh-saltwater interface.

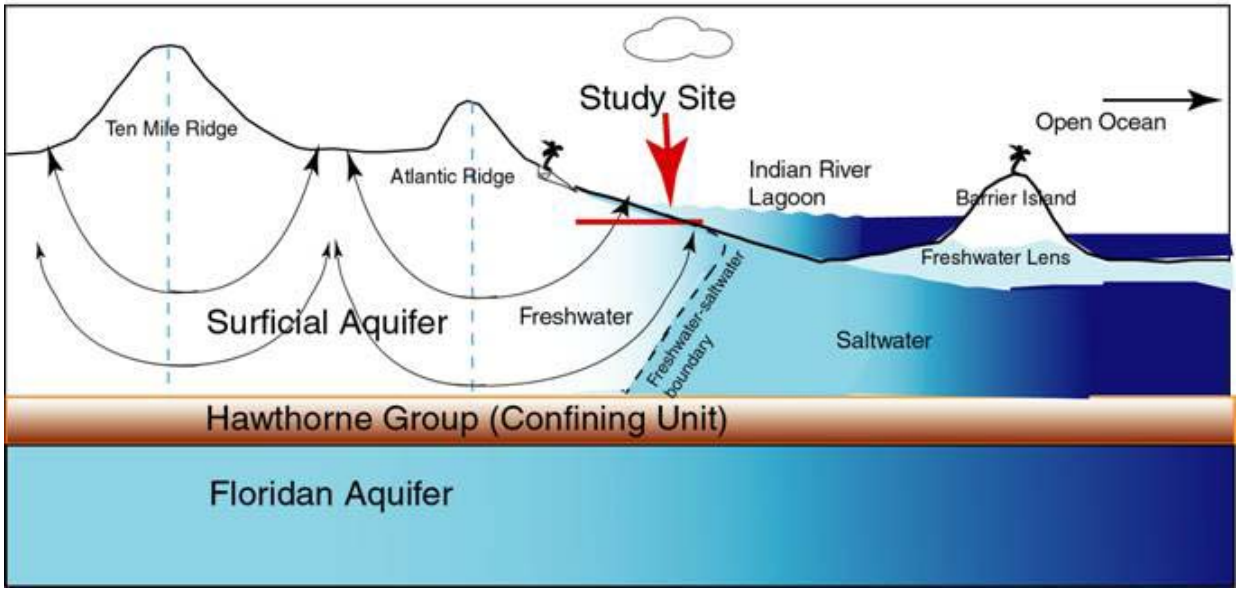

Figure 1-3. Highly schematic conceptual diagram of flowpaths of water near the Indian River Lagoon. Water divides are shown by blue dashed lines. The black dashed line represents the freshwater-saltwater boundary. The red line shows the sampling transect.

CHAPTER 2
INFLUENCE OF SEALEVEL RISE ON IRON DIAGENESIS IN AN EAST FLORIDA SUBTERRANEAN ESTUARY

Introduction

Only a few recent studies have addressed the link between SGD and Fe distributions in subterranean estuaries (e.g., Testa et al., 2002; Spiteri et al., 2006). In Waquoit Bay, Massachusetts, dissolved Fe concentrations decrease in the subterranean estuary because of changing oxidation-reduction potential (oxidation of dissolved Fe bearing hypoxic fresh groundwater plume by oxic marine SGD), and increase in pH (Charette et. al. 2005; Spiteri et al., 2006). These Fe-oxides trap reactive phosphorus when they precipitate (Charette et al., 2005). In contrast, dissolved Fe concentrations increase at the freshwater-saltwater boundary in the marsh sediments at Moses Hammock, Georgia, where elevated dissolved organic carbon (DOC) concentrations at the boundary resulted in high Fe-oxide reductions (Snyder et al. 2004). Controls on Fe-oxide diagenesis thus appear to vary depending local conditions within a particular subterranean estuary.

Rising sealevel will shift the subterranean estuary landward along with the associated SGD and zones of Fe-diagenesis. This landward shift should bring terrestrial sediments into the estuarine environment and move estuarine sediments that have been diagenetically altered by flows within the subterranean estuary into the marine environment. Estimated global average sealevel rise is about 1.96 mm/year over the past 200 years (e.g., Jevrejeva et. al., 2008). Recent sealevel rise estimated for Florida ranges between 1.7 and 2.4 mm/year (Penland and Ramsey, 1990), suggesting sealevel rise in Florida is similar to the global average. In the flat-lying coastal areas of Florida, coastlines have thus moved inland several tens of meters over a few centuries, displacing subterranean estuaries landward. Despite the potential for extensive movement of subterranean estuaries and diagenetic alteration of sediments in the subterranean estuary, no

study has ever evaluated its influence on Fe cycling. Consequently, in this chapter I evaluated how flow in a subterranean estuary of Indian River Lagoon, Florida influences Fe diagenesis and assessed how sealevel rise affects the diagenesis.

Location and Background

Our study site is the subterranean estuary of the Indian River Lagoon, Florida (Figure 2-1a). The main lagoon is part of the larger interconnected Indian River Lagoon system that also includes the Mosquito and Banana River lagoons. This lagoon system is a north-south trending, 195-km long estuary extending southern peninsular Florida. The present study area (28^{o}08.0' N and 80^{o}37.5'W) is in the central Indian River Lagoon.

The hydrostratigraphy of the field area is subdivided into three units: 1) the unconfined Surficial Aquifer, which is composed of sand, silt, clay, shell and dolomitic limestones of the Holocene Anastasia Formation; 2) the confined Floridan Aquifer, which is composed of Late Paleocene to Oligocene limestone; and 3) the confining unit, which separates the Floridan and Surficial aquifers, and is composed of sand, silt and clay of the Miocene Hawthorne Group (Toth, 1988; Scott, 1992). The Hawthorne Group is more than 30 m thick in the study area, fully confining the Floridan Aquifer, and thus all terrestrial SGD in the study area is from the Surficial Aquifer. Sediments are predominantly sandy with a porosity of around 0.45. In the upper 300 cm of lagoon sediments, permeability varies from 10^{-2} to 10^{-8} cm/sec, but is more homogeneous in the top 70 cm sediments, ranging from 10^{-2} to 10^{-4} cm/sec (Hartl, 2006).

Indian River Lagoon is a microtidal, shallow water (average depth 1 to 2 meters), wave-dominated estuary (Smith, 1987), where flow rates and magnitudes of terrestrial and marine SGD are well studied (Cable et. al., 2004; Martin et. al., 2004, 2006; 2007; Smith et al. 2006, 2008a, b). Submarine groundwater discharge has been estimated for Indian River Lagoon using seepage meters, chemical and thermal tracers, and modeling. Typical values for total SGD are

found to be around 10 cm/day (Belanger and Walker, 1990), but numerical modeling suggests terrestrial SGD ranges from 0.14 to 0.36 cm/day (Pandit and El-Khazen, 1990). This discrepancy was resolved by recognizing that marine SGD contributes more than 90% of the total SGD in this area (Martin et al., 2007). At our study site, the rate of terrestrial SGD decreases linearly with offshore distance and terrestrial SGD ceases at the freshwater-saltwater boundary (Smith et. al., 2006, 2008b; Martin et. al., 2007). In a previous study, the seepage face boundary was defined to occur between 20 and 22.5 m offshore based on the salinity distribution (Martin et al., 2007). In this study, however, the seepage face boundary is defined as water with 300 mM Cl, because water column chlorinity outside the seepage face of the subterranean estuary is above this value but in the seepage face ranges between 250 mM to 300 mM (see Martin et al., 2007). This Cl boundary occurs about 25 m offshore. The estimated residence time of terrestrial SGD in the subsurface is approximately 5 to 7 months based on the lag between rainfall and discharge (Smith et al., 2008b). Chloride concentrations, sampled intermittently between November 2004 and April 2007, suggest discharge from the seepage face was steady state over this time (Martin et. al., 2007). Saltwater intrusion temporarily shifted the seepage face landward during tropical storm Tammy (4th October 2005) and Hurricane Wilma (24th October 2005) (Smith et al., 2008a). This large scale perturbation required about 3 to 6 months for the seepage face to return to the pre-storm conditions (Smith et. al., 2008a).

Four major depositional environments, including marine, brackish, lacustrine, and lagoonal, were identified in the Surficial Aquifer by Hartl (2006). Four sediment cores were collected at the most seaward edge of our study site (CIRL39; 250 m offshore). These cores were composed of black sediments of marine origin in approximately the upper 2 m. These black marine sediments were underlain by orange sediments of terrestrial origin, which extended to the

base of the cores and thus have an unknown thickness, but were presumed to extend to the underlying Pleistocene coquina of the Anastasia Formation (Hartl, 2006). Hartl (2006) found sediment at 95 cmbsf at CIRL39 is approximately 500 years old using ^{14}C dating technique on plant materials and wood debris. The water column thickness at this site is 80 cm, but the lagoon water level is 25 cm higher than the mean sealevel, suggesting the depth of the plant material and wood debris is 150 cm below mean sea level. Dividing this depth of sediments by the time of deposition, the estimated average sealevel rise in Indian River Lagoon subterranean estuary is about 3 mm/year over this time. This rate of sealevel rise is similar to the global sealevel rise estimated by Jevrejeva et. al. (2008), and is also similar to the relative sealevel change estimated for Florida (Penland and Ramsey, 1990). At this rate, transgression of the modern seepage face would have taken about 300 years (e.g. Hart, 2006).

Methods

Porewater was collected between 18 and 22 April, 2007, using multilevel piezometers (multisamplers; Martin et al., 2003). Multisamplers were installed 0, 5, 10, 15, 17.5, and 20 m offshore within the seepage face, 22.5 m offshore at the landward side of the freshwater-saltwater boundary, 30 m offshore immediately seaward of the boundary, and 250 m offshore (Figure 2-1b). The stations for the nearshore multisamplers sites (i.e. 0-30 m offshore) are designated as EGNxx (Eau Gallie North), where xx represents the distance offshore. The farthest offshore station (250 m) is designated CIRL39 (Central Indian River Lagoon #39) from previous studies (Cable et al., 2006; Hartl et al., 2006; Martin et al., 2006, 2007; Smith et al., 2008a, b). Porewaters were extracted from the seepage face at various depths depending on the depth of each multisampler port in the seepage face.

Water was pumped from each port through an overflow cup while monitoring conductivity, temperature, and dissolved oxygen with a YSI model 556MPS multiprobe meter.

When these parameters stabilized, samples for metal analyses were filtered through a 0.45 µm canister filter into acid-washed HDPE bottles, immediately acidified to pH values < 2 with distilled trace metal grade nitric acid, and stored at 4^{o}C until analyzed. Separate aliquots of the porewater were processed in the field immediately after sampling to measure sulfide (S^{2-}) concentrations using the p-phenelynediamine – $FeCl_3$ technique (Gieskes et al., 1991). The samples were analyzed with a Milton Roy Spectronic 401 spectrophotometer within 6 to 10 hours of collection. Standards were prepared after each multisampler collection and measured in sequence with the samples so that samples and standards reacted over the same time periods.

Dissolved Fe and Mn concentrations were analyzed using a single collector ICP-MS (Finnegan Element II). The measured concentrations are assumed to be largely reduced Fe and Mn because solubilities of their reduced species are several orders of magnitudes higher than corresponding oxidized forms at ambient pH values. Each sample was diluted 50 times with 5% distilled nitric acid spiked with 8 ppb rhodium, which is used as an internal standard to correct for instrumental drift. Elemental concentrations were quantified using in-house gravimetrically prepared standards and a pair of external standard, NASS 5 (Canadian seawater standard) and SLRS 4 (Canadian river water standard). The precision and accuracy of the technique were calculated by comparing multiple measurements of the external standard SLRS4 (Table 2-1). The detection limit for Fe and Mn with this technique is about 0.003µM, and both Fe and Mn concentrations were occasionally below this value. Concentrations of Cl and sulfate (SO_4^{2-}) were analyzed by ion chromatography using a Dionex DX500 automated ion chromatograph with a precision of about 3% of the measured values.

Sediment samples were collected by vibracoring approximately 1 m north of the multisampler transect. Six cores of about 2 to 2.5 meters in length were collected from EGN0,

EGN10, EGN20, EGN22.5, EGN30, and CIRL39. These cores were returned to the laboratory where they were split and passed through a Geotek multi-sensor core logger (MSCL, http://www.geotek.co.uk.mscl/html). The MSCL calibrated color core imaging system was used to photograph the cores and measure the wavelengths of light reflected from the surface of the split cores. The wavelength was detected as red, blue, and green to produce the core image.

Ninety five subsamples of sediment (~1 g) were collected from cores at sites EGN0, EGN10, EGN20, and EGN30 at depths matching the depths of the port of the corresponding multisampler. Additional subsamples were collected from cores at EGN22.5 and CIRL39 at approximately 10 cm intervals throughout the core. Each subsample was measured for total C and S concentrations using a Carlo Erba 1500 CNS Elemental Analyzer. Precision was found to be 1% of the measured value based on 10 measurements of Atropine as a check standard. Concentrations of inorganic C (i.e. carbonate minerals) were measured with an automated Coulometer with a precision of 0.016%. The difference between total C and inorganic C concentrations was used to estimate OC concentrations. Same sediment samples, which were collected from cores at EGN0, EGN10, EGN20, EGN22.5, EGN30, and CIRL39 at various depths, were leached for Fe-oxides and Fe-sulfides according to the technique described by Hall et al. (1996). Iron and manganese concentrations in the leachates were measured at the University of Florida using the Element II ICP-MS. Scanning electron microscopy (SEM) and qualitative X-ray diffraction (XRD) analyses were made on 5 sediment samples representing the different color zones. These samples included three samples from orange sediments collected at 145 cmbsf from EGN0, EGN20, and EGN30, one sample from black sediments collected at 45 cmbsf at EGN20, and one sample from white sediments collected at 75 cmbsf at EGN30.

Results

Porewater Chemistry

Across the seepage face, total dissolved Fe and Mn concentrations vary by 6 and 3 orders of magnitude, respectively, ranging from 0.009 to 286 µM for Fe and 0.05 µM to 2.9 µM for Mn (Figure 2-2). The highest concentrations occur near the freshwater-saltwater boundary at depths greater than 66 cmbsf. The lowest concentrations occur at the site closest to shore, where maximum upward flow occurs (e.g., Martin et al., 2007) and 250 m offshore, which is beyond the influence of the seepage face (Figure 2-2). Dissolved Fe maxima occur at progressively greater depths with increasing distance from shore. At EGN0 and EGN5, the dissolved Fe maxima occur between 30 and 50 cmbsf and the maxima increase in depth to 140 cmbsf at EGN30. Dissolved Mn maxima occur at slightly shallower depths than the Fe maxima. Like Fe, Mn maxima become progressively deeper with distance offshore from about 15-25 cmbsf at EGN5 to 55-75 cmbsf at EGN20. All Fe and Mn maxima from the seepage face sites occur within the terrestrial orange sediments. Conversely, at CIRL39, both Fe and Mn maxima occur at 10 cmbsf. The Fe concentrations at the maxima increase from 1.05 µM at EGN0 to 286 µM at EGN22.5 and decrease to 0.49 µM at CIRL39. Similarly, the Mn concentrations at the maxima increase from 0.28 µM at EGN0 to 2.9 µM at EGN22.5 and decrease to 0.56 µM at CIRL39.

Dissolved sulfide profiles show offshore variations, but pH and DIC concentration-depth profiles are similar across the subterranean estuary. Similar to Fe and Mn maxima, dissolved sulfide maxima become deeper and broader with distance offshore, but unlike Fe and Mn, this trend continues offshore to CIRL39 (Figure 2-3a). The maxima deepen from about 20 cmbsf at EGN5 and EGN15 to around 50 cmbsf at EGN30. The highest dissolved sulfide concentration (200 µM) occurs at 120 cmbsf at CIRL39. All of the sulfide maxima occur within the marine black sediments. All sampling sites show DIC concentrations increase with depth, while a sharp

decrease in pH of about 1 pH unit is observed from the water column to the shallowest porewater sampled and then exhibit little or no variation below 10cmbsf (Figure 2-3a).

Sediment Chemistry

Vibracores taken from the seepage face show systematic color variations from orange to white to black from the bottom to the top of the cores taken from EGN0 to EGN30 (Figure 2-4). Thicknesses of the black sediments increase from about 17 cm at EGN0 to around 68 cm at EGN30. In some cores, black sediment interfinger with the orange and white sediments, but these interfingering black sediments have low sulfide concentrations compared to black sediments near the sediment-water interface. The core from CIRL39 differs from the other cores in that is has only black sediments from the base of the core at 230 cmbsf to 45 cmbsf and the upper 45 cm of the core contains white to grayish-white sediment. No orange sediment was found in the core we collected from CIRL39, although orange sediment was found at this site in a previous study at depths below about 250 cmbsf, deeper than our core (Hartl, 2006).

SEM and XRD analyses showed no mineral phases of Fe or Mn-oxides and Fe-sulfide, suggesting any overgrowth of secondary minerals and pyritization is minor in the sediments. Sediment leaching experiments showed black sediments are Fe-sulfide rich, and orange sediments have Fe-oxide coatings. The leaching results also showed that the black sediments have orders of magnitude higher S and OC concentrations (0.16 wt. % and 0.34 wt. %, respectively) and an order of magnitude lower Fe-oxide concentrations (0.03 wt. %) than the orange sediments (average 0.04 wt. % S and OC, and 0.2 wt. % Fe-oxide) (Figure 2-3b, and 2-4). Sulfur and OC concentrations have maxima in the near-surface black sediments across the seepage face, but at CIRL39, both S and OC concentrations increase steadily with depth. This sulfur is associated with Fe-sulfides based on the leaching experiments. Sulfur and OC concentrations are orders of magnitude higher in sediments at CIRL39 than in the seepage face,

with S concentrations ranging from 1.27 to 1.81 wt. % between 179 and 191 cmbsf and OC ranging from 1.16 to 1.83 wt. % between 90 and 110 cmbsf.

Discussion

Sources and Sinks of Dissolved Fe

In marine systems, OC is sequentially remineralized by terminal electron acceptors according to their Gibbs free energy yields in the order of oxygen, nitrate, Mn oxides, Fe-oxides, SO_4^{2-}, and CO_2 (Froelich et al., 1979; Burdige, 2006). Among these terminal electron acceptors, Mn-oxides and Fe-oxides occur in the solid phases and the rest are dissolved. In the Indian River Lagoon subterranean estuary, oxygen concentrations are low in all of the porewater (Martin et al., 2007), and nitrate concentrations average around 29 μM at EGN0, but was <0.3 μM offshore of EGN0 (Dorsett, 2009). These low concentrations suggest that oxygen and nitrate have been exhausted during OC remineralization, suggesting that Fe and Mn-oxides are important terminal electron acceptors for the OC remineralization.

The dissolved Fe maxima occur within Fe-oxide-coated orange sediments of Indian River Lagoon, suggesting the source of dissolved Fe is locally derived from reduction of the Fe-oxide coatings (Figures 2-2, 2-3, and 2-4). The identification of the orange sediments as having a terrestrial origin (Hartl, 2006) suggests the origin for Fe-oxide differs from similar orange sediments that were found in Waquoit Bay, Massachusetts. In Waquoit Bay, Fe-oxides were deposited within the subterranean estuary as dissolved Fe flowed upward into oxidized sediments (Charette and Sholkovitz, 2002; Charette et al. 2005). Iron-oxides were observed to produce elevated dissolved Fe concentrations as a result of elevated DOC concentrations and greater reducing conditions at the freshwater-saltwater boundary in Moses Hammock, Georgia (Snyder et al., 2004). Although in Indian River Lagoon, orange sediments have lower OC concentrations

than the overlying estuarine black sediments, it appears that Fe-oxide reduction by OC in the orange sediments is responsible for elevating the dissolved Fe concentrations.

The presence of dissolved sulfide maxima in the OC-rich black sediments indicates SO_4^{2-} is being reduced there, but good linear correlations between SO_4^{2-} and Cl^- concentrations suggest there is only a minor amount of sulfate reduction. Nonetheless, the sulfide generated during sulfate reduction appears to react with the dissolved Fe that flows upward with terrestrial SGD, precipitating solid Fe-sulfides as shown by the elevated solid S concentrations in the black sediment (Figures 2-3 and 2-4). Manganese does not show any systematic variation with porewater sulfide and sedimentary S (Figures 2-3 and 2-4) suggesting Mn-sulfide phases are not important sinks for dissolved Mn.

Iron-sulfide concentrations in the black sediments vary little with distance offshore, but the thickness of black sediments increases offshore suggesting that the total amount of Fe-sulfide accumulating in the sediments increases offshore. This increase reflects a longer time of accumulation for the offshore sediments than near shore sediments, which would have been recently inundated by sealevel rise. Precipitation of Fe-sulfides represents a sink for Fe dissolved from the underlying Fe-oxide coating that flows upward with the terrestrial SGD.

Non-local exchange will bring oxygenated water across the sediment-water interface, thereby limiting sulfide production in shallow sediments. Terrestrial SGD restricts non-local exchange in the seepage face (Smith et al., 2008a), thereby allowing precipitation of Fe-sulfides there. Non-local exchange at CIRL39 could explain the presence of white sediments above the Fe-sulfide stained black sediment offshore of the seepage face. At this location, the lack of terrestrial SGD allows rapid recirculation resulting from bioirrigation to decrease the residence time of lagoon water in the upper 50 cmbsf to less than a day (Martin et al., 2004, 2006). This

exchange creates oxic conditions near the sediment-water interface, leading to dissolution of Fe-sulfides. The dissolution of Fe-sulfides could be responsible for the dissolved Fe concentrations maximum at 10 cmbsf at CIRL39. The non-local exchange should also flush dissolved Fe from the sediment, resulting in overall low Fe concentration. The lack of white sediments at the sediment-water interface within the seepage face reflects a less vigorous non-local exchange as a result of damping by upward flow of terrestrial SGD (Smith et al. 2008b). Similarly, the white sediments separating black and orange sediment within the seepage face sediments represent sediments that have had most of their Fe-oxides leached but lack corresponding precipitation of Fe-sulfides. The variation in the location of Fe sources and sinks, depending on whether terrestrial or marine SGD dominates, indicates that hydrogeology plays a role in Fe diagenesis in the subterranean estuary and its flux from the sediment.

Relation between Terrestrial SGD and Fe-Diagenesis

Distribution of dissolved Fe reflects the position of the freshwater saltwater boundary of the subterranean estuary because of the geochemical conditions associated with the boundary (Snyder et al. 2004; Charette et al., 2005; Spiteri et al., 2006). In Waquoit Bay, pH increases from 5.5 nearshore to 7.9 at the freshwater-saltwater boundary of the subterranean estuary, and dissolved Fe concentration are low where pH is high at the boundary (Spiteri et al., 2006). In contrast, Indian River Lagoon pH profiles vary little across the seepage face, but elevated dissolved Fe concentrations occur at the freshwater-saltwater boundary, suggesting pH can not cause elevated Fe concentrations at the boundary (Figure 2-3). Boundaries between freshwater and saltwater coincide with elevated DOC concentrations at Moses Hammock, Georgia, where DOC concentrations increase from 250 µM in the freshwater zone to about 1050 µM at the freshwater-saltwater boundary (e.g. Snyder et al., 2004). Unlike Georgia site, in the Indian River Lagoon DOC concentration profiles in porewater (Dorsett, 2009), and sediment bound OC, Fe-

oxide concentrations vary little with offshore, but the quality of DOC changes to marine suggesting DOC may influence elevated Fe concentrations. Additionally, SGD decreases from nearshore to the freshwater-saltwater boundary, thus elevated Fe concentrations at the boundary can be due to SGD.

Different sources of SGD (e.g., marine or terrestrial) have different redox conditions because of differing amounts of time since the water was in contact with atmospheric oxygen. According to the Ghyben-Herzberg and Cooper (1959) flow models, terrestrial SGD at the freshwater–saltwater boundary has longer flowpaths and slower flow rates than at discharge points closer to shore (e.g., Figure 1-2; and Cooper, 1959; Fetter, 2001; Martin et. al., 2007). Consequently, terrestrial SGD at the distal end of the seepage face (i.e., near the freshwater – saltwater boundary) should have longer residence times in the subsurface and more reducing conditions than elsewhere in the seepage face. In contrast, oxidizing conditions would be expected at the sediment-water interface where non-local exchange of marine SGD brings dissolved oxygen to the shallow sediments (Figure 1-2). Upward flow of terrestrial SGD at Indian River Lagoon limits the depth of penetration of the non-local exchange to about 40 cmbsf (Smith et al., 2008a), which is shallower than the base of the black sediments and thus does not carry DOC into the orange sediments to influence the Fe diagenesis. Flow rates of terrestrial SGD decrease from a maximum of around 0.5 m^3/day/meter at the shoreline to 0.018 m^3/day/meter at the freshwater-saltwater boundary (Martin et al., 2007). These variations in flow and its correspondence to dissolved Fe across the subterranean estuary of the Indian River Lagoon suggests either longer flowpaths and associated reducing conditions at the boundary causes higher Fe-oxide reductions, and/or slower flow rates of terrestrial SGD allow a greater accumulation of reduced Fe at the boundary.

Sealevel Rise and Reverse Redox Zonation

The freshwater-saltwater boundary is transient, and can change its position over short-term (months to years) and long-term scales (100 of years). Short-term changes result from episodic storm events and seasonal fluctuations of aquifer recharge, which can alter flow within the subterranean estuary and thus Fe-diagenesis (Michael et al, 2005; Smith et al., 2008b). Such diagenetic changes are limited to porewater chemistry and unlikely to be recorded in the chemical composition of the sediments. Chemical composition of sediments in Indian River Lagoon, particularly the Fe and sulfide compositions of the sediment, appears to record long-term changes in the position of the subterranean estuary. The orange sediments could not have formed under the current hypoxic/anoxic conditions present within the seepage face. During lower sealevel, these sediments would have been part of the vadose zone and been exposed to the atmosphere (Figure 2-5), allowing precipitation of Fe-oxide coatings on quartz sands (e.g., Skolasinska, 2006). Consequently, the Fe-oxide coatings represent relict conditions when the seepage face was farther offshore than its current location. As sealevel rose, the seepage face migrated landward and brought Fe-coated sediments into the seepage face, when the deposition of estuarine black sediments was initiated at the top of orange sediments. In the Indian River Lagoon, some black sediments interfinger with orange sediments, and these interfingering black sediments have different chemical compositions (low OC and S) than the estuarine black sediments, suggesting they may have formed either by multiple fluctuations of the water table by storms or floods, when these sediments were onshore, or multiple sequences of inundation of terrestrial deposits during transgression.

Under normal burial diagenesis Fe-oxide reduction occurs at shallower depths than SO_4^{2-} reduction because of the higher energy yields of Fe-oxides than SO_4^{2-} (Froelich et al., 1979; Burdige et al., 2006). In contrast, in the Indian River Lagoon subterranean estuary, the SO_4^{2-}

reduction zone overlies Fe-oxide reduction zone. This reversal of the normal burial diagenetic sequence results from variations in OC and Fe-oxide concentrations, as well as the type of OC contained within the sediments. Organic carbon present in orange sediments is terrestrial and thus more likely to be refractory than the OC within the black sediment, which is marine (e.g., Suess et al., 1980). Further, because Fe-oxides are absent in the black sediments, SO_4^{2-} must become the terminal electron acceptor after oxygen and nitrate are depleted.

The rate of marine transgression of the seepage face is estimated by dividing the thickness of water column, 27 cm, plus the thickness of black sediments at the freshwater-saltwater boundary, 53 cm at EGN30, with the rate of sealevel rise, 3 mm/year, estimated from Hartl (2006). This estimation suggests the landward edge of the subterranean estuary was located around EGN30 about 270 years ago. As sealevel has risen, the subterranean estuary would have shifted landward while retaining its relative configuration. This migration of the subterranean estuary has resulted in the current distribution of solid and dissolved Fe concentrations across the seepage face.

In summary, in the Indian River Lagoon subterranean estuary, Fe-oxide reduction and Fe-sulfide precipitation occur within the seepage face where terrestrial SGD dominates and Fe-sulfide dissolution occurs outside the seepage face, where non-local exchange (marine SGD) dominates. This dependence of the Fe sources and sinks on sources of SGD reflects the importance of hydrology on Fe diagenesis in the subterranean estuary. Elevated dissolved Fe concentrations occur at the seaward end of the seepage face, although diagenetic sources of Fe are constant across the seepage face. Only flow rates and lengths of flowpaths vary across the seepage face. Therefore, although common burial diagenetic reactions occur within the subterranean estuary, they are modified in both space and time by SGD.

Conclusions

Variations in dissolved Fe concentrations across the seepage face at the Indian River Lagoon are significantly larger than what would be expected from simple mixing between freshwater and saltwater. In Indian River Lagoon sediments, Fe-oxides are an important oxidant for OC remineralization. The amount and location of the remineralization are controlled by SGD, which influences redox conditions in the subterranean estuary. Submarine groundwater discharge allows dissolved Fe to accumulate at the freshwater–saltwater boundary because of slower flow rates of terrestrial SGD. One sink for dissolved Fe is Fe-sulfide, which precipitates in an OC-rich sedimentary layer. The precipitated Fe-sulfides are remobilized at the sediment-water interface beyond the seepage face when oxygen-rich lagoon water recirculates through the shallow sediments. Iron exchange between solid and dissolved phases in Indian River Lagoon thus occurs in three steps: dissolution of Fe-oxides, precipitation of dissolved Fe as Fe-sulfides, and subsequent oxidation of the Fe-sulfides.

Sealevel rise is reflected in thickening of marine black sediments with offshore distance. Sealevel rise allows dissolved Fe to flux from the sediment to the water column by transgressing the subterranean estuary and transposing Fe-oxide rich sediment into the reducing environment of the subterranean estuary, along with pushing Fe-sulfide-rich sediments seaward of the seepage face where they can be re-oxidized. Because Fe-oxides are an important oxidant for OC remineralization, the magnitude and distribution of OC remineralization utilizing Fe-oxides as a terminal electron acceptor is dependent on modern hydrologic conditions, e.g., rates and sources of SGD, superimposed on the long term effects of rising sealevel.

Table 2-1. Analytical certainty of the measured external standard SLRS4.

	UF Values (ppm)	STD. Dev.	Certified Values (ppm)	STD. Dev
Mn	0.00324	0.00056	0.00337	0.00018
Fe	0.11012	0.00398	0.103	0.005

* UF means values measured in University of Florida
STD. Dev means standard deviations of the measurements.

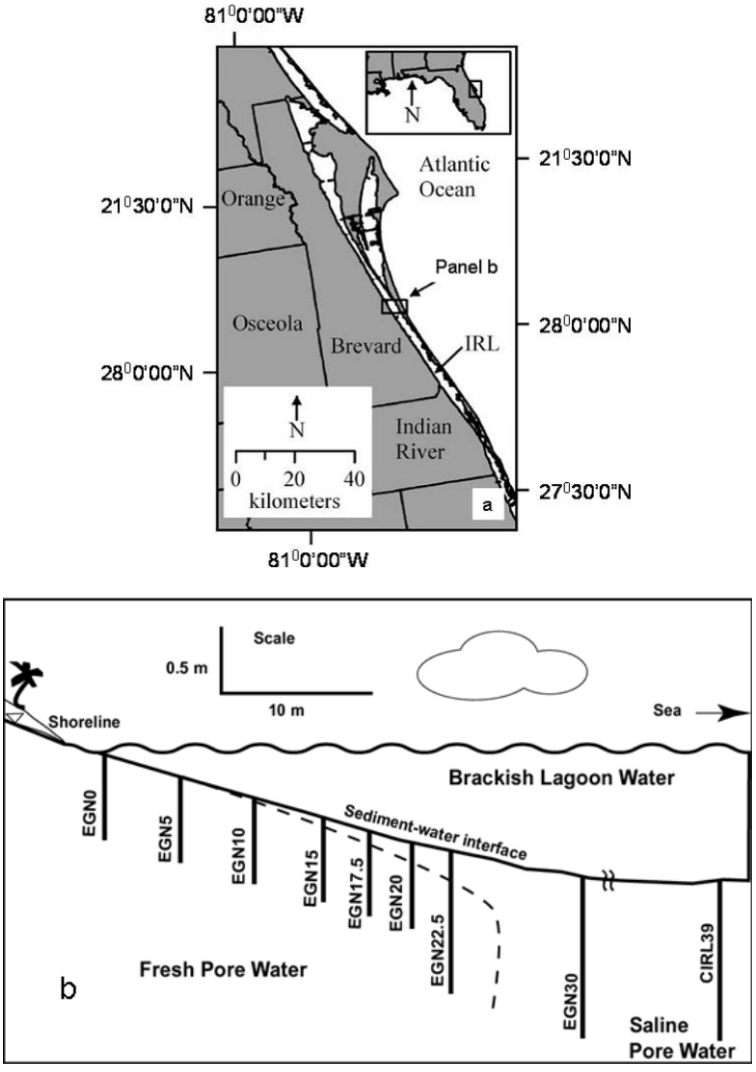

Figure 2-1. Location of the study site. a) geographic location of the transect, and b) cross-sectional view of the transect and location of multisamplers. The dashed line is the fresh-saltwater boundary at Cl concentrations of 300µM. (Note: multisamplers have different lengths and CIRL 39 is 250m offshore).

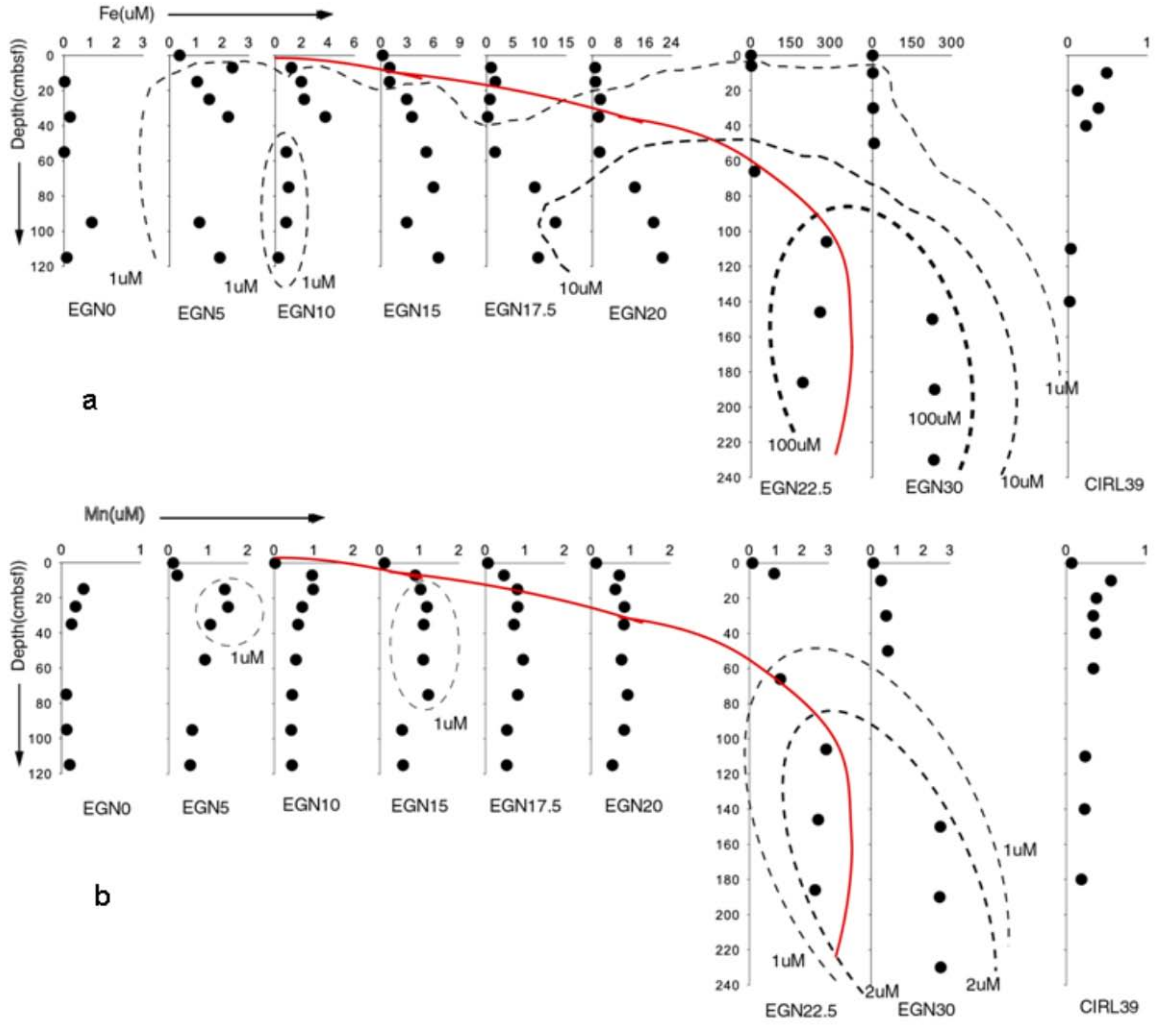

Figure 2-2. Dissolved concentrations of metals. a) Fe, and b) Mn across the seepage face. Dashed lines are contoured concentrations with the contour interval of 1, 10, and 100 µM in a), and 1 and 2 µM in b). Solid red line shows the 300 mM Cl concentration, representing the fresh-saltwater boundary.

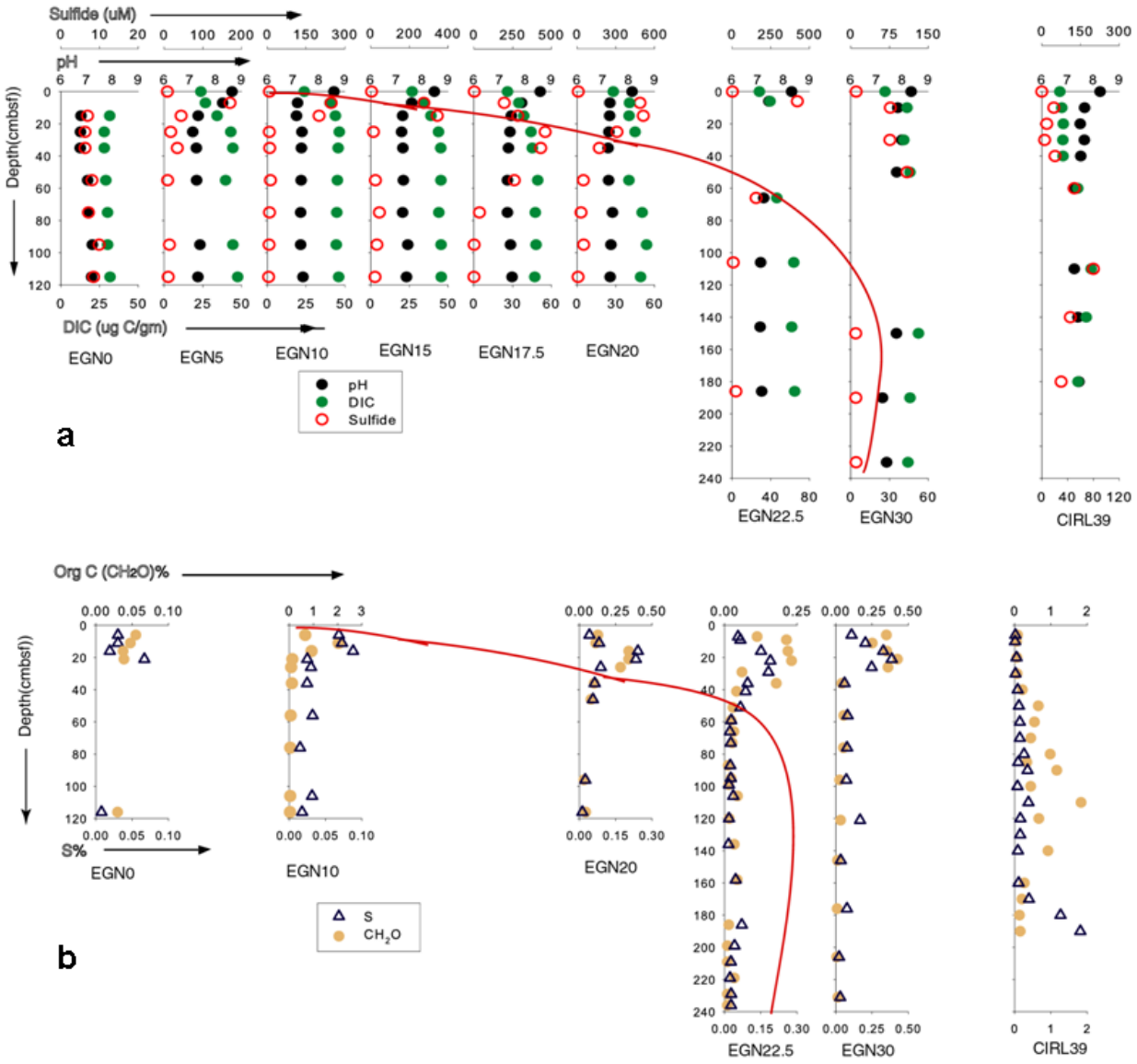

Figure 2-3. Depth profiles of water quality parameters. a) porewater pH, DIC, and sulfide, b) S and OC (CH_2O) in sediments. Solid red line shows the 300 mM Cl concentration, representing the fresh-saltwater boundary.

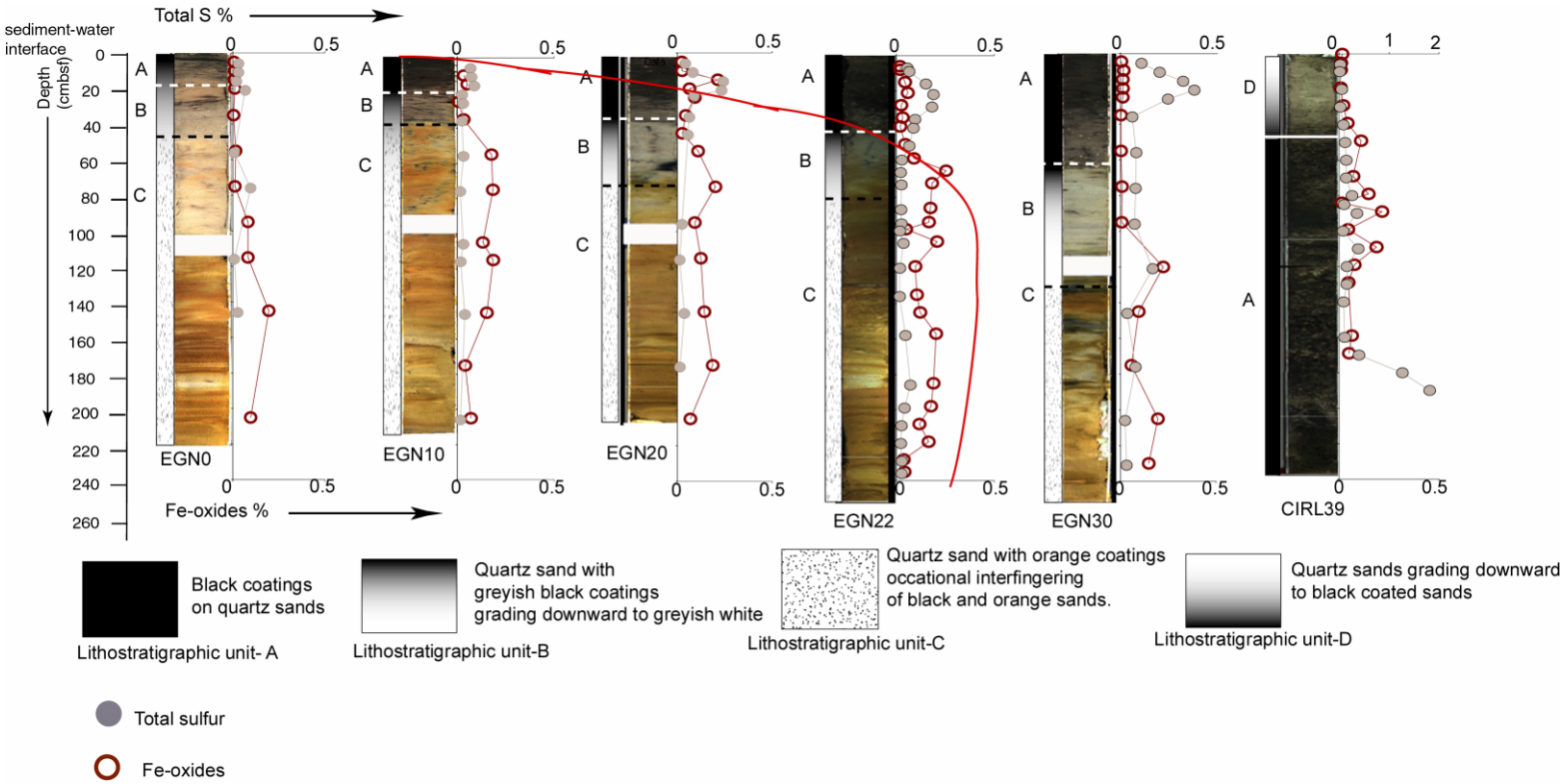

Figure 2-4. GEOSCAN images of five vibracores collected from the seepage face along with their lithostratigraphic unit description, and associated Fe-oxide and sedimentary sulfur concentrations. The white dashed line, black dashed line, and white solid line are the boundaries between A-B, B-C, and D-A, respectively. (Note: the change in the scale of the sulfur concentrations for CIRL39).

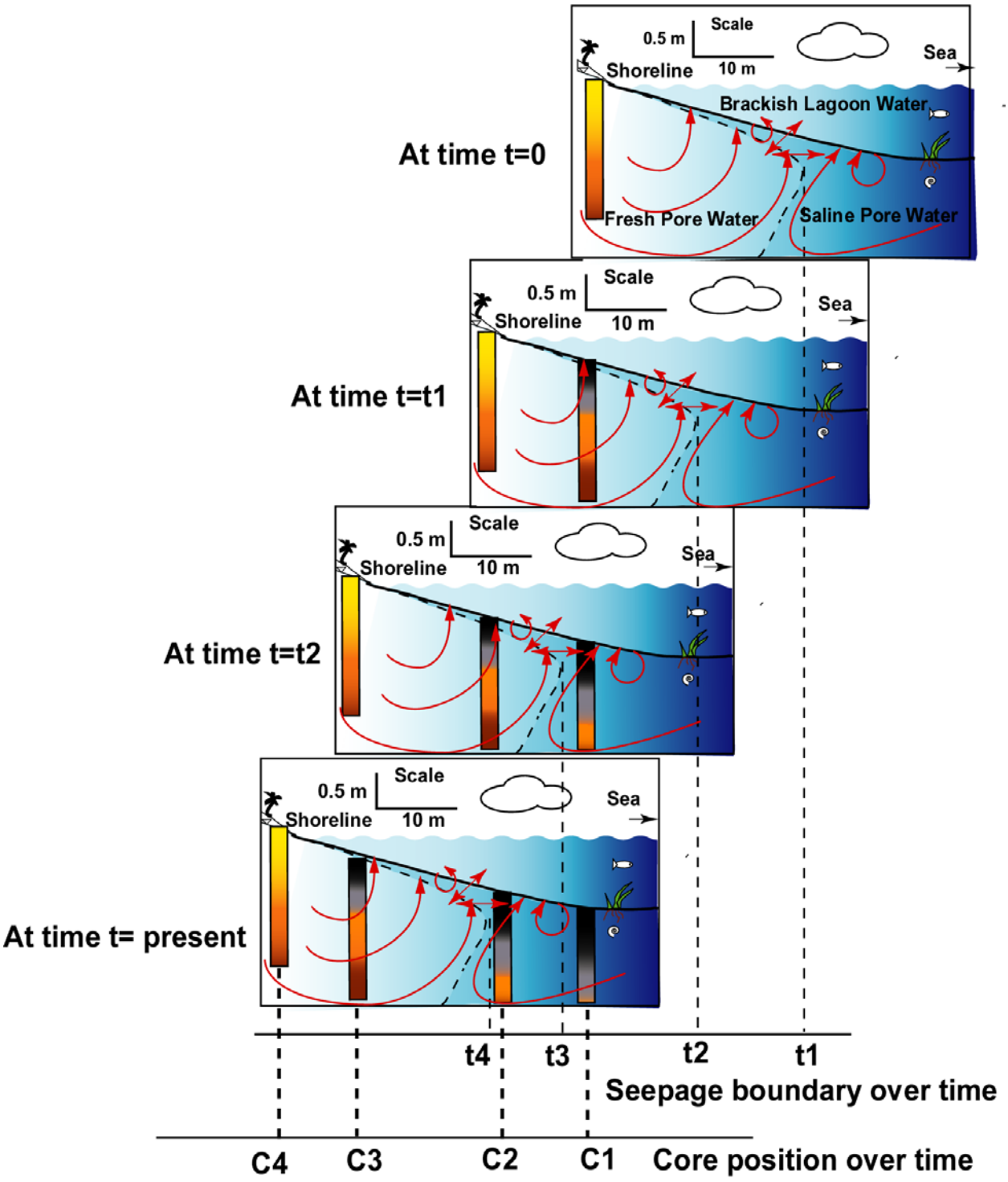

Figure 2-5. Diagram for the evolution of the seepage face as sea level rose over the past 270 years. Core C4 is present day EGN0, and C1 is present day CIRL39; at time t = t0, C1 was at C4.

CHAPTER 3
REACTIVE-TRANSPORT MODEL OF IRON DIAGENESIS AND ASSOCIATED ORGANIC CARBON REMINERALIZATION IN A FLORIDA (USA) SUBTERRANEAN ESTUARY

Introduction

Rates of Fe-oxide reduction and associated magnitudes of OC oxidation can be estimated in marine sediments using reactive-transport models (Van Cappellen and Wang, 1995). These models are typically applied to sediment systems where there are no SGD, e.g. marine sediments or coastal sediments farther offshore. A few models also consider the influence of freshwater discharge on Fe diagenesis (Spiteri et al. 2006, 2008). Models are often based on mass exchange between dissolved Fe and solid Fe-oxides, but can be complicated by other reactions, such as Fe-sulfide precipitation and dissolution (Berner, 1980), changes in pH (Spiteri et al., 2006), or reduction of Fe-oxides by electron donors other than OC (Postma, 1985). Similarly, estimates of OC reduction can be complicated if OC is remineralized by terminal electron acceptors other than Fe-oxides (Froelich et al., 1979; Van Cappellen et. al., 1998).

The linkages between Fe-oxide reduction and OC oxidation, coupled with the hydrogeology of the subterranean estuary, raise the question of whether the subterranean estuary sediments act to sequester OC or produce a net flux of oxidized carbon (e.g., CO_2) from the sediments. Consequently, in this chapter I developed a reactive-transport model of Fe-oxide dissolution and the loss of dissolved Fe to solid Fe-sulfide in the subterranean estuary of Indian River Lagoon, Florida. Unlike many existing reactive-transport models (e.g. Berner, 1980), this model includes advective transport by terrestrial SGD along with diffusion. I used a comparison of estimated and measured solid Fe-sulfide concentrations to validate the model. The model thus provides a means to quantitatively assess the magnitude, locations, and sources of OC remineralization caused by reduction of Fe-oxides within a subterranean estuary.

Fe Dissolution and Precipitation Model

Model Conceptualization

Two reactions are considered for the production and consumption of dissolved Fe in Indian River Lagoon sediments, which can be represented by:

$$C_6H_{12}O_{6(OrgC)} + 42CO_2 + 24Fe(OH)_{3(Fe-oxide)} \xrightarrow{R_1} 24Fe^{+2}{}_{(Fe_{aq})} + 48HCO_3^- + 18H_2O \quad (1) \qquad (3\text{-}1)$$

$$Fe^{2+}{}_{(Fe_{aq})} + HS^- \xrightarrow{R_2} FeS_{(Fe-sulfide)} + H^+ \qquad (3\text{-}2)$$

Equation 3-1 (e.g. Stumm and Morgan, 1996) represents the production of dissolved Fe during reduction of amorphous Fe-oxides by OC at the rate of R_1. Equation 3-2 (e.g., Berner, 1980) represents the consumption of dissolved Fe by precipitation of amorphous Fe-sulfide at the rate of R_2. The reaction rates R_1 and R_2 depend on the first order kinetic rate constants (1/sec) of reactions 1 and 2, represented by K_1 and K_2 respectively. The rate of Fe-oxide dissolution, R_1, can be obtained by multiplying the rate constant K_1 with measured solid Fe-oxide concentrations (Equation 3-3).

$R_1 = K_1 * [\text{Fe-oxide}]$ (3-3)

Similarly, the rate of Fe-sulfide precipitation, R_2, can be obtained by multiplying dissolved Fe concentrations with the corresponding rate constant K_2 (e.g., Van Capppellen and Wang, 1995)

$R_2 = K_2 * [\text{Fe}]$ (3-4)

Although K_2 is assumed to be constant with depth, dissolved Fe concentrations vary with depth (Figure 3-2) indicating that R_2 also must vary with depth. The coefficients K_1 or K_2 are often called pseudo-rate constants (see Berner, 1980) for early diagenetic models, and they depend on activity coefficients, chemical potentials, and ionic strength, which vary across the seepage face and thus K_1 and K_2 are expected to vary.

We assume both equations (3-1) and (3-2) are kinetically driven, and neither Fe-oxide dissolution nor Fe-sulfide precipitation reach the equilibrium to allow reverse reactions. Oxidation of dissolved Fe is not included in the model, because reducing conditions in the Indian River Lagoon subterranean estuary prevent formation of Fe-oxides. Also, terrestrial SGD continuously removes dissolved Fe from the zone of Fe-oxide reduction so that dissolved Fe never attains equilibrium with Fe-oxides. Fe-oxides coating terrestrial sediments have been continuously supplied to the subterranean estuary from onshore as the field site was transgressed at a rate faster than they are reduced by terrestrial SGD (Chapter 2), and thus reactant Fe-oxides are not exhausted. Based on this information, equation (3-1) is assumed to be a forward and continuous reaction over time that supplies sufficient dissolved Fe for continuous Fe-sulfide precipitation, and consequently, equation (3-2) is also assumed to be a forward reaction.

Reactive-transport models were developed to estimate the offshore variation of Fe-oxide dissolution and Fe-sulfide precipitation. The modeled domain was set equal to the sampling domain at each station. Because of differences in dissolved Fe concentrations among the three lithostratigraphic units, three different zones are assumed to represent differences in the Fe diagenetic reactions. The uppermost zone extends from the sediment-water interface to the bottom of the black sediments. The intermediate zone ranges from bottom of the black sediments to the depth of the dissolved Fe maxima. The lowermost zone extends from the depth of the dissolved Fe maxima to the bottom of the sampling domain (Figure 3-1). In the upper zone dissolved Fe concentrations decrease upward as a result of precipitation of Fe as Fe-sulfides. In the intermediate zone, although dissolved Fe concentrations decrease upward, sediment color is orange and not black and there is little sedimentary sulfur, suggesting Fe removal is not due to precipitation of Fe-sulfide. The most likely reason for Fe removal in this intermediate zone is the

dissolved Fe adsorption onto Fe-oxides, which is a common step during microbial Fe-oxide reduction (Lovley et al., 1987; Icopini et al., 2004). In the bottommost zone, dissolved Fe concentrations increase upward as a result of dissolution of Fe oxides. In each zone, only one reaction (either precipitation of Fe, adsorption of Fe, or dissolution of Fe-oxides) is assumed. Different values of K_2 are assumed for the upper and intermediate zones based on different sediment types and corresponding reactions in each zone. These two values are represented as K_{2a} for the Fe precipitation as Fe-sulfides in upper zone and K_{2b} for the Fe adsorption in the intermediate zone respectively. The reaction constants for Fe-oxide dissolution, for Fe-sulfide precipitation, or for dissolved Fe adsorption (K_1, K_{2a}, or K_{2b}) are assumed to be constant with depth at the "average rate constant" (e.g., Wang and Van Cappellen, 1996), although values of K_1 or K_2 vary from one sample site to another.

Numerical Solutions

In the zone where Fe-oxide dissolution occurs, the early diagenetic equation (e.g. Berner, 1980) for Fe^{2+} production can be represented by

$$\frac{\partial C}{\partial t} = D_s \frac{\partial^2 C}{\partial z^2} - \omega \frac{\partial C}{\partial z} + K_1 C_{solid} \qquad (3\text{-}5)$$

Similarly, in the upper and intermediate zones where Fe is removed from porewaters, its consumption can be represented by

$$\frac{\partial C}{\partial t} = D_s \frac{\partial^2 C}{\partial z^2} - \omega \frac{\partial C}{\partial z} - K_2 C \qquad (3\text{-}6)$$

where C is the dissolved Fe concentration (μM) to be modeled; C_{solid} is the measured Fe-oxide concentrations in sediment leachates (sediment wt% converted to μM), which are corrected for porosity(Φ), and sediment density(ρ); t is the time for non-steady state models; K_1 is the first order Fe-oxide dissolution rate constant; K_2 is the first order Fe-removal rate constant; z is depth

below the sediment-water interface (positive downward); ω is the advection rate of terrestrial SGD (negative downward); and D_s is the molecular diffusion of dissolved Fe at infinite dilution (D), which has been corrected for tortuosity. The value of D for Fe is $7.2*10^{-6}$ cm^2/sec (Li and Gregory, 1974), and the correction for tortuosity is (e.g. Berner, 1980; Bodreau, 1996)

$$D_s = \frac{D}{(1-2*\log(\phi))} \tag{3-7}$$

The porosity and sediment density for Indian River lagoon sediments are 0.45 and 2.67gm/cm^3, respectively (Hartl et. al., 2006), yielding a value of D_s of $2.77*10^{-6}$ cm^2/sec, which we assume remains constant throughout the subterranean estuary. Advection of terrestrial SGD decreases offshore (e.g. Martin et al., 2007) according to:

$$\omega = 0.16-0.0064x \tag{3-8}$$

where, x is the offshore distance in meters, and ω is in cm/day. The subterranean estuary at our site is steady state during the time of sampling (Martin et al., 2007), thus $\frac{\partial C}{\partial t} = 0$.

Measurements of solid Fe-oxide concentrations are available only where cores were collected (i.e., EGN0, EGN10, EGN20, and EGN22.5), but these sites show little differences in concentrations across the seepage face. We thus assume Fe-oxide concentrations for site EGN15, and EGN17.5 are similar and use Fe-oxide data from EGN20 for modeling purposes at these two stations.

Equations (3-5) and (3-6) were solved numerically by a two point boundary solving technique. Details of the numerical solving technique are available in Glover et al. (2006) and Press et al. (1992). The modeled domain extends from the sediment-water interface to 115 cm below sea floor (cmbsf) at sites EGN0 to EGN20, and to 186 cmbsf at EGN22.5. The model domain was divided into N number of 1-cm long cells. The upper and lower boundary conditions

follow Dirichlet boundary conditions, and use the measured dissolved Fe concentrations at the sediment-water interface and bottom of the sampling domain, respectively.

The only model parameters are K_1, K_{2a}, and K_{2b} which were adjusted to minimize the difference between measured and modeled dissolved Fe concentrations. We used the Nelder-Mead optimization technique (Nelder and Mead, 1965), to find the values of K_1, K_{2a}, and K_{2b} in their corresponding zones. Using the modeled values of K_1 K_{2a}, and, K_{2b}, the rate of Fe-oxide dissolution or Fe-sulfide precipitation was estimated at each cell using equations (3-3) and (3-4), respectively. By adding the R values for each cell, $\sum R$, the total mass exchange from solid to fluid or fluid to solid in the oxide dissolution or sulfide precipitation zone can be obtained for each site. The entire thickness of the Fe oxide dissolution zone was not sampled and thickness of the black sediments varies offshore, resulting in different thicknesses of the zones at each site. To overcome this problem, average fluxes per unit cross sectional area (i.e., the depth integrated flux values) of Fe-oxide dissolution and Fe-sulfide precipitation (mg/cm^2/year) were obtained by multiplying the summed value, $\sum R$ (units of mg/cm^3/year) by the thickness, L (units of cm) of the corresponding zones respectively (Wang and Van Cappellen, 1996). No porewater data are available from the oxide reduction zone at sites EGN15 and EGN20 and thus depth integrated fluxes of Fe-oxide dissolution are not available from these two sites. Iron-oxide dissolution is compared below from the remaining four sites, EGN0, EGN10, EGN17.5, and EGN22.5.

Annual amounts of total OC remineralized by Fe-oxide reduction was estimated by dividing the depth integrated Fe-oxide reduction by 4, which is the stoichiometric ratio of Fe-oxides to OC oxidation shown in equation 3-1. Since there are two zones where dissolved Fe can be removed, the total amount of Fe removal was found by summing the accumulation from both zones. Offshore variations in the precipitation of Fe-sulfides and remineralization of OC were

estimated based on the production of dissolved Fe from Fe-oxides, modified by the amount of Fe-sulfides precipitated and adsorbed from dissolved Fe.

Model Validation and Results

The reactive-transport model was validated by comparing measured concentrations of Fe-sulfides with the amount estimated by the model. Site EGN22.5 was chosen for this comparison because it occurs at the seepage face boundary, and thus has an integrated record of sulfide precipitation as the seepage face was transgressed during sea level rise (Chapter 2). The rate of Fe-sulfide precipitation is variable with distance offshore, and thus we assume Fe-sulfide precipitation also varied through time as EGN22.5 was transgressed. The amount of Fe-sulfide accumulated at EGN22.5 as sea level transgressed the seepage face can thus be estimated by plotting the amount of Fe-sulfide precipitated at each site versus the time since the site was flooded, and integrating the area under the curve (Figure 3-2a). The Fe-sulfide precipitation rates are divided into five segments, with each segment representing linear change in the rate of Fe-sulfide precipitation between two adjacent sampling sites. The total amount of Fe-sulfide at the base of the black sediment zone thus includes Fe-sulfide that precipitated during the entire transgression at rates depending on the age of the sediment. Age of the sediment was estimated from the local rate of sea level rise given by Hartl et al. (2006).

The average concentration of Fe-sulfide estimated from the model for the 66-cm thick black sediments at EGN22.5 is 0.13 wt%, similar to the measured average of Fe-sulfides of 0.16 wt%. Although the total amount of Fe-sulfides that occurs in the sediment is similar to the model estimate, the measured and modeled distributions differ (Figure 3-2b). The model estimates show Fe-sulfide concentrations increase continuously with depth to around 60 cmbsf, but measured Fe-sulfide concentrations pass through a maximum around 25 cmbsf. Possible causes of this difference are discussed below.

Model results are presented in Figure 3-5, which shows estimates of dissolved Fe at each site, and in Table 3-1, which gives estimates of average reaction rates for Fe-sulfide precipitation, Fe-oxide reduction, and OC remineralization by Fe-oxide reduction at each site. The first order pseudo reaction rate constant of Fe-oxide dissolution, K_1, varies within the same order of magnitude, ranging from a value of $3.78*10^{-12}$ 1/sec at EGN0 to $8.90*10^{-12}$ 1/sec at EGN22.5 (Figure 3-4a). The rate decreases slightly from EGN0 to EGN10 and then increases monotonically to EGN22.5. In general, K_2 from the upper two zones decreases offshore; particularly in the black sediments, where K_{2a} decreases from a value of $21.9*10^{-8}$ 1/sec at EGN0 to $0.64*10^{-8}$ 1/sec at EGN22.5. The value of K_{2b} is lower than K_{2a}, decreasing from $5.74*10^{-8}$ 1/sec at EGN0 to $0.76*10^{-8}$ 1/sec at EGN22.5. The total amount of Fe-oxide dissolution does not show any offshore trend and has little variation across the seepage face, ranging from 0.054 mg/cm^2/year at EGN0 to 0.242 mg/cm^2/year at EGN22.5 at (Figure 3-6b). Estimates of total OC remineralization associated with total Fe-oxide dissolution are also similar across the seepage face, ranging from 0.0135 mg/cm^2/year at EGN0 to 0.061 mg/cm^2/year at EGN22.5 (Figure 3-6b). Despite the offshore decrease in K_{2a} and K_{2b}, the total amount of Fe-sulfide that precipitates within the upper two zones varies little across the seepage face, ranging from 0.05 mg/cm^2/year at EGN0 to 0.33 mg/cm^2/year at EGN20, but increases 10 times to about 2.46 mg/cm^2/year at the seaward edge of the seepage face because of the elevated dissolved Fe concentrations there (Table 3-1).

Discussion

Hydrological Controls on Fe-Diagenesis

Fe-oxide reduction

The first reactive-transport model developed to estimate influence of terrestrial SGD on Fe diagenesis was a finite element model to estimate Fe-oxide precipitations (Spiteri et al., 2008)

but did not consider the influence of Fe diagenesis on OC remineralization. This previous model used a single value of first order rate constant of Fe-oxide dissolution of 8.8×10^{-5} 1/sec throughout the subterranean estuary, regardless of the variation in flow rates of terrestrial SGD. The assumption of a single value of first order rate constant is a common practice, but for early diagenetic models the pseudo first order rate constant can vary from one site to another depending on reactivity of OC (Berner, 1980; Burdige, 1991), particularly in a dynamic system where flow rates of terrestrial SGD and associated porewater chemistry are known to change from onshore to freshwater-saltwater boundary (Martin et al., 2007). Additionally, Spiteri et al. (2008) assumed no flux impermeable boundaries at the bottom and the top of the modeled domain, because the model domain covered the entire thickness of the coastal aquifer in which the subterranean estuary occurs. However, in the Indian River Lagoon location the entire thickness of the subterranean estuary was not sampled leaving dirichlet boundary conditions as the only choice. Results from the Spiteri et al.'s (2008) model showed pH change in the subterranean estuary of Waquoit Bay controls dissolved Fe oxidation, rather than oxidizing condition at the freshwater-saltwater boundary.

In this modeling approach, dissolved Fe is transported by diffusion and vertical flow of terrestrial SGD. The flow rate is constant with depth at a particular site, but decreases offshore by an order of magnitude from EGN0 to EGN22.5 (Martin et al., 2007). These slower flows of terrestrial SGD transport dissolved Fe from the Fe-oxide reduction zone to the Fe-sulfide precipitation zone at slower rates with distance offshore and thus the influence the chemical composition of the porewater. Also, flows of terrestrial SGD oppose non-local exchange and limit the penetration depth of non-local exchange to upper 40 cm depths and thus oxidation of Fe-sulfides in shallow sediments (e.g. Smith et al. 2008a, 2008b; Chapter 2). Although oxic

water brought by non-local exchange could be important for preventing Fe-oxide dissolution, non-local exchange has been ignored here because it can not penetrate to depths where Fe-oxides are reduced. Variations in flow rates of terrestrial SGD thus influence kinetics of the Fe-sulfide precipitation, Fe-oxide reduction, and thus the associated rate of OC remineralization.

Another important factor in the rate of the reduction of Fe-oxides is their concentrations in the sediment. Because these concentrations are similar across the seepage face, there is a limited variation in the rate of Fe-oxide reduction with distance offshore (Figure 3-6b). In other coastal marine settings, the distributions of dissolved Fe concentrations relate systematically to the amount of OC in the sediment. For example, in sediments of the Skagerrak (between Norway and Denmark), the distribution of dissolved Fe was controlled by the rate of Fe-oxide reduction resulting from variations of OC concentrations (Canfield et al., 1993a, 1993b; Wang and Van Cappellen, 1996). In Georgia Bight marsh sediments, elevated Fe concentrations occurred at the freshwater-saltwater boundary due to higher availability of OC there than onshore (Snyder et al., 2004). In contrast, in the Indian River Lagoon subterranean estuary the quantity of OC associated with Fe-oxides reduction zones (orange sedimnents) is orders of magnitude less than Skagerrak and Georgia Bight sediments. Also, OC concentration in orange sediments is constant offshore around 0.04 wt%, regardless of offshore variations in dissolved Fe concentrations (Figure 2-3b). The variation in dissolved Fe concentration across the seepage face results from variations in flow rates of terrestrial SGD, which either flushes dissolved Fe from the near shore orange sediments because of faster flow rates, or allows dissolved Fe to accumulate in the orange sediments at the freshwater-saltwater boundary because of slower flow rates there.

Fe-sulfide precipitation and oxidation

In contrast to Fe-oxide reduction rates that vary little across the seepage face, the rate of Fe-sulfide precipitation increases offshore as a result of the increase in dissolved Fe

concentrations (Table 3-1). Regardless of the offshore increase in Fe-sulfide precipitation rate, the rate constant for Fe-sulfide precipitation decreases by an order of magnitude from near shore to the seepage face boundary (Figure 3-4a). Also, the rate constant of Fe adsorption decreases offshore. This decrease in the rate constant corresponds to an increase in the amount of non-local exchange across the sediment-water interface as the strength of terrestrial SGD decreases offshore (e.g., Smith et al., 2008b), suggesting non-local exchange is an important control of Fe-sulfide precipitation.

Field measurements of dissolved oxygen (DO) concentrations show the water column has about nine times higher average DO concentrations (about 9 mg/L) than porewaters. Non-local exchange thus supplies oxygen from water column to the porewaters in the subsurface. Smith et al. (2008b) showed penetration depth of non-local exchange ranges from 15 cmbsf nearshore to 47 cmbsf at the seepage face boundary, with an associated exchange rate of 95.7 cm/day nearshore to 6.9 cm/day offshore (Smith et al., 2008b). Based on this information, approximately 0.123 mg/day oxygen flows to sediment nearshore, which is four times less than the value at the seaward end of the seepage face, about 0.423 mg/day. The larger amount of oxygen entering the sediment offshore may limit the amount of Fe-sulfide that could precipitate and can oxidize the Fe-sulfides that are precipitated there. These effects of non-local exchange leaching Fe-sulfide have been observed in sediment approximately 250 m seaward of the seepage face, where black sediments at the sediment-water interface have been leached to grayish-white sediments by oxidizing Fe-sulfides (Chapter 2).

A leached sediment cap is absent at the sediment-water interface at the seaward edge of the seepage face even though rate constants of Fe-sulfide precipitation are an order of magnitude lower at the seepage face boundary than nearshore. The lack of leached sediment within the

seepage face reflects restrictions on non-local exchange from vertical flow within the seepage face, thereby limiting leaching of Fe-sulfides (e.g., Martin et al., 2007). In addition, the vertical flow of terrestrial SGD within the seepage face continuously supplies dissolved Fe to the zone of Fe-sulfide precipitation, and allows precipitation of Fe-sulfides. In contrast outside the seepage face, supply of dissolved Fe from Fe-oxide reduction zone to Fe-sulfide precipitation zone would be limited because of the slower diffusive transport process there.

Fe Diagenesis and its Relation to the Source and Availability of OC

Although the elevated Fe concentration at the seepage face boundary is not controlled by OC distribution, the overall low amount Fe-oxide reduction in the seepage face compared to other coastal sediments may be caused by the limited availability of OC and/or its terrestrial origin. The general value of Fe-oxide reduction by OC is 7.84 mg/cm^2/year for coastal sediments experiencing normal burial diagenesis and unaffected by SGD (Van Cappellen and Wang, 1995). The general modeled value of OC concentrations for coastal sediments is more than 1 wt% (Van Cappellen and Wang, 1995), which is orders of magnitude higher than the measured OC in the Fe-oxide-rich sediments of Indian River Lagoon, of around 0.04 wt%. In the Indian River Lagoon seepage face the average rate of Fe-oxide reduction is about 0.213 mg/cm^2/year (Table 3-1), more than an order of magnitude lower than the coastal sediments. This low rate in Indian River Lagoon sediments may reflect the low OC concentrations of the sediment. Alternatively, lower OC remineralization rates could be due to the terrestrial source of the OC. Planktonic marine OC tends to be more labile than terrestrial OC, which contains refractory residue of continental cellulose (Suess, 1980) and thus Fe-reducing microbes remineralize marine OC more easily than terrestrial OC. Consequently, lower rate of Fe-oxide reduction could be due to the terrestrial origin of the orange sediments (Hartl, 2006), where Fe-oxide reduction occurs. Iron-

oxide reduction is missing in the zone of marine black sediments, where OC is of marine origin, like regular coastal sediments.

Deposition of terrestrial OC has been found to be limited in estuaries around the world. In Gironde surface estuary, south western France, 80% of terrestrial particulate OC (POC) was oxidized in the surface estuary (Fontugne and Jouannneau, 1987). Riverine OC had widely ranging $\delta^{13}C$ values (varying between -26 and -30 $^{0}/_{00}$) in nine estuaries of the European Atlantic coast, but within the estuaries were modified to a uniform value (-26 $^{0}/_{00}$), which is closer to the local marine end member, -20 $^{0}/_{00}$, suggesting that terrestrial OC gets removed in estuaries and marine OC gradually gets accumulated (Middelburg and Herman, 2007). Local redox conditions control OC oxidation by Fe-oxides and thus can be site specific. For example, in Waquoit Bay the subterranean estuary is intermittently exposed to the atmosphere during low tide, driving Fe-oxide precipitation rather than dissolution (Charette et al., 2005) unlike Indian River Lagoon, which is continuously submerged and thus remains anoxic (Chapter 2).

The total amount of terrestrial OC remineralized by Fe-oxides during transgression across the seepage face can be estimated from the modeled OC remineralization rate. The OC remineralization rate varies little with offshore distance (Figure 3-4b), remaining around about 5.34×10^{-2} mg/cm^2/year (Table 3-1). Transgression across the 25 m wide modern seepage face took around 280 years (Chapter 2). Assuming an average thickness for the Fe-oxide reduction zone of at least 50 cm and sediment density of 2.67 gm/cm^3, the total mass of sediment within a 1 m strip of the seepage face is 33.38 kg. The total amount of OC remineralized in this zone thus can be obtained by multiplying the average OC oxidation rate by the time for transgression and the unit area of the seepage face (25 m^2). This calculation indicates that approximately 3.74 kg of OC, or about 1.12 wt %, was oxidized during the transgression of the seepage face. The current

concentration of OC in the orange sediments averages around 0.04 wt %. Assuming about 1.12 wt% of the OC was oxidized, the original concentration would have been around 1.16 wt % and about 96.5 % of this original concentration would have been oxidized as the seepage face was transgressed. However, OC concentrations in orange sediments are constant at 0.04 wt%, thus EGN0 and EGN22.5 have the same amount of OC. This distribution of OC suggests either OC oxidation was not constant at 5.34×10^{-2} mg/cm^2/year and varied in the seepage face over the past 280 years, or the terrestrial OC supply from the anoxic coastal aquifer has decreased over time. Alternatively, the OC measured in the orange sediments is the left over OC after Fe-oxide reduction, both at EGN0 and EGN22.5. If this is true, then the reaction front of Fe-oxide reduction would have moved progressively downward with distance offshore, leaching upper part of orange sediments to white, so that Fe-oxides can utilize OC from deeper sediments.

In contrast to removal of terrestrial OC, the the thickness of black sediments, and thus the amount of marine OC, increases offshore from 15 cm at EGN0 to 60 cm at EGN22.5. These black sediments have an average of 0.34 wt % of OC. Therefore, the amount of marine OC buried in the 25-m-long sediment-wedge is about 35 kg, which is 10 times more than the amount of terrestrial OC that was removed by reduction of Fe-oxides. In the Indian River Lagoon subterranean estuary, there appears to be a net removal of DOC formed from terrestrial OC through reduction of Fe-oxides, and a net accumulation of marine OC (solid) overlying the terrestrial sediments following transgression.

Accumulation of Fe-Sulfide with Sealevel Rise

Although both the modeled and measured Fe-sulfide concentrations are similar (0.13 wt % and 0.16 wt %, respectively), the modeled Fe-sulfide concentrations increase with depth, while the measured Fe-sulfide concentrations show a near surface maximum. This difference reflects the assumption in the model that once Fe-sulfides form, they continue to be accumulated over

time. As a consequence of this assumption, the bottom-most black sediments have the longest amount of time to accumulate Fe-sulfide. Why there is a difference between observed and modeled Fe-sulfide depth distributions is unknown to us, however several speculations can explain this difference. One of them is Fe-sulfide precipitated only at the dissolved sulfide maximum, and our assumption of Fe-sulfide deposition over the entire thickness of black sediments is wrong. Alternatively, if the modeled distribution of Fe-sulfides at EGN22.5 is correct, then observed higher abundances near the sediment–water interface indicate that Fe-sulfides were remobilized at the base of black sediments. The process that can remobilize Fe-sulfides at 66cmbsf is unknown to us, but can not be non-local exchange, because non-local exchange cannot penetrate that deep into the sediments of the seepage face. .

Conclusions

The rate of Fe-oxide dissolution remains approximately constant across the 25-m wide seepage face of the subterranean estuary in Indian River Lagoon, Florida, but dissolved Fe concentrations increase by three orders of magnitude from near shore to seaward edge of the seepage face. Flow velocity of terrestrial SGD decreases by 10 times from near shore to the seaward edge of the seepage face. The correspondence of the differences in these two rates indicates that dissolved Fe either accumulates within the Fe-oxide dissolution zone at the seepage face boundary because of slower flow rates there than onshore, and/or flushes out from the Fe-oxide dissolution zone nearshore because of faster flow rates there. Either way this relation between flow rates and dissolve Fe distributions shows Fe distribution is controlled by hydrology. Previous studies suggested higher dissolved Fe concentrations at the salinity boundary are due to higher Fe-oxide reduction rates, resulting from either higher OC availability and/or due to longer contact time between OC and Fe-oxides at the boundary than onshore. Our study for the first time shows, the transport mechanism of SGD is equally important and can

cause elevated Fe concentrations at the boundary without varying the Fe-oxide reduction rate. The first order rate constant of Fe-sulfide precipitation in black sediments decreases sharply from onshore to the seaward edge of the seepage face reflecting gaining strength of non-local exchange. This distribution of Fe diagenesis shows hydrology controls Fe diagenesis in the seepage face.

Iron-oxide diagenesis drives OC remineralization in the terrestrial orange sediments of Indian River Lagoon, which were deposited prior to the transgression of the seepage face. This study shows that terrestrial DOC has been removed from the orange sediments during sea level rise. These terrestrial sediments are overlain by black marine OC rich sediments that were deposited in the seepage face following transgression. These black sediments have 10 times more marine OC than the amount of terrestrial OC removed during transgression. These black sediments have few terminal electron acceptors, including Fe oxides, available to remineralize the marine OC present there. Although some of the OC in marine black sediments are lost during sulfate reduction, little sulfate reduction occurs as shown by the linearity between sulfate and salinity and thus a major fraction of the marine OC remain sequestered in black sediments. Thus, in the subterranean estuary of Indian River Lagoon, terrestrial OC is remineralized while marine OC accumulates in sediment.

Table 3-1. Model results

Offshore distance (m)	0	10	15	17.5	20	22.5
K_1 (1/sec)	3.78×10^{-12}	1.81×10^{-12}	†	4.99×10^{-12}	†	8.90×10^{-12}
K_{2a} (1/sec)	21.9×10^{-8}	2.80×10^{-8}	3.63×10^{-8}	3.91×10^{-8}	0.27×10^{-8}	0.64×10^{-8}
K_{2b} (1/sec)	5.74×10^{-8}	5.36×10^{-8}	0.29×10^{-8}	1.39×10^{-8}	0.48×10^{-8}	0.76×10^{-8}
Fe-sulfide precipitation ($mg/cm^2/year$)	0.00076	0.0327	0.094	0.0757	0.0163	0.207
Fe-adsorption ($mg/cm^2/year$)	0.1796	0.0195	0.128	0.2230	0.3140	2.249
Total Fe removal ($mg/cm^2/year$)	0.050	0.052	0.222	0.299	0.330	2.456
Fe-sulfide dissolution ($mg/cm^2/year$)	0.054	0.483	†	0.073	†	0.242
Fe-oxide dissolution ($mg/cm^2/year$)	0.0135	0.121	†	0.018	†	0.061

Since we have truncated Fe-oxide compartments at most of the stations, along with total Fe-oxide dissolution we reported the average Fe-oxide dissolution and associated average OC remineralization.
† dissolved Fe production zones were not sampled and thus not included in the modeled domain.
**At station 10 m offshore the intermediate compartment is missing.

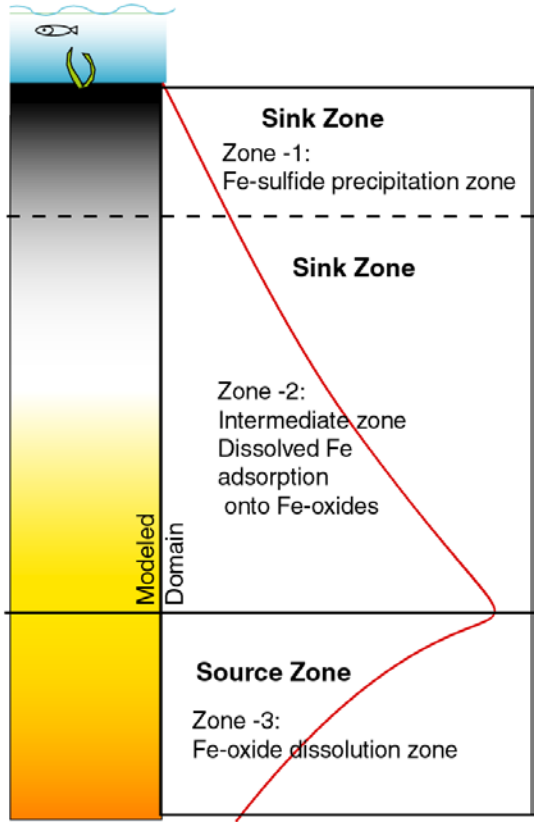

Figure 3-1. Conceptual model domains. The red line represents a generalized dissolved Fe profile, and the left panel represents the corresponding sediment color. Two zones act as sinks for dissolved Fe and have been conceptualized based on the differences in lithostratigraphic units. The upper sink zone occurs in the black sediments, and the lower sink zone occurs at the transition from black to orange sediments.

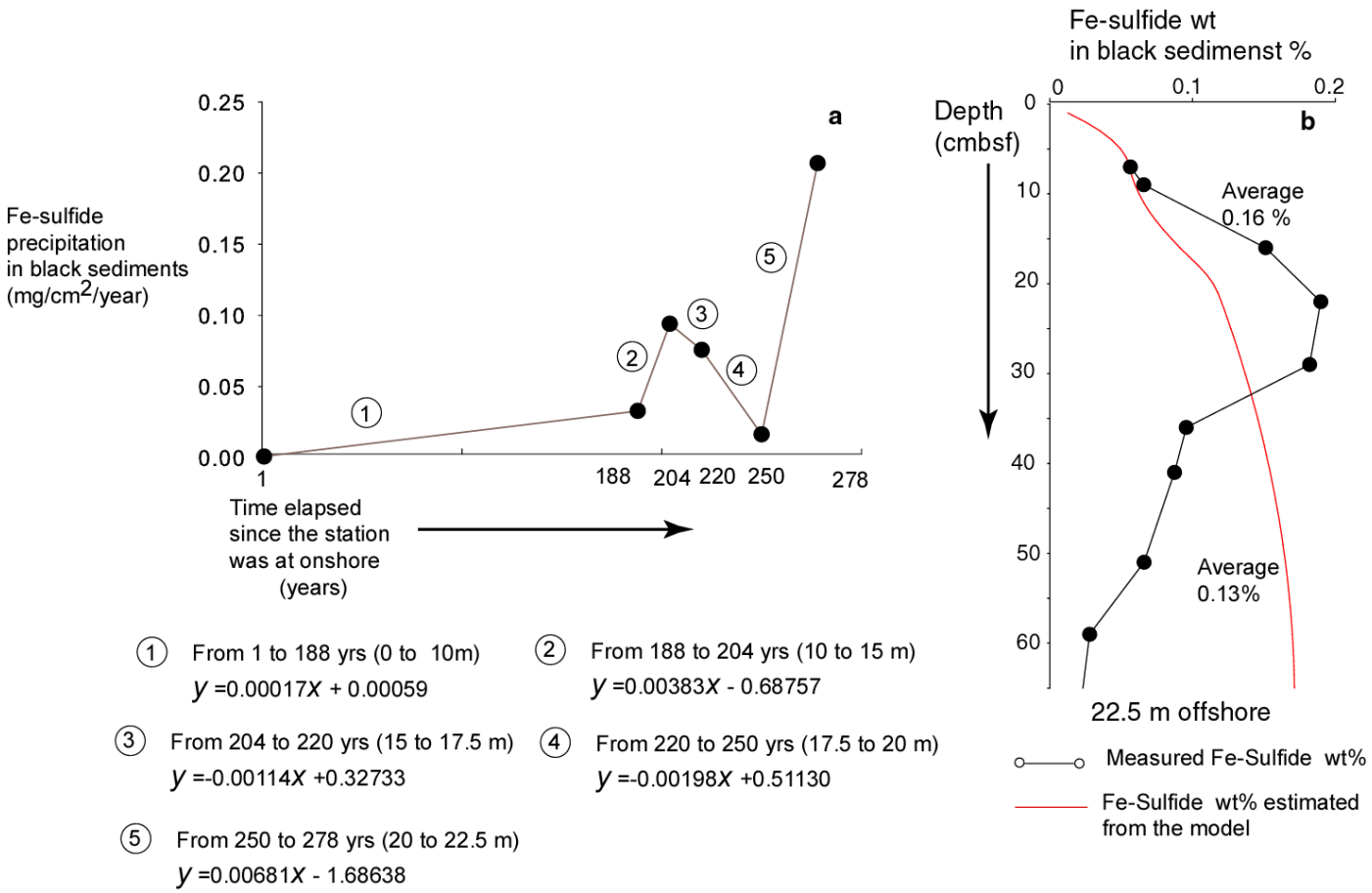

Figure 3-2. Variation in Fe-sulfide precipitation rate (mg/year) with sea level rise. a) the Fe-sulfide precipitation curve is divided into six linear segments across the seepage face for calculating total Fe-sulfide precipitated at the seepage face boundary, and b) comparison between measured and modeled Fe-sulfide wt % at the seepage face boundary.

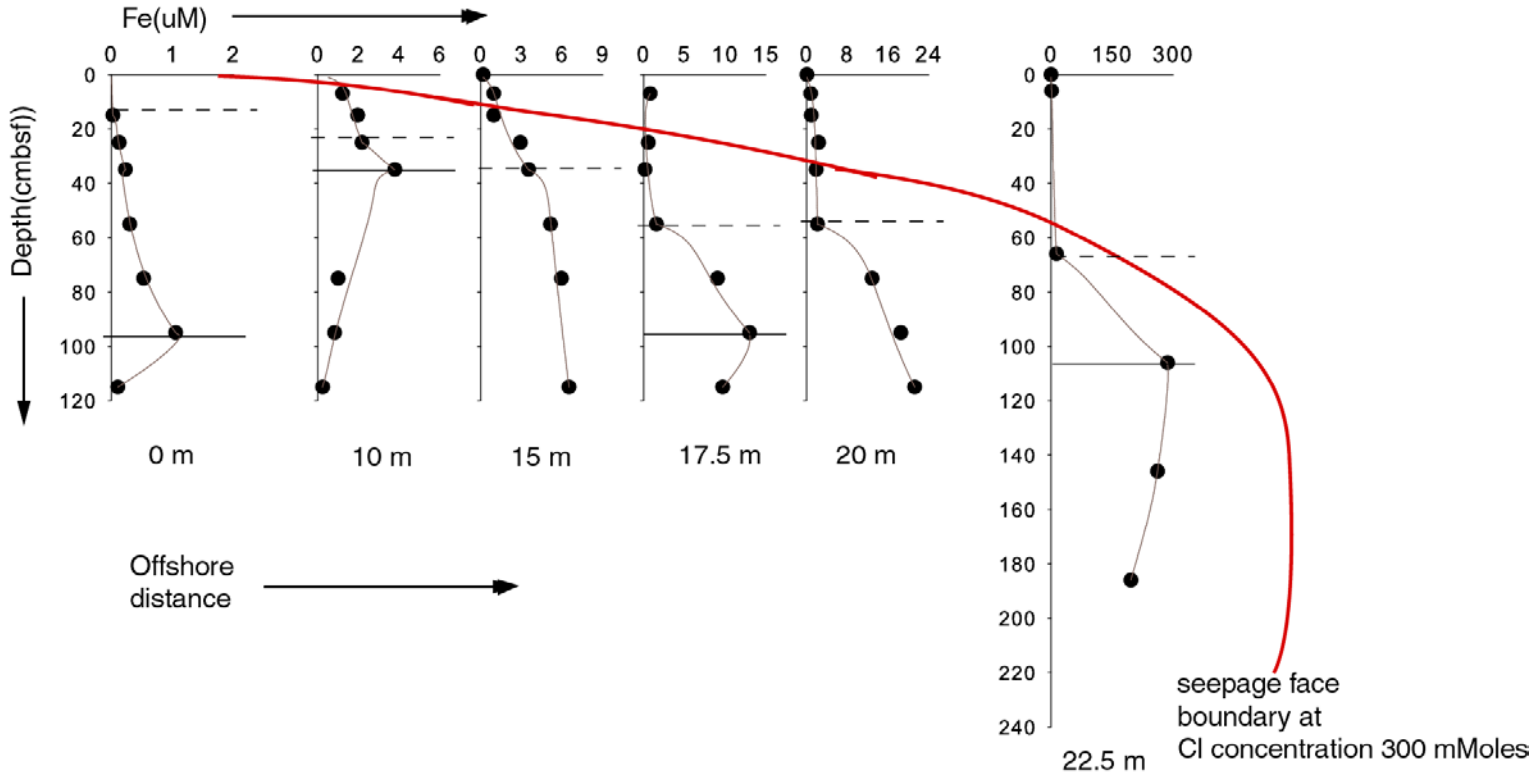

Figure 3-3. Dissolved Fe model. Solid dark circles represent measured dissolved Fe concentrations at discrete depths, and dark grey curved lines represent dissolved Fe models. The straight dashed lines represent the boundary between upper and intermediate zones used in the model, and the straight solid lines represent the boundary between intermediate and bottom zones. The red line represents the upper part of the freshwater-saltwater boundary of the subterranean estuary, the seepage face boundary.

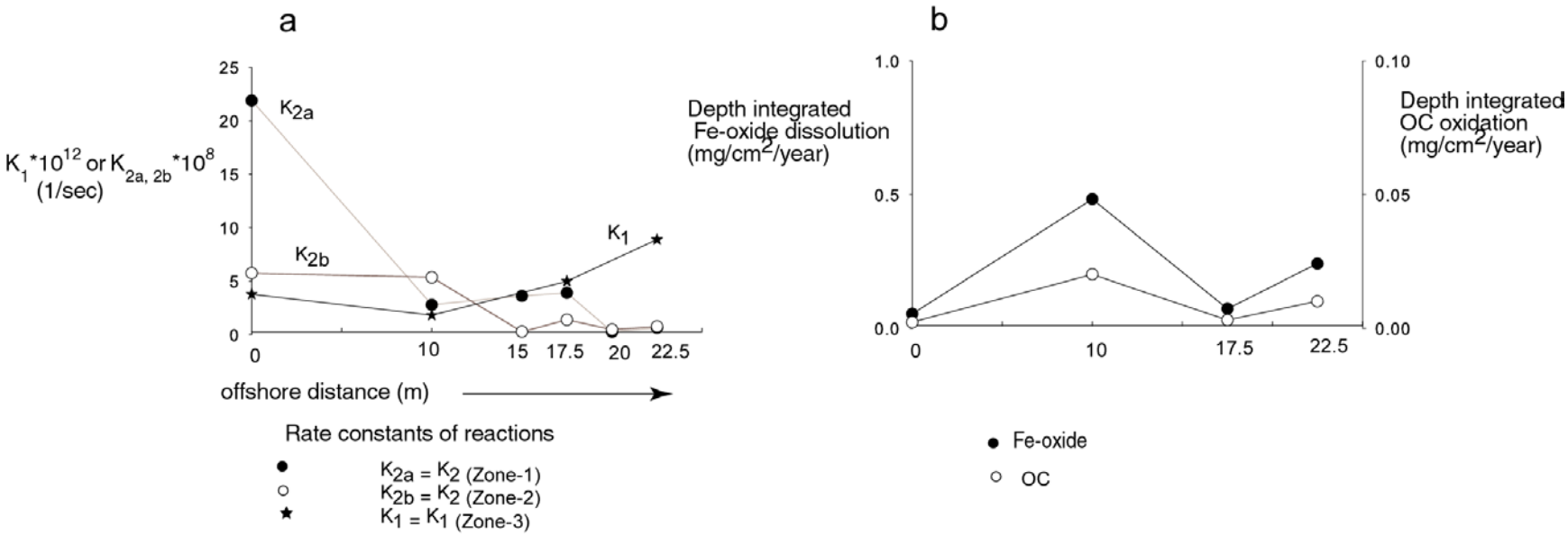

Figure 3-4. Variation in rate constants, Fe-oxide dissolution rate, and OC remineralization rate across the seepage face. a) variation in first order kinetic rates of Fe-sulfide precipitation from upper and intermediates zones, and Fe-oxide dissolution from bottom zone, b) variation in Fe-oxide dissolution rates (mg/year), and total OC remineralization rates (mg/year) from zone 3 at each site with distance offshore.

CHAPTER 4
INFLUENCE OF AQUIFER RECHARGE ON IRON AND ORGANIC CARBON DIAGENESIS IN THE SEEPAGE FACE OF A SUBTERRANEAN ESTUARY

Introduction

The position of the freshwater-saltwater boundary can change temporally at time scales ranging from days (e.g., in areas with high tidal range and following storms) to months (e.g., seasonally), to a few hundred years (e.g., sea level rise) (Taniguchi et al., 2003; Michael et al., 2005; Smith et al., 2008b). Movement of the freshwater-saltwater boundary should affect geochemical conditions associated with the boundary, and thus should alter dissolved Fe distributions and other reaction products resulting from Fe diagenesis. This shift of the boundary results from several causes including storm surges and the amount of terrestrial SGD, which is controlled by the aquifer recharge (Michael et al., 2005; Smith et al., 2008a). In this chapter, I present results showing how annual recharge to the coastal aquifer affects fluxes of dissolved Fe and OC remineralization in the seepage face. Times series of the fluxes are estimated with the numerical reactive-transport model of dissolved Fe developed in Chapter 3 at eight different sampling periods over a period of three years.

Methodology

Recharge Estimation

The monthly recharge to the Surficial Aquifer is calculated from the difference between the monthly average precipitation and the monthly average of evapotranspiration, the ‘effective precipitation’. The monthly precipitation and temperature data is obtained from the Melbourne station, which is within few kilometers from the study area, (source of the evaporation, precipitation, and temperature data: St. John watershed Management District, Florida; Southwest Regional Climate Center, and

NOAA National Weather Service Forecast Office, Florida). The monthly potential evapotranspiration (PET) is calculated from Thornthwaite's method,

$$E = 1.6(\frac{10T}{I})^{a} \tag{4-1}$$

Where E is the monthly PET to be calculated (e.g., Thornthwaite, 1944), T is the average monthly temperature, I is the annual (12 months) sum of monthly heat index values $(\sum_{1}^{12} i)$. The equation to calculate 'i' is given by

$$i = (\frac{T}{5})^{1.514} \tag{4-2}$$

The equation to calculate 'a' is given by

$$a = (6.75x10^{-7} xI^{3}) - (7.71x10^{-5} xI^{2}) + (1.79x10^{-2} xI) + 0.49 \tag{4-3}$$

Model Conceptualization

Details of modeling techniques are discussed in Chapter 3. Using two sink zones and one source zone, it was possible to explain the observed Fe profiles in April 2007 when Fe maxima were limited only to bottom zone of orange Fe-oxides (Figure 4-1a). However, two other types of Fe depth-profiles are observed in other time periods (Figure 4-1). One has a shallow Fe maxima (Figure 4-1b), and other has two different rates of Fe-oxide dissolution (Figure 4-1c). For example, shallow Fe maxima were observed at EGN20 in November 2004, and February 2005 (Appendix –I). These shallow Fe maxima occur in black sediments, and dissolved Fe concentrations increase again in orange sediments. Consequently, dissolution of Fe-oxides according to equation (3-1) cannot explain the occurrence of shallow maxima, and the only possible source of dissolved Fe in the black sediments is Fe-sulfide dissolution (e.g., Dos Santos and Stumm, 1992), as shown by:

$$FeS + H_2O \xrightarrow{R3} FeOH_2 + S^{2-} \tag{4-4}$$

Equation (4-4) shows that Fe-sulfide dissolves at the rate of R_3. Dissolution of Fe-sulfides near the sediment-water interface could result from oxidation of Fe-sulfide by O_2 circulated from the overlying water column by non-local exchange.

The reaction rates R_1, R_2, and R_3 depend on the first order kinetic rate constants (1/sec) of reactions 3-1, 3-2 and 4-4, represented by K_1, K_2, K_3 respectively, where K_2 represents K_{2a} in the Fe-sulfide precipitation zone and K2b in the dissolved Fe adsorption zone. For profiles where the Fe-oxide dissolution rate is different in the upper and lower part of the source zone (zone-3), the Fe-oxide reduction zone is divided into two subzones (Figure 4-1c). Consequently, different values of "average rate constants" are assumed for the upper and lower Fe-oxide reduction zones, K_{1a} and K_{1b}, respectively. These kinetic rates are multiplied by the concentrations of the corresponding reactant to obtain the dissolution rate of Fe-oxides, along with precipitation and dissolution rates of Fe-sulfides.

$$R_1 = K_1 * [\text{Fe-oxide}] \quad (4\text{-}5)$$

$$R_2 = K_2 * [\text{Fe}] \quad (4\text{-}6)$$

$$R_3 = K_3 * [FeS_2] \quad (4\text{-}7)$$

It is assumed in Chapter 2 that reactions, shown by equations (3-1) and (3-2), are kinetically driven and I follow the same assumption here. Simultaneous presence of dissolution and precipitation of Fe-sulfides questions whether the equation (4-4) is kinetically driven or is equilibrium controlled. In a dynamic system, where groundwater continuously flows upward, equilibrium between dissolved Fe and Fe-sulfides can not occur. Furthermore, I separated the zone for Fe-sulfide dissolution from Fe-sulfide precipitation zone in the model (Figure 4-1b), and thus equation (3-5) and equation (4-4) occur at different depths and both can still be kinetically driven.

Results

Aquifer Recharge

The amount of effective precipitation to the coastal aquifer dropped from about 40 cm/year to about -10 cm/year from 2004-2005 to 2006-2007 (Figure 4-2). Average monthly effective precipitation (precipitation – PET) at the study area dropped from about 13 cm/month to about 9 cm/month from 2004-2005 to 2006-2007. However, the average monthly potential evapotranspiration (PET) remained the same, about 10 cm/month, from 2004 to 2007.

Salinity and Dissolved Fe Distributions

Distribution of extrapolated Cl concentrations shows 300 mM Cl contour (seepage face boundary) progressively moved landward, by approximately 5 m, from November 2004 to September 2007 (Figure 4-3). From November 2004 to September 2005, the 300 mM Cl contour was located about 25 m offshore. In May 2006, the boundary moved landward by 1 to 2 m from its original position to the EGN22.5. In October 2006, the 300 mM Cl contour occurred between EGN20 and EGN22.5. In April 2007 and September 2007, the 300 mM Cl isohaline contour occurred between EGN15 and EGN20. Along with the landward movement of the boundary, a saline water plume with chlorinity higher than 350 mM, gradually appeared at the seaward edge of seepage face. This saline water plume was observed only in the April and September 2007 sampling times, when chlorinity was highest at the seaward edge of seepage face, compared to other sampling times.

At all sampling times, an elevated Fe concentration zone, where Fe concentrations are higher than 100 µM, is observed at the seepage face boundary (Figure 4-4). This elevated Fe concentration zone, which was nearly centered at the seepage face boundary,

moved landward from November 2004 to September 2007. This elevated concentration zone was located more than 25 m offshore until October 2006. In April and September 2007, this elevated Fe concentration zone occurred between 20 and 22.5 m offshore. Also, maximum dissolved Fe concentration in the elevated concentration zone increased from about 200 µM to about 400 µM.

Estimated Rate Constants and Rates

Distribution of dissolved Fe concentrations and corresponding models for May 2005 sampling time are shown in Figure 4-5, and for samples from other sampling times are given in Appendix-A. Values of model-estimated first-order rate constants for Fe-oxide dissolution, dissolved Fe adsorption, Fe-sulfide precipitation, and corresponding fluxes of Fe and OC remineralization are given in Appendix-B. Dissolved Fe depth profiles at each site show irregular variations over time, by having Fe maxima at different depths in orange sediments, and occasionally having shallow maxima at the base of black sediments. In general, K_{2a} values range between 10^{-9} to 10^{-7} mg/cm^2/year. An offshore decrease in the rate constant of Fe-sulfide precipitation (K_{2a}) was observed in April 2007 (Chapter 3). A similar trend of was observed in September 2007, but was absent at other sampling times. The rate constants of Fe-sulfide dissolution, K_3, are orders of magnitude lower than rate constants of Fe-sulfide precipitations (K_{2a} and K_{2b}) and generally range between 10^{-12} to 10^{-13} mg/cm^2/year. Similar to the rate constants, rates of Fe-sulfide precipitation and dissolution do not show any temporal variation.

Like rates constants of Fe-sulfide precipitation, rate constants of Fe-oxide dissolution, K_{1a}, do not show any temporal trends and no offshore trend is observed at any sampling time. Three year averages of Fe-oxide dissolution and corresponding OC remineralization are around 0.768 mg/cm^2/year and 0.192 mg/cm^2/year, respectively.

Discussion

Temporal Variations in Aquifer Recharge and Shift of the Seepage Face Boundary

Similar to our study area, work elsewhere has shown that aquifer recharge varies temporally, thereby causing variations in terrestrial SGD, which in turn causes shift of the seepage face boundary at timescales (months to years), (Smith et al., 2008a; Charette, 2007). For example, seasonality is observed in SGD in areas where precipitation dominates aquifer recharge. The conventional Ghyben-Herzberg conceptualization suggests that SGD should be highest during wet seasons of spring and winter, when aquifer recharge is highest, compared to dry seasons of summer (Ghyben, 1901; Herzberg, 1959). However, highest recharge can occur in summer months if precipitation dominates evapotranspiration. For example, in the Ganges Delta, monsoon precipitation dominates over evapotranspiration in summer resulting in the highest recharge in summer. The greatest amount of SGD occurs a few months after the highest recharge, in the winter (Moore, 1997). In subterranean estuaries of Pamet River and Waquoit Bay, and along the South Atlantic Bight, the highest amount of SGD was observed during dry summer months, though recharge was highest during winter and spring months (Michael et al., 2005; Charette, 2007; Moore, 1996). It was suggested these few months lag between the highest recharge and highest SGD resulted from the groundwater residence and travel time in the coastal aquifer (Michael et al., 2005; Smith et al., 2008a). These differences can be smaller between summer and winter values of terrestrial SGD, if there is very little recharge in summer. For example, the Pettaquamscutt estuary of the Rhode Island Sound, receives the highest SGD in summer, but the summer and winter values of terrestrial SGD were within the same order of magnitude, 2.1 and 6.9 L/ m^2/day,

respectively, because of the higher evapotranspiration in summer decreased the SGD (Kelly and Moran, 2002).

In the Indian River Lagoon, the aquifer recharge, as calculated from effective precipitation values to the Surficial Aquifer, in 2004 and in 2005, was 5 times higher than in 2006 and 2007. The seepage face boundary was 25 m offshore in 2004 and 2005, but was 20 m offshore in 2006 and 2007. This correspondence between recharge and changing position of the seepage face boundary suggests shift resulted from variations in aquifer recharge (Smith et al., 2008a; Charette, 2007).

Link between Fe Distributions and the Seepage Face Boundary

Dissolved Fe concentrations are known to be altered by subsurface geochemical and physical conditions, such as OC availability (Snyder et al., 2004), changes in redox conditions (Charette et al., 2005), presence of sulfide (Burdige, 2006), and variations in pH (Spiteri et al, 2008). These previous studies showed most of these geochemical conditions vary from nearshore to the freshwater-saltwater boundary, and influence dissolved Fe concentrations across the seepage face. However, these subsurface geochemical controls of Fe concentrations do not vary offshore in the Indian River Lagoon study area. For example, pH remains near neutral, OC availability (0.04 wt%) and solid Fe-oxide concentrations (about 0.3 wt%) remain unchanged in the Fe-oxide reduction zones, regardless of the distance offshore. Consequently, our dissolved Fe concentration models show Fe-oxide reduction rates, and Fe-sulfide precipitation rates are similar near shore and at the seepage face boundary. Despite the similar reaction rates of Fe across the seepage face, dissolved Fe concentrations increase from onshore to the seepage face boundary suggesting variations in reactions rates cannot cause elevated Fe concentrations at the boundary. Flow rates of terrestrial SGD in the Indian River

Lagoon subterranean estuary decreases by an order of magnitude from 0.5 m^3/day/meter This link between flow rates of SGD and Fe distributions (Chapter 2) suggested that elevated Fe concentrations at the seepage face boundary are primarily hydrology controlled and that slower flow rates of terrestrial SGD at the boundary accumulate dissolved Fe in the source zone at the seepage face boundary.

Shift of the Seepage Face Boundary and Variations in Fe Flux

The link between the seepage face boundary and elevated Fe concentration zone suggests that variations in Fe and OC fluxes can be caused by variations in the position of the seepage face boundary. In the Indian River Lagoon, both the seepage face boundary and corresponding elevated Fe concentration zones had shifted landward by about 5 meters from November 2004 to September 2007 (Figures 4-3 and 4-4). Fluctuation of the seepage face boundary was observed in the Pamet River Estuary, where flux of dissolved inorganic nitrogen (nitrate + ammonium) to the subterranean estuary decreased from 21 moles/m^2/year in July 2001 to 8.1 moles/m^2/year in July 2002 , but increased to 41 moles/m^2/year in March 2003 (Charette, 2007). Similar variations in Fe and associated OC fluxes with the shift of the seepage face boundary are thus expected in the Indian River Lagoon.

Calculations of Fe and OC fluxes from the seepage face are associated with certain assumptions. In the Indian River Lagoon, non-local exchange cannot penetrate to the depth where Fe-oxide reduction occurs. Within the seepage face, terrestrial SGD opposes non-local exchange, and thus terrestrial SGD is assumed to be the primary transport mechanism of dissolved Fe, and the model ignored non-local exchange. The shallow Fe maximum is observed mainly at the site EGN20, and lacks offshore and temporal trends, therefore is assumed to be local. Rate constants of Fe-sulfide dissolution associated with

these shallow maxima in the black sediments are orders of magnitude lower than rates of Fe-sulfide precipitation in adjacent zones, and thus it has been assumed that Fe-sulfide dissolution has little influence over the Fe flux, and that black sediments are overall sinks of dissolved Fe.

Model results show reactions rates of dissolved Fe production are nearly constant, averaging 0.768 mg/cm^2/year, from November 2004 to September 2007 (Appendix B). The observed length of the seepage face decreased from 25 m in November 2004 to about 20 m in September 2007 (Figure 4-3), thus the area under the seepage face decreased from 25 m^2 to 20 m^2 assuming the unit width (1m) of the seepage face. Multiplying the spatially averaged Fe-oxide dissolution rate by the area under the seepage face provides an estimate of the dissolved Fe flux from Fe-oxides. This flux of dissolved Fe decreased from 192 g/year to 154 g/year from November 2004 to September 2007 from the strip of the seepage face. Consequently, the terrestrial OC remineralization, which is one fourth of the Fe-oxide dissolution according to equation (3-1), decreased from 48 g/year to 38 g/year over the three years. In Chapter 3, it was shown that OC (probably DOC) was removed from the Indian River Lagoon seepage face, while solid marine OC is sequestered (Chapter 3). The landward shift of the seepage face enriches the seepage face relatively with marine OC, assuming burial rate of marine OC remain unchanged.

Seasonality is not observed in the dissolved Fe distributions. Based on radon modeling, Smith et al. (2008b) showed a 3-4 months lag is present between recharge and SGD at our study site. However, no relationship exists between dissolved Fe concentrations and recharge values over the previous 3 to 4 months (Figures 4-2, and 4-4). Unlike dissolved Fe, dissolved uranium (U) distribution shows seasonal variations,

and variations due to episodic events (Smith et al, in progress). Uranium concentrations were highest right after Hurricane Wilma in 2006 (Smith et al., 2008a). Unlike Fe, U maxima occur at shallow depths. Charette et al. (2007) suggested terrestrial SGD can have three different types of flowpaths: shallower flowpaths, intermediate flowpaths, and deeper flowpaths. Sources of shallow flows are associated with the tidal pumping near shore, whereas sources of deeper flows are inland portion of the coastal aquifer. Assuming these three distinct types of flowpaths also occur in the subterranean estuary, the discrepancy between Fe and U distribution suggests they are controlled by flow paths at different depths in the Surficial Aquifer. Presence of seasonal variations of dissolved U and its responses to episodic events thus suggest dissolved U is likely related to the shallow portion of the coastal aquifer, which is perturbed by the episodic events and has short groundwater residence time (3 to 4 months). In contrast, lack of seasonality and response to episodic events suggest dissolved Fe distribution is more likely related to the deeper portion of the aquifer, which is undisturbed by the episodic events and seasonal fluctuations, but responds to the annual changes in the aquifer recharge.

Conclusion

This study showed the seepage face boundary shifted landward by 5 m from November 2004 to September 2007. This shift of the seepage face boundary decreased the distance offshore and thus the area of the seepage face. The seepage face boundary shifted landward because of the decrease in aquifer recharge. Potential evapotranspiration did not change over the three years time, but the precipitation was lowered by 1.5 times. Reactions rates of dissolved Fe production and consumption did not change over three years time of sampling, but the flux decreased from 192 g/year to 153 g/year. The flux of terrestrial OC remineralization from Fe-oxide reduction decreased from 48 g/year to 38

g/year (the amount estimated over the strip of the seepage face). Consequently by controlling SGD, aquifer recharge ultimately controls the temporal variations in Fe flux and associated OC flux from a subterranean estuary.

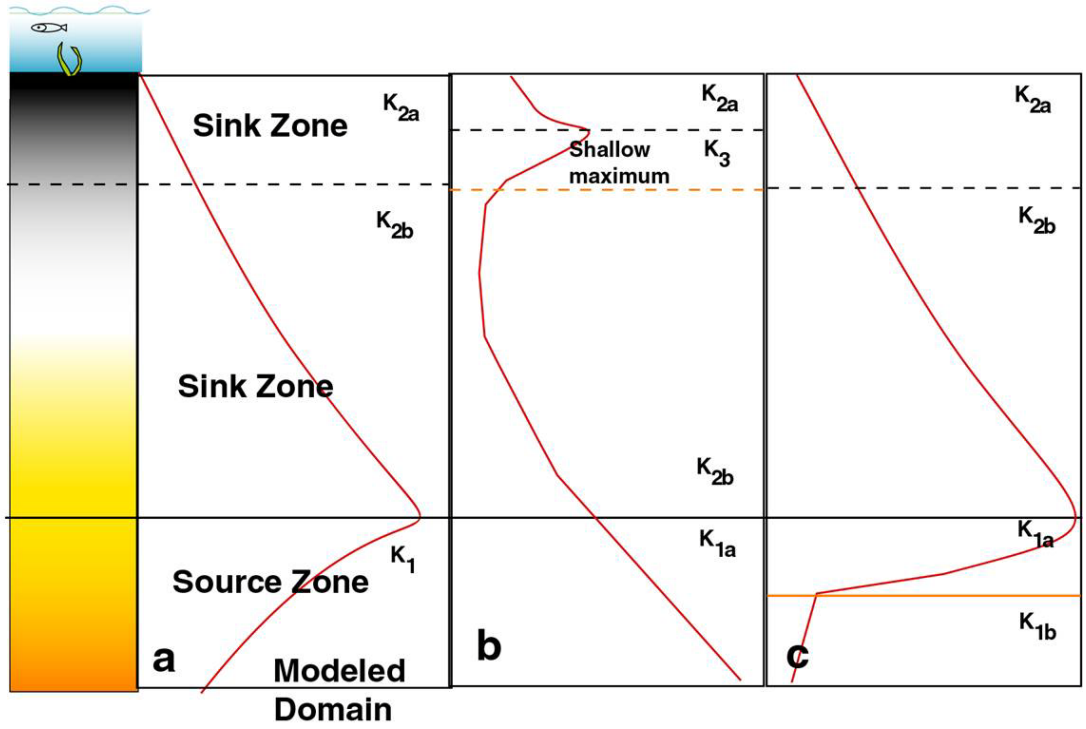

Figure 4-1. Variable dissolved Fe profiles and corresponding conceptual model domains. a) depth-profile type with single Fe maximum, b) depth-profile type with two Fe maxima, and c) depth-profile type with variable rate of Fe production. In a) the black dashed line represents the boundary between upper and lower Fe-sulfide precipitation zone, and the solid black line represents the boundary between Fe-sulfide precipitation zone and Fe-oxide dissolution zones. In b) the zone between black and orange dashed lines represents a local Fe-sulfide dissolution zone. In c) the solid orange line separates the upper and lower Fe-oxide dissolution zones.

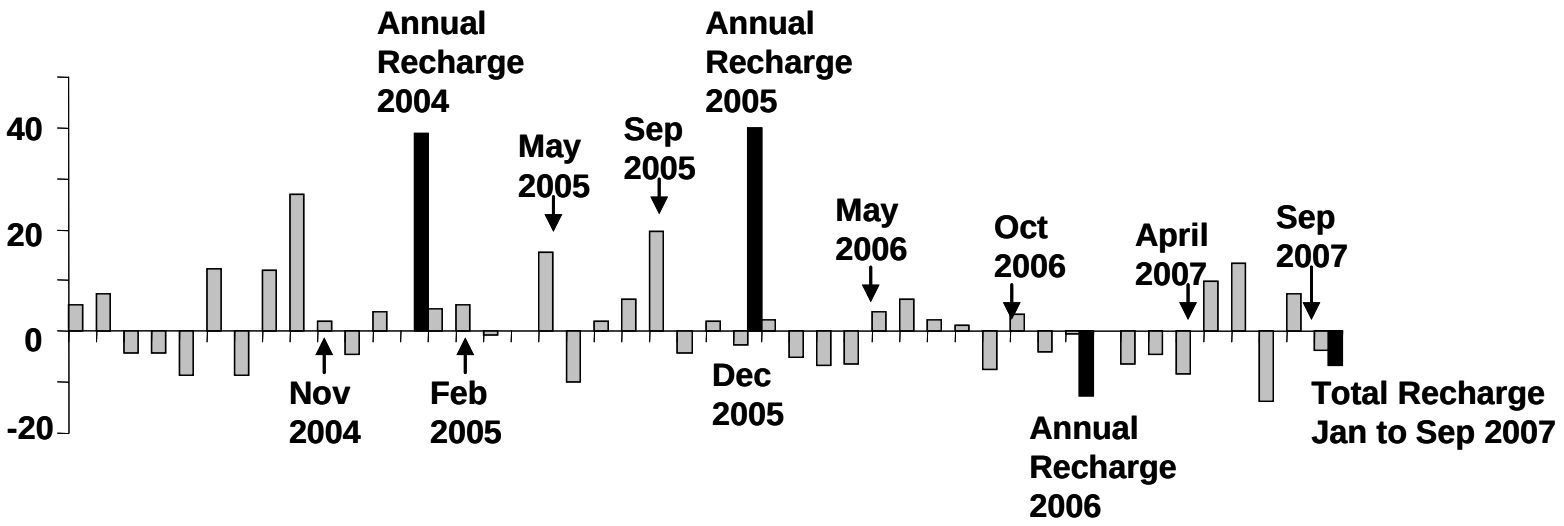

Figure 4-2. Temporal variation in aquifer recharge from November 2004 to September 2007. Light grey bars represent monthly recharge, and dark grey bars represent total annual recharge. Sampling times are indicated by small arrows associated with the dates. (Note: in 2007 total recharge was calculated from the beginning of January to the end of September, the last time of sampling).

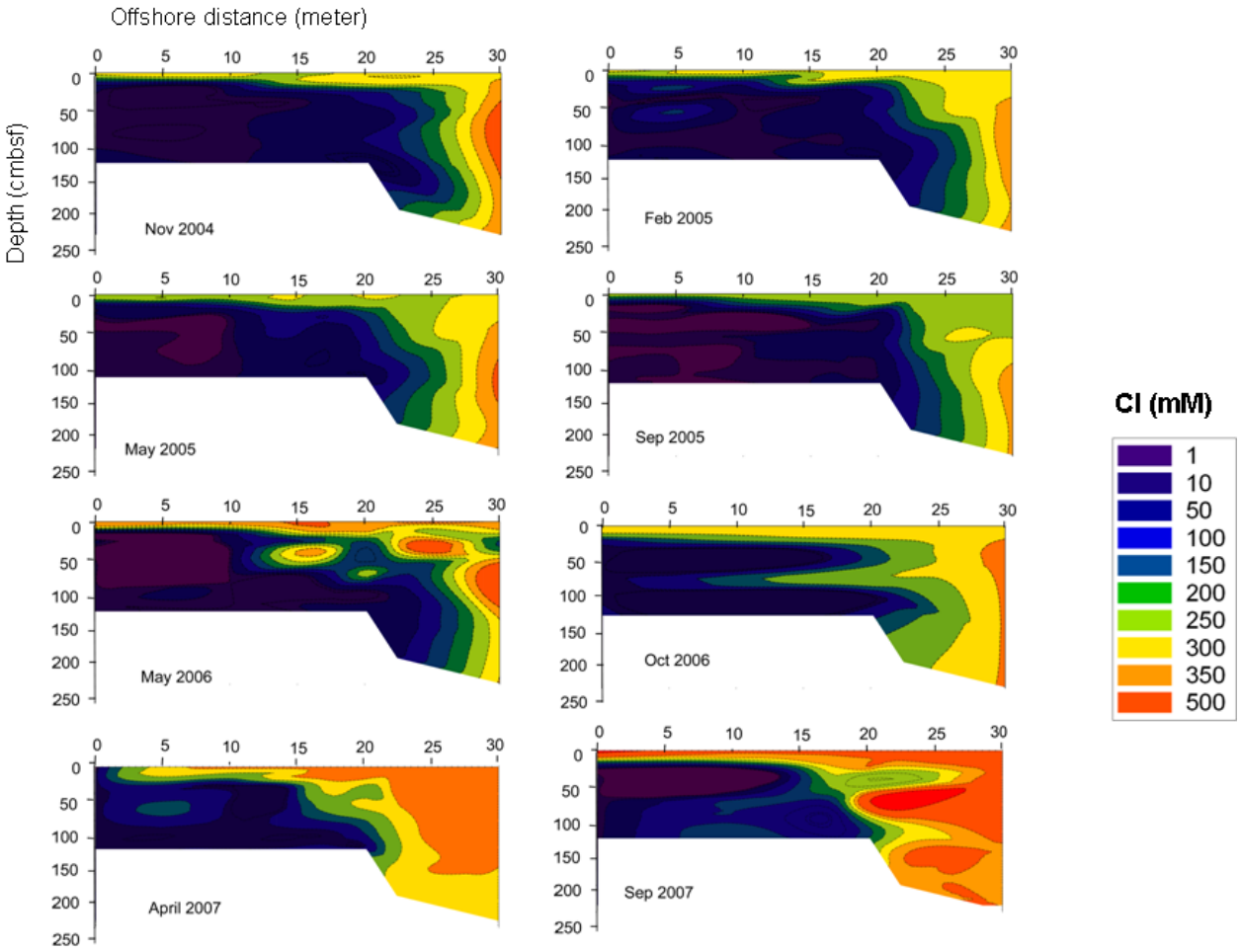

Figure 4-3. Temporal variations in Cl concentrations from November 2004 to September 2007. The yellow and light green boundary represents the 300mM Cl contour, thus the seepage face boundary at the time of sampling.

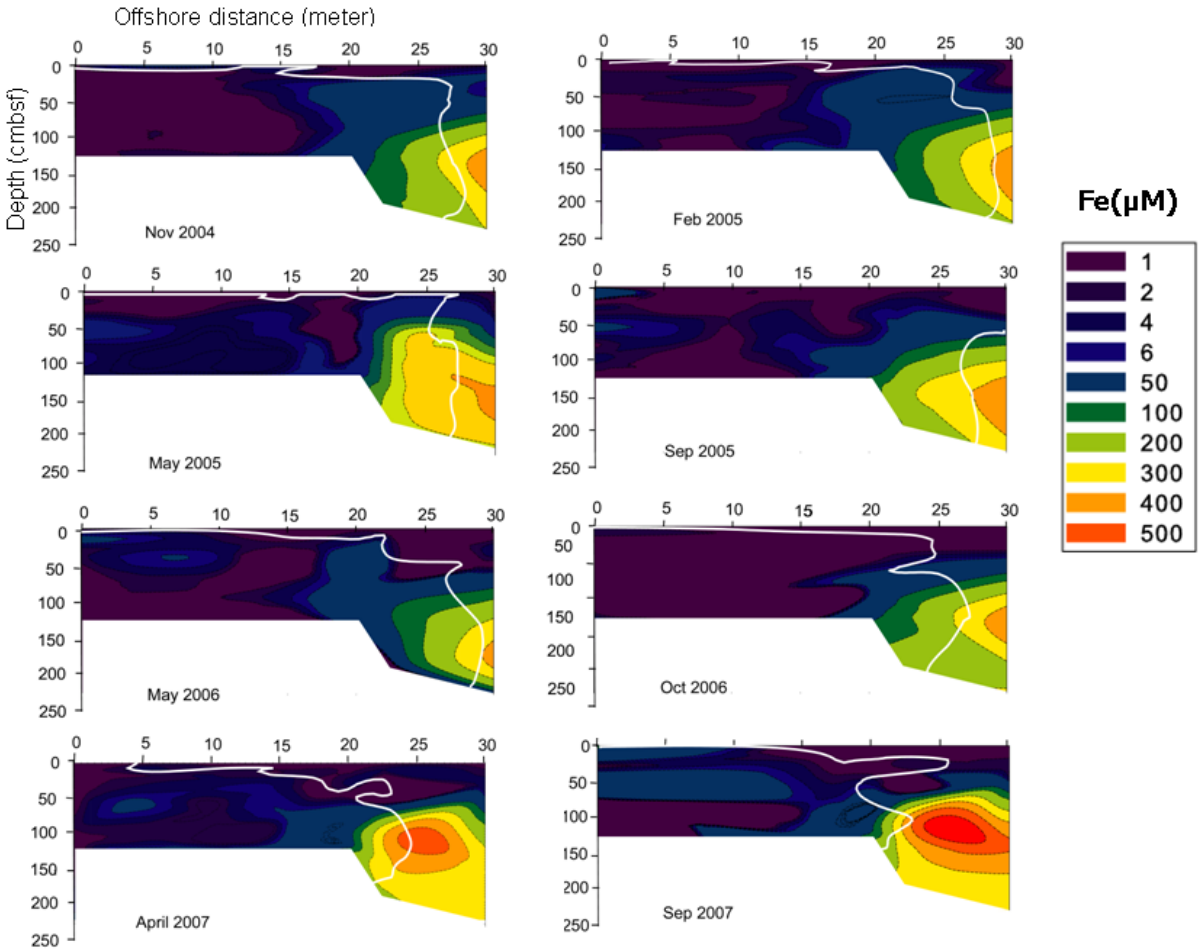

Figure 4-4. Temporal variations in distribution of dissolved iron (Fe) from November 2004 to September 2007. The white line represents the Cl contour at 300 mM at the time of sampling..

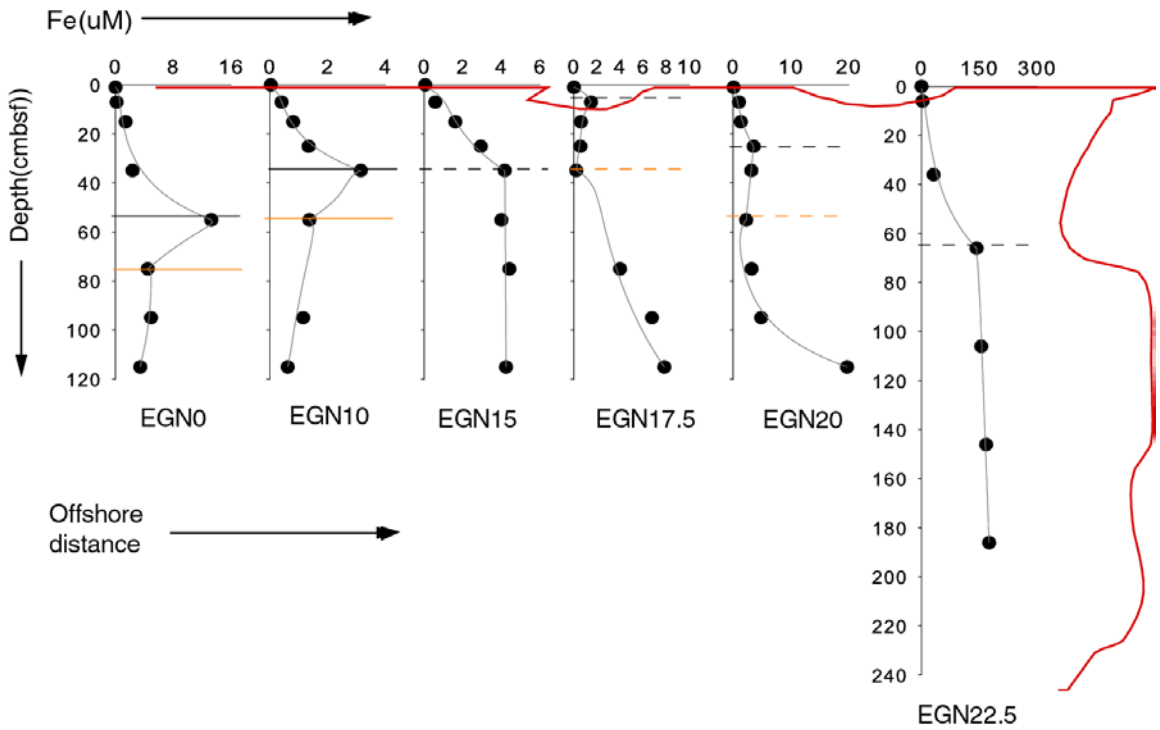

Figure 4-5. Dissolved Fe model in May 2005. Solid dark circles represent measured dissolved Fe concentrations at discrete depths, and dark grey curved lines represent dissolved Fe models. The straight dashed lines represent the boundary between upper and intermediate zones used in the model, and the straight solid lines represent the boundary between intermediate and bottom zones. The red line is the 300 mM Cl contour.

CHAPTER 5
IDENTIFICATION OF PATHWAY OF IRON DIAGENESIS IN AN EAST FLORIDA (USA) SUBTERRANEAN ESTUARY USING IRON ISOTOPES

Introduction

Diagenetic reactions are commonly disrupted in nearshore environments by the submarine groundwater discharge (SGD) (Church, 1996; Moore and Church, 1996; Taniguchi et al., 2003; Charette et al., 2005; Martin et al., 2007). With well-defined fractionation factors, it should be possible to identify the pathway Fe diagenesis in nearshore coastal sediments.

The fractionation of Fe isotopes between two phases A and B is often reported by the fractionation factor, α, which is designated as

$$\alpha_{A-B} = \frac{(^{56}Fe/^{54}Fe)_A}{(^{56}Fe/^{54}Fe)_B} \quad (5\text{-}1)$$

For fractionations of only a few per mil, α can be approximated from:

$$1000*\ln \alpha_{A\text{-}B} = \delta^{56}Fe_A - \delta^{56}Fe_B \quad (5\text{-}2)$$

Difference in measured δ^{56}Fe values between phase A (porewaters) and phase B (sediments) will provide an idea about the pathway of chemical reactions of Fe. This difference in measured δ^{56}Fe values may not give α at the time of reaction, particularly when sediment-bound Fe represents a long term average, and thus α is modeled often from porewater isotope values (e.g Rouxel et al., 2008).

In this chapter, I measured δ^{56}Fe values in porewater and sediments in the subterranean estuary of the Indian River Lagoon (Figure 2-1), and use these differences in δ^{56}Fe values of porewaters and sediments to identify the pathways of Fe-diagenetic reactions. Similar to early diagenetic models of total Fe concentrations in Chapter 3, porewater ^{56}Fe and ^{54}Fe numerical models are developed to estimate α at the time of kinetic reactions (Van Cappellen and Wang, 1995, Wang and Van Cappellen, 1996, Rudinicki et al.2001, Rouxel et al., 2008).

Methods

Analytical Techniques

Iron isotopes values were measured using a Neptune multicollector inductively coupled plasma mass spectrometer at Woods Hole Oceanographic Institution (WHOI), and corresponding δ^{56}Fe values were reported. For porewater samples, Fe concentrations were grouped into high salinity samples (salinity higher than 10 ppt), and low salinity samples (salinity less than 10 ppt) groups to avoid seawater matrix effects. A seawater standard (seawater doped with Fe isotope standard) was loaded to the column to check the matrix effect. Sediment bound iron was extracted from 1 g of sediments by dissolving the bulk sediment in 10 ml aqua regia (30% nitric acid and 10% hydrochloric acid), which removed Fe-oxide coating from the surface of the sediments to the acid solution, but was not strong enough to dissolve framework silicates. The acid solution containing the dissolved Fe-oxide coatings was evaporated overnight on a hot plate, and 5 ml of 6N HCl was added to the precipitate and then centrifuged in Falcon centrifuge tubes. The Fe was dissolved from the supernatant leachate using column chemistry.

Anbar et al (2004). showed isotopic fractionation similar to microbial Fe-oxide reduction is possible during column chemistry, but the published records showed the method followed here does not fractionate Fe during column chemistry (Escoube et al., 2009; Rouxel et al., 2008). Details of column chemistry technique and analysis protocol in Ion coupled plasma mass spectrometer (ICP-MS) are already available elsewhere (e.g. Rouxel et al., 2008; Dauphas et al., 2009), but briefly, Bio-Rad AG1X8 mesh size 100 resin was used for the Fe column chemistry. The IRMM-014 was used as a primary standard for Fe isotope measurements in the ICP-MS, but to check column yield and precision of measurements another in-house standard SRM-3149 was loaded to the column, and was doped with seawater. This SRM-3149 was measured using the ICP-MS and compared with IRM-014 in all four runs, and four repeated measurements were in

taken in the middle of each run. These measurements were consistent with in and among runs, suggesting there is no mass drift effect on isotope measurements. The average value of SRM-3149 from all runs is given in Table 5-1. Yield from the column was also tested by using Ferrozine technique on acid solution passed through columns, after the Fe was eluted from the column. Since Fe can fractionate during column chemistry, extra caution was taken during column chemistry. During analysis on ICP-MS, Cr, Ni, and Cu isotopes were also measured on Faraday cups along with Fe isotopes, so that isobaric interference of ^{54}Cr on ^{54}Fe and ^{58}Ni on ^{58}Fe can be checked. The ^{58}Fe was analyzed because fractionation between $^{56}Fe/^{57}Fe$ should be similar to $^{57}Fe/^{58}Fe$, because both pairs have mass difference of 1. For the same reason $^{65}Cu/^{63}Cu$ was compared to $^{56}Fe/^{54}Fe$. Three to four repeated measurements of each sample were taken, and the mass dependent Fe fractionation and thus the quality of the isotope data were verified by plotting $\delta^{56}Fe$ and $\delta^{57}Fe$ values from sample measurements on the mass dependent fractionation line (Figure 5-1).

Fe isotope model

The Fe isotope model is a modification of the model presented in Chapter 3. The model was developed at site EGN20, because it is near the seepage face boundary, which has previously been shown to be the most reactive location of the seepage face (Chapters 2 and 3). In this porewater Fe isotope model, sedimentary $\delta^{56}Fe$ data was not included, because sediments in the seepage face represent averaged Fe accumulation over 300 years of sealevel rise, rather than fractionation at the time of diagenetic reactions (Chapter 2). The mixing of isotopes between the Fe-oxide reduction zone and the sulfate reduction zone was modeled by the advection and diffusion of Fe. Total Fe concentrations, which were obtained from the reactive-transport model in Chapter 3, were multiplied by the relative abundance of ^{56}Fe, 0.9175 (91.75%), to obtain the ^{56}Fe concentrations. I did not use measured Fe concentration values at WHOI in the model,

because at WHOI Fe concentrations were measured by summing all four Fe isotopes that were measured in the column elutes. In University of Florida (UF) Fe concentrations were measured directly in the acidified porewater samples (which includes both soluble and colloidal), resulting a difference between UF and WHOI total Fe concentrations. The model requires coupling total Fe concentrations and δ^{56}Fe values to estimate α (Rudinicki et al., 2001), thus I used total Fe concentrations measured at UF to estimate ^{56}Fe.

Once ^{56}Fe concentrations are known, a diagenetic equation was written for ^{56}Fe. The reaction zones sampled at EGN20 are only the Fe sinks; the Fe-oxide reduction zone was below the sampled depth (Chapter 2, Figure 2-2a). Consequently, the diagenetic equation for ^{56}Fe diagenesis at EGN20 can be written as

$$D_s \frac{\partial^2 (^{56}Fe)}{\partial x^2} - \omega \frac{\partial (^{56}Fe)}{\partial x} - ^{56}K_2 * ^{56}Fe = 0 \quad (5\text{-}3)$$

The rate constant for ^{56}Fe, $^{56}K_2$, is related to the fractionation factor α and $^{54}K_2$, according to the following equation

$$\alpha = \frac{^{56}K_2}{^{54}K_2} \quad (5\text{-}4)$$

$^{56}K_2$ is estimated from the ^{56}Fe model (equation 5-32) and substituted into equation (5-4). By rearranging (5-4) to

$$^{54}K_2 = \frac{^{56}K_2}{\alpha} \quad (5\text{-}5)$$

From equation 5-5, $^{54}K_2$ can be expressed in terms of α and $^{56}K_2$, and thus the diagenetic equation for ^{54}Fe can be written in terms of $^{56}K_2$ as

$$D_s \frac{\partial^2 (^{54}Fe)}{\partial x^2} - \omega \frac{\partial (^{54}Fe)}{\partial x} - (^{56}K_2 / \alpha) * ^{54}Fe = 0 \quad (5\text{-}6)$$

The ^{54}Fe concentrations are calculated from δ^{56}Fe values and ^{56}Fe abundance (equation 5-7).

$$(^{56}Fe/^{54}Fe_{sample}) = [(\delta^{56}Fe_{measured}/1000)+1]*(^{56}Fe/^{54}Fe)_{std} \quad (5\text{-}7)$$

The ^{54}Fe model from equation (5-6) is optimized to match calculated ^{54}Fe values using the Nelder-Mead optimization technique (Nelder and Mead, 1965), and was solved for α. This α is α_{2a} in the Fe-sulfide precipitation zone, and α_{2b} in the dissolved Fe adsorption zone. Unlike calculated ^{56}Fe, the ^{54}Fe was not calculated from its abundance, because ^{54}Fe abundance is orders of magnitude less than ^{56}Fe.

Results

Two trends of porewater δ^{56}Fe values and porewater Fe concentrations were observed across the seepage face within the orange sediments. At EGN20, both porewater δ^{56}Fe values and porewater Fe concentrations decrease upward within the orange sediment from 115 cmbsf to 55 cmbsf from -0.83 $^{o}/_{oo}$ to -1.76 $^{o}/_{oo}$ for δ^{56}Fe values, and 21.22 to 2.17 μM for Fe concentrations. In contrast, at EGN22.5 and EGN30, porewater δ^{56}Fe values within the orange sediments decrease upward, while the Fe concentrations increase upward (Figure 5-2a). In the black sediments, from the seepage face porewater δ^{56}Fe values increase upward (Figure 5-2). In contrast to the black sediments from the seepage face, porewater δ^{56}Fe values in the black sediments at CIRL39 decrease upward, from 0.89 $^{o}/_{oo}$ at 140 cmbsf, to 0.29 $^{o}/_{oo}$ at 10cmbsf. Porewater δ^{56}Fe values show relatively constant values of about + 0.24 $^{o}/_{oo}$ near the sediment-water interface (upper 7 cmbsf) at all sites, regardless of whether sediments are black (in the seepage face) or white (at CIRL39) Porewater δ^{56}Fe values the black-orange sediment interface are less than 0 $^{o}/_{oo}$ within the seepage face, but are higher than 0 $^{o}/_{oo}$ at the seepage face boundary (Figure 5-3).

The δ^{56}Fe values of the solid Fe-oxides in the orange sediments remain constant around 0 $^{o}/_{oo}$. The δ^{56}Fe values of black sediments range from about -1 $^{o}/_{oo\ to}$ -0.5 $^{o}/_{oo}$ within the seepage

face. Black sediments at CIRL39 differ from the black sediments of the seepage face, by having higher δ^{56}Fe values that range between 0.29 $^{o}/_{oo}$ to 0.89 $^{o}/_{oo}$. Sediment δ^{56}Fe values are always heavier in the orange sediments and are lighter in the black sediments than the porewater δ^{56}Fe values, irrespective of the location of the site in the seepage face (Figure 5-2b).

Discussion

Tracing sources and sinks of Fe

In this discussion section first I will identify the pathway of Fe diagenesis (sources and sinks), by directly comparing δ^{56}Fe values from porewater and sediments (equation 1-1), and then will discuss the modeled value of α, estimated from equation (5-6). Orange sediments have δ^{56}Fe values in porewater -1 to-2 $^{o}/_{oo}$ lighter than the associated relatively unfractionated sedimentary δ^{56}Fe values. This value is similar to the δ^{56}Fe value expected during dissimilatory Fe-oxide reduction (DIR) (Fredrickson et al., 1998; Schauble et al., 2001; Johnson et al., 2002, e.g. in 2004a; Beard et al. 2003). Assuming porewater Fe at our site is essentially Fe^{2+}, such similarities in δ^{56}Fe values indicate *in situ* Fe-oxide reduction produced dissolved Fe at our site, and thus isotope data supports previous conclusion from Chapter 2. Similar δ^{56}Fe values in porewater, -1.5 $^{o}/_{oo}$ are possible during phototrophic oxidation of Fe^{2+} to poorly crystalline hydrous ferric oxide (HFO) when there was no HFO present initially at the beginning of the reaction (Croal et al., 2004). Additionally Fe^{2+} can become isotopically lighter during microbial precipitation of Fe-oxides (see introduction), and thus additional evidence is required to identify the oxic versus anoxic conditions (e.g. Johnson et al., 2008). In the Indian River Lagoon subterranean estuary, concentrations of dissolved O_2 in porewaters is low, less than 1 ppm, suggesting Fe-oxide reduction is causing the lighter δ^{56}Fe values in the dissolved Fe than corresponding sediments (Figure 5-2; Chapter 2). In Lake Nyos, Cameroon, where SO_4^{2-}

concentrations were low, and NO_3^- concentrations were close to zero like Indian River Lagoon, Fe^{2+} was produced by DIR, and $\delta^{56}Fe$ values of dissolved Fe decreased by 1.8 $^{o}/_{oo}$ (Teutsch et al., 2009). Similarities of isotope values between Lake Nyos and Indian River Lagoon suggest DIR is causing Fe-oxide reduction in Indian River Lagoon. Unlike the porewater values, $\delta^{56}Fe$ values do not change for the Fe-oxides in the orange sediments in Indian River Lagoon, because the abundance of Fe in the sediment is 4 orders of magnitude higher than porewater abundance.

Large fractionation of dissolved Fe isotopes would be expected from Fe-oxide reduction, but Fe-oxide reduction is not a single step process and instead occurs through multiple steps (Figure 5-4). For example, Fe-oxides often get dissolved by formation of ligands, and then equilibrium fractionation occurs between Fe^{3+} ligand ($[Fe^{3+}(H_2O)_6]^{6+}$), and Fe^{2+} ligand $(Fe^{2+})(H_2O)_6]^{2+}$), and $\delta^{56}Fe$ values of porewater become 2.74 $^{o}/_{oo}$ lighter (Brantley et al. 2001, 2004; Johnson et al. 2002). However, under early diagenetic conditions, the inorganic formation of Fe^{3+} ligands from Fe-oxides is unlikely because solubilities of various forms of Fe-oxides are low, thus formation of ligands and Fe-oxide reductions are microbially mediated (Lovley, 1987, Thamdrup, 2000; Johnson et al., 2004a; Hyacinthe et al, 2006). Later studies showed ligand bound dissolution of Fe-oxides are kinetically not possible and instead a reactive Fe^{3+} layer is formed onto Fe-oxides (Figure 5-8), which subsequently reduce to Fe^{2+} (Crosby et al. 2005, 2007).

Iron isotope data reflects different steps of DIR in the Indian River Lagoon. Porewater $\delta^{56}Fe$ values decrease both upward below and above the dissolved Fe maxima (Figure 5-2). If DIR was a single step dissolution process of Fe-oxides to Fe^{2+}, then the isotopically lightest porewater value should have occurred where the dissolved Fe concentration is highest. Crosby et al.(2005) showed microbial Fe-oxide precipitation occurs first by sorption of dissolved Fe on

newly formed Fe-oxides, then by electron exchange between Fe^{2+} and Fe^{3+}, and finally by formation of a reactive Fe^{3+} coating on the Fe-oxide surfaces. Presumably a similar sequence would occur in reverse during microbial Fe-oxide dissolution. Sorption of dissolved Fe to the Fe-oxyhydroxides would make porewater lighter (Jeon et al., 2003; Mikutta et al., 2009, Teutsch et al., 2005; Crosby et al., 2007). About -3.5 $^{o}/_{oo}$ fractionation for Fe^{2+} during sorption was suggested by Teutsch at al. (2005). In an experiment, Icopini et al. (2004) showed the $\delta^{56}Fe$ values of Fe^{2+} are 1.2 $^{o}/_{oo}$ lighter than the source goethite, and one-third of dissolved Fe produced from Fe-oxide reduction were sorbed back on the surface of goethite. Consequently, only two third of the dissolved Fe was available in the solution. Because of adsorption, $\delta^{56}Fe$ values of remaining dissolved Fe became 0.8. $^{o}/_{oo}$ lighter and thus the total fractionation was -2 $^{o}/_{oo}$ during DIR. Similarly, in the Indian River Lagoon in the upper part of the dissolved Fe maxima, the observed upward decrease in Fe^{2+} concentrations and $\delta^{56}Fe$ values suggest dissolved Fe produced from Fe-oxides was sorbed back on to Fe-oxide surfaces and only a portion of dissolved Fe produced from Fe-oxides was transported along with SGD to the black sediments, where bacterial SO_4^{2-} reduction (BSR) occurs.

In contrast to unfractionated Fe-oxides coatings on orange sediments, black Fe-sulfide sediments have negative $\delta^{56}Fe$ values, and porewaters have positive $\delta^{56}Fe$ values that increase upward through the black sediments, reflecting Fe-sulfide precipitation in the porewater (e.g. Johnson et al., 2004a). Experiments have shown there is a +0.3 $^{o}/_{oo}$ fractionation of porewater during Fe-sulfide precipitation (Butler et al., 2005). Porewater $\delta^{56}Fe$ values were found to increase by about 1 $^{o}/_{oo}$ during Fe-sulfide precipitation in the Santa Barbara Basin, California (Severmann et al., 2006). Similarly in Indian River Lagoon, about +1 $^{o}/_{oo}$ maximum difference is observed in porewaters $\delta^{56}Fe$ values associated with Fe-sulfides in the seepage face (Figure 5-1).

In both areas, Fe-oxide reduction and Fe-sulfide precipitation occur and $\delta^{56}Fe$ values in porewater show mixed isotope signature of these two reactions (Figure 5-4). At the Santa Barbara Basin, SO_4^{2-} reduction zone underlies Fe-oxide reduction zone, and positive fractionation of porewater during Fe-sulfide precipitation has caused $\delta^{56}Fe$ values of $Fe(OH)_3$ to be lighter with a range between -1.7 $^{o}/_{oo}$ and -0.7 $^{o}/_{oo}$ than Fe-sulfides, with a range between -0.4 $^{o}/_{oo}$ to +0.4 $^{o}/_{oo}$ (Severmann et al., 2006). In contrast, at Indian River Lagoon, SO_4^{2-} reduction zone overlies the Fe-oxide reduction zone, and upward flow of porewater by SGD from Fe-oxide reduction zone to Fe-sulfide precipitation zone resulted in modestly negative (where Fe-oxide reductions dominate isotope signature) to modestly positive (where BSR dominates isotope signature) $\delta^{56}Fe$ in porewaters, as suggested by Johnson et al. (2008).

Influence of hydrology on Fe isotope fractionation

Previous study showed in the subterranean estuary Fe isotope fractionation was much larger than expected from laboratory experiments or in marine sediments where there is no flow of SGD (Beard and Johnson 2004; Teutsch et al., 2005; Rouxel et al., 2008). In the Indian River Lagoon, the influence of hydrology on the Fe isotopic signatures of the porewater and sediments is shown by the link between gaining strength of non-local exchange and increasing $\delta^{56}Fe$ values at the black-orange sediment interface with distance offshore (Figure 5-3). Within the seepage face of the Indian River Lagoon, non-local exchange penetrates to the depth of the black-orange sediment interface, where the most negative $\delta^{56}Fe$ values in porewater profiles occur. At the black-orange sediment interface, $\delta^{56}Fe$ values become positive with distance offshore. This link between non-local exchange and $\delta^{56}Fe$ values at the black-orange sediment interface indicates that as non-local exchange gains strength. SO_4^{2-} reduction increases and dominates the mixed Fe isotopes signature, over the Fe-oxides reduction (Figure 5-4).

Near the sediment-water interface (upper 10 cmbsf), porewater $\delta^{56}Fe$ values are nearly constant, about + 0.24 $^{o}/_{oo}$, at all sites including CIRL39 (Figure 5-2). These small positive $\delta^{56}Fe$ values in porewater near the sediment-water interface suggest oxidation of Fe-sulfides by O_2 carried with the non-local exchange. Evidence of Fe-sulfide dissolution is observed in the upper 10cmbsf at CIRL39, where black sediments were leached to white and a shallow dissolved Fe maximum occurs (Figures 2-2, 2-4) and porewater $\delta^{56}Fe$ values at CIRL39 decrease toward the sediment-water interface.

Modeled Rate of Isotope Fractionation

Equation (5-6) is used to estimate fraction factors α and thereby to understand the influence of hydrology on porewater Fe isotope fractionation. Model results are given in Table 5-2, and ^{56}Fe and ^{54}Fe models are shown in Figure 5-5. For simplicity, α value reported in the Table 5-2 are converted to per mil by subtracting 1 from the estimated α, and multiplying the difference by 1000. The model shows about -1.1$^{o}/_{oo}$ fractionation in porewaters from 55-115 cmbsf depths at EGN20, supporting the inference that Fe sorbs onto Fe-oxides. The model verifies that the observed profile of ^{56}Fe and ^{54}Fe can be simulated with constant fractionation rate. Considering the constant rate of fractionation, decrease in porewater $\delta^{56}Fe$ values in orange sediments from about -0.5 $^{o}/_{oo}$ at 115 cmbsf to about -2 $^{o}/_{oo}$ at 55 cmbsf suggests initial $\delta^{56}Fe$ values at 115 cmbsf (meteoric groundwater) was slightly higher than initial $\delta^{56}Fe$ values at 55 cmbsf (subterranean estuary porewater). In the Waquoit Bay subterranean estuary, $\delta^{56}Fe$ values of groundwater end member were 3-4 $^{o}/_{oo}$ higher than porewaters in the subterranean estuary (Rouxel et al., 2008). The same could be true for Indian River Lagoon, where relatively high $\delta^{56}Fe$ values of groundwater may have lowered the net observed $\delta^{56}Fe$ values produced by Fe-oxide reduction.

In the black sediments, estimated fractionation of porewater by about +8 $^{o}/_{oo}$, was higher than what would have expected from the single step Fe-sulfide precipitation from dissolved Fe of about +1 $^{o}/_{oo}$ (e.g., Butler et al., 2005; Severmann et al., 2006). The overall agreement of the model with the ^{56}Fe and ^{54}Fe concentrations, and the match between fractionation factors from this study and previous studies in the dissolved Fe sorption zone suggests our model is correct. Under natural conditions Fe can fractionate by about 10 $^{o}/_{oo}$ (Beard and Johnson, 2004) and +8 $^{o}/_{oo}$ fractionation is within this range. Such anomalously high values may result from additional fractionation of Fe during multiple stages of Fe-sulfide precipitation (Ostwald ripening). Also, Fe isotope fractionation has been shown to vary over time, because of the variations in the colloidal sources of Fe (Ingri et al. 2006). This change in fractionation occurs during storm events when Fe colloids were mainly Fe-C colloids with δ^{56}Fe values of -0.13 $^{o}/_{oo}$, but in calm periods the colloids are mainly Fe-oxyhydroxides with δ^{56}Fe values of +0.31$^{o}/_{oo}$. Hydrology of the Indian River Lagoon seepage face varies with episodic events like storms (Smith et al., 2008b), and it takes about 3 months to regain the previous hydrologic conditions. Dissolved Fe concentration depth profiles at EGN20 also vary over time (Appendix-A), suggesting episodic variations in Fe may cause additional fractionation in porewater from black sediments. We lack supporting data such as measurements of particulate, colloidal, soluble phases of Fe, measurement of bacterial counts, separation of dissolved Fe^{2+} from dissolved Fe^{3+}. These limitations do not allow us to identify the physical reasons causing such anomalously high fractionation of porewater from the Fe-sulfide zone. Future studies are thus necessary to acquire all these above mentioned ancillary data, to model Fe isotope fractionations at other sites in the seepage face, and to identify temporal variations in Fe isotopic signatures.

Conclusion

In Indian River Lagoon, Fe isotopes in porewater and sediments bear mixed signatures of Fe-oxide reduction and Fe-sulfide precipitation. In the seepage face, adsorption of dissolved Fe on the Fe-oxides during DIR produces the observed variations in δ^{56}Fe values in porewaters from the orange sediments. The light isotopes produced during DIR flow upward with terrestrial SGD to the black sediments, where δ^{56}Fe values in porewater become heavier because of Fe-sulfide precipitation. Consequently, the lightest δ^{56}Fe values are observed at the black-orange sediment interface. At the seepage face boundary, this lightest δ^{56}Fe values at the black-orange sediment interface is missing because the Fe-sulfide precipitation has taken over the Fe-adsorption pathway with gaining strength of non-local exchange. Such modifications of Fe isotopes by hydrology of the subterranean estuary suggest the Fe isotope signature is altered during early digenetic reactions in subterranean estuary sediments and may contribute to the Fe isotope values in the open oceans.

Table 5-1. Accuracy and precision of measurements, and value of the in-house isotope standard.

	Average UF Values (ppm)	Standard. Deviation.	Certified Values (ppm)	Standard. Deviation	Average WHOI δ^{56}Fe Values
Dissolved Fe	0.11012	0.00398	0.103	0.005	
Internal Isotope Standard SRM-3149					0.43 (from 4 runs. In each run standard was analyzed for 4 times)

Table 5-2. Model Results at EGN20.

l	Total Fe Model	^{56}Fe Model	Modeled Fractionation factor
Total Fe K_{2a} (1/sec)	0.27 x10^{-8}	-	-
Total Fe K_{2b} (1/sec)	0.48 x10^{-8}	-	-
$^{56}K_{2a}$ (1/sec)	-	0.2764 x10^{-8}	-
$^{56}K_{2b}$ (1/sec)	-	0.4843 x10^{-8}	-
α_{2a} ($^{o}/_{oo}$)	-	-	+8.6
α_{2b} ($^{o}/_{oo}$)	-	-	-1.1
Total Fe-sulfide precipitation in upper zone (mg/cm^2/year)	0.0163	-	-
Total dissolved Fe adsorption in lower zone (mg/cm^2/year)	0.3140	-	-
Total Fe-loss (mg/cm^2/year)	0.330	-	-

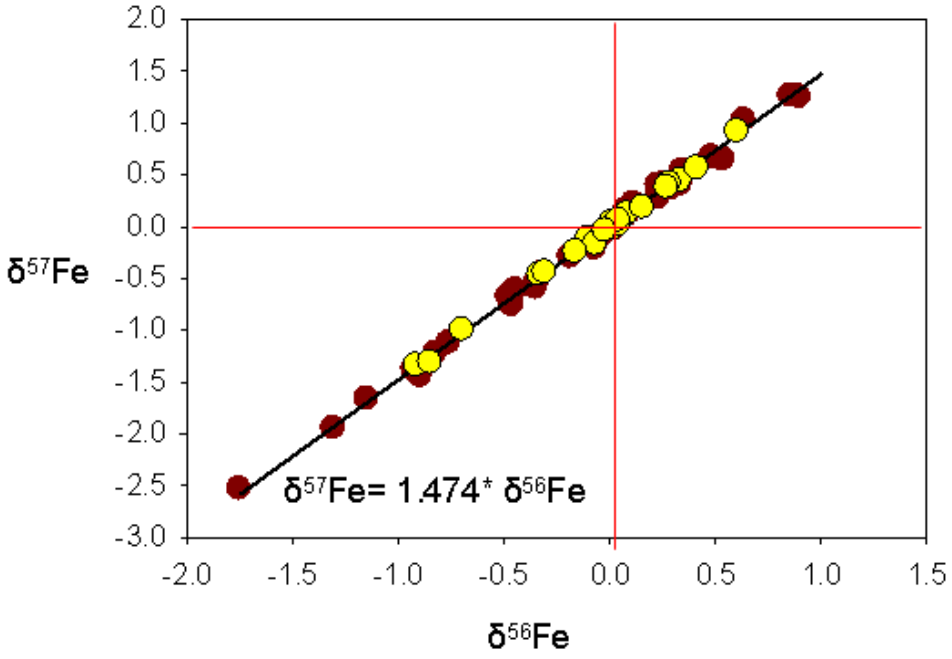

Figure 5-1. Verification of the mass dependent fractionation of the measured samples. Brown circles represent porewater, and yellow circles represent sediment isotope data. The straight line represents mass dependent fractionation line.

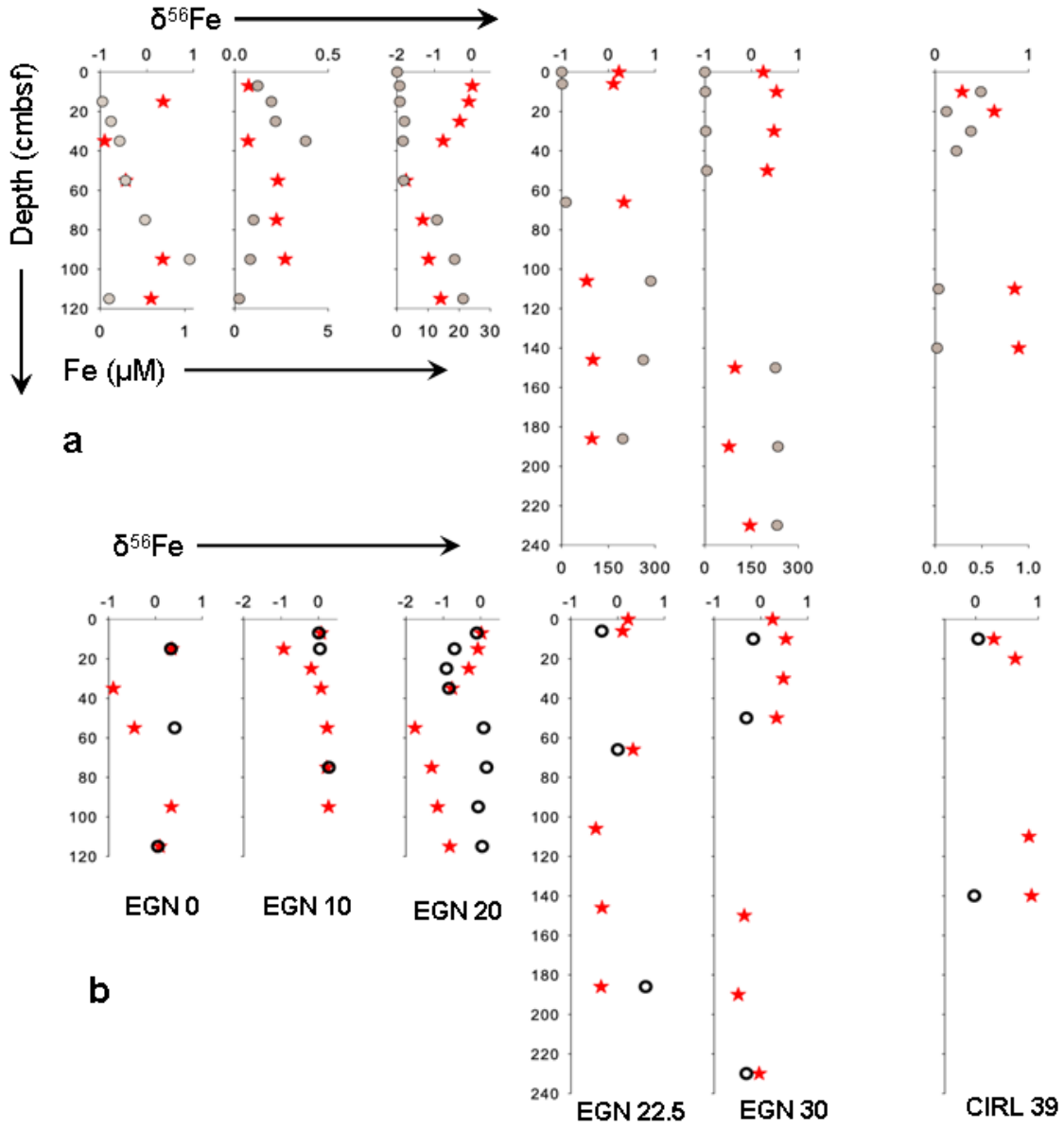

Figure 5-2. $\delta^{56}Fe$ values in porewater and sediments, and corresponding Fe concentrations in porewater. a) $\delta^{56}Fe$ values in porewaters and sediments across the seepage face, b) comparison of $\delta^{56}Fe$ values in porewater and dissolved Fe concentrations. Red asterisks show $\delta^{56}Fe$ values in porewaters, open circles show $\delta^{56}Fe$ values in sediments, and solid circles show dissolved Fe concentrations

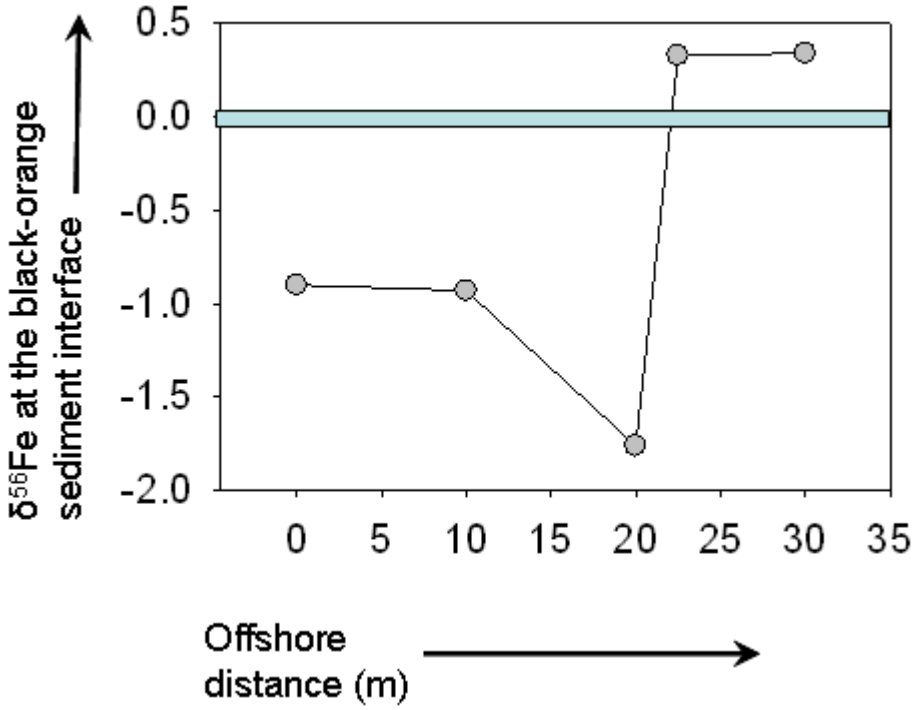

Figure 5-3. Offshore variation in porewater $\delta^{56}Fe$ values at the black-orange sediment interface. The highlighted zone represents $\delta^{56}Fe$ values of zero.

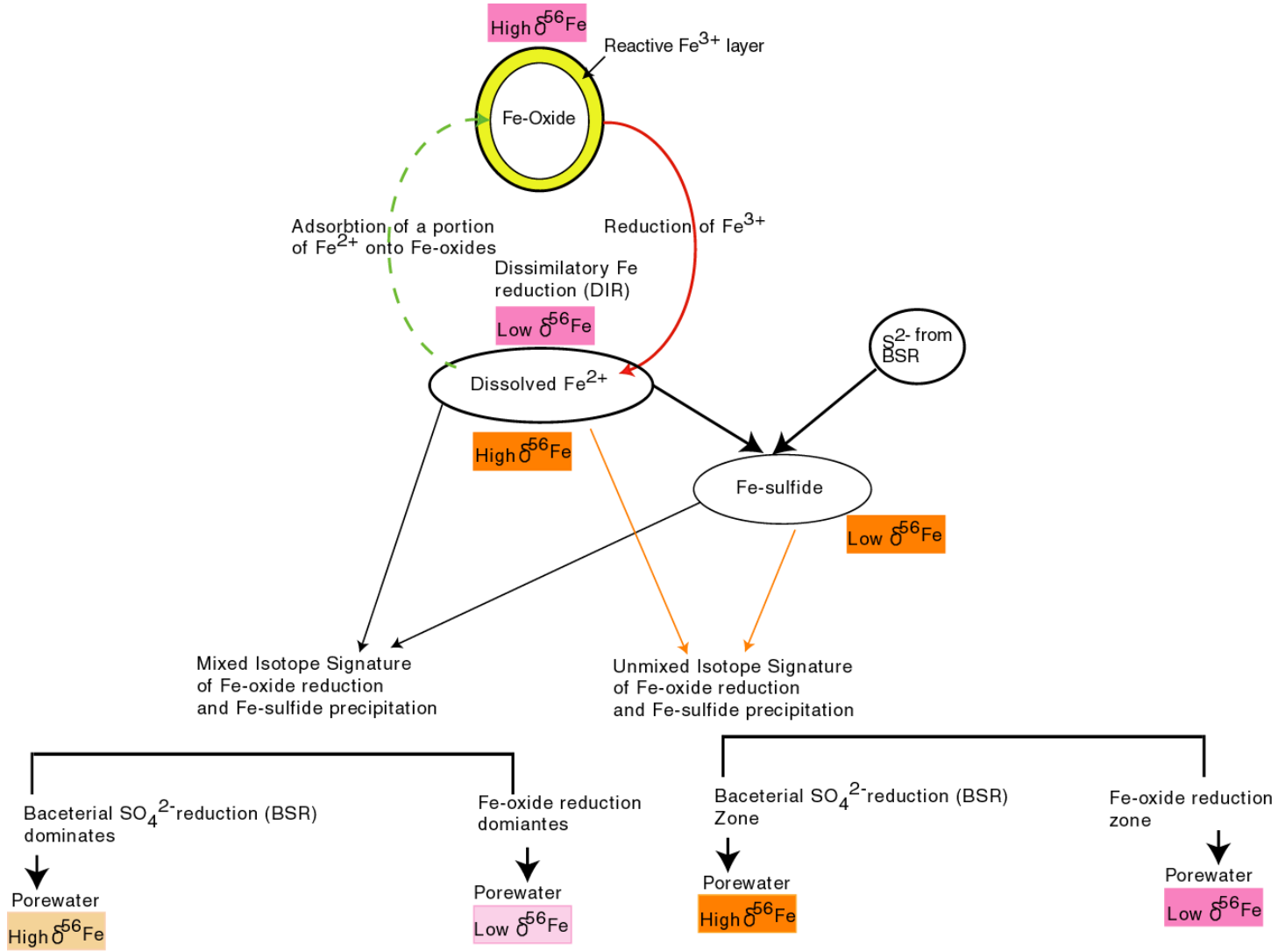

Figure 5-4. Diagram of Fe isotope fractionation in presence of SO_4^{2-} and Fe-oxide reduction.

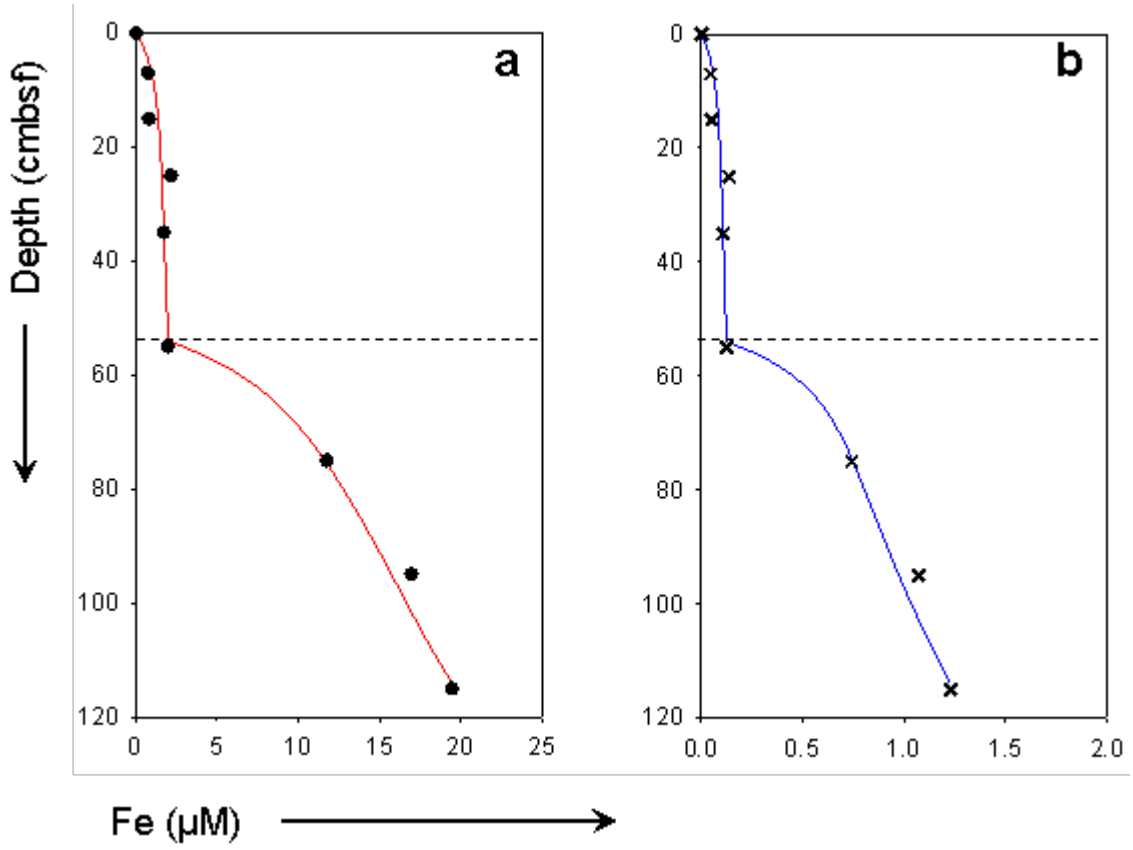

Figure 5-5. Fe isotope models. a) ^{56}Fe concentration model, b) ^{54}Fe concentration model. The solid circles and cross marks represent calculated ^{56}Fe and ^{54}Fe values, respectively. The solid red line represents ^{56}Fe model, and blue line represents ^{54}Fe model.

CHAPTER 6
CONCLUSIONS

Summary and Conclusions

Iron (Fe) is an important micronutrient that can influence OC remineralization under anoxic conditions. Previous studies have shown that Fe diagenesis in the subterranean estuary is influenced by hydrogeology, particularly when reduced Fe is transported to more oxidizing zones by terrestrial SGD, where it precipitates as Fe-oxides. However, in the previous studies no Fe-oxide reduction was observed in the subterranean estuary, thus the amount of OC remineralization during Fe-oxide reduction in the subterranean estuary was unknown. Results from work presented here indicate for the first time that Fe-oxides are reduced in the seepage face of the subterranean estuary, thereby impacting the diagenesis of the sedimentary OC there. Differences in the results presented here and previous work indicate that Fe diagenesis depends on the local geological environment, especially the types of sediments that make up the seepage face.

Sediments from the Indian River Lagoon seepage face are orange in color in the deeper parts, but are black in color near the sediment-water interface. Sequential leaching techniques applied to these sediments show the orange color is due to Fe-oxide coating on quartz sands, and the black color is from Fe-sulfides. Sediment S, OC, and porewater S^{2-} maxima and Fe minima occur in black sediments, and dissolved Fe maxima occur in underlying orange sediments. This distribution of Fe, S, and OC suggests that Fe-oxides dissolve to form Fe maxima in the porewater profiles and these maxima are enhanced by the removal of dissolved Fe by precipitation of Fe-sulfides in the black sediments. The black sediments contain 7 times more OC than the orange sediments and high OC contents drive minor amounts of SO_4^{2-} reduction.

Maxima of the porewater Fe concentrations are around 1 μM at the shoreline and about 0.5 μM 250 m offshore, more than 200 m seaward of the seepage face. The Fe maximum is about three orders of magnitude higher at the seaward end of the seepage face than near shore or far offshore. Elevated Fe concentrations at the distal end of the seepage face result either from highly reducing conditions caused by long residence time of flows, or from accumulation of dissolved Fe due to slow flow rates of terrestrial SGD, which is10 times lower at the boundary than shoreline. This conceptual model of the link between hydrology and Fe diagenesis in the subterranean estuary has been quantified in a numerical model that estimates the rates of Fe-oxide reduction and Fe-sulfide precipitation. Modeled Fe-oxide reduction rates vary little across the seepage face, averaging around 0.213 mg/cm^2/year. The nearly constant Fe-oxide reduction rates indicate elevated dissolved Fe concentrations at the seepage face boundary are not due to higher reducing conditions than near shore, but instead are due to slow flow velocities of terrestrial SGD at the seepage face boundary. In contrast to the constant Fe-oxide reduction rates, the average rate constants of Fe-sulfide precipitation decreases from 21.9 x 10^{-8} 1/sec to 0.64 x 10^{-8} 1/sec from the shoreline to the seepage face boundary, because of an increase with distance from the shoreline of non-local exchange.

At the site 250 m offshore, white sediments occur in the upper 50 cmbsf. These white sediments indicate that non-local exchange, which carries oxygen-rich surface water into the sediments, causes oxidation of Fe-sulfide in the black sediments. Non-local exchange is limited within the seepage face because of the upward flow of terrestrial SGD. Because terrestrial SGD also transports Fe into the sulfate reduction zone, Fe-sulfide accumulates there, rather than being removed. Therefore, various sources and flows of SGD cause differences in sources and sinks of Fe within and outside the seepage face of the subterranean estuary.

These results indicate that Fe fluxes from the Indian River Lagoon subterranean estuary occur in three steps. The first two steps occur within the seepage face with the reduction of Fe-oxides from the orange sediments and precipitation of dissolved Fe as Fe-sulfides in the black sediments. The third step, re-oxidation of the Fe-sulfides, occurs outside the seepage face, in the saltwater zone of the subterranean estuary.

A previous study showed that orange sediments are of terrestrial origin and black sediments are of marine origin. These black sediments thicken seaward as a result of sealevel rising at the rate of about 3mm/year, indicating the current seepage face was transgressed over approximately the past 300 years. As the subterranean estuary is transgressed, the sediments which act as sources and sinks of dissolved Fe continuously move offshore effectively transporting Fe deposited in the terrestrial sediments into the lagoon water column.

Indian River Lagoon concentrations have low concentrations of dissolved O_2 and NO_3^-, which are the energetically favored electron acceptors in OC remineralization. Consequently, the observed Fe oxide reduction should be important for most of the OC remineralization in these sediments. Modeled rates of OC remineralization by Fe-oxides vary little across the seepage face, averaging 5.34×10^{-2} mg/cm^2/year. The increasing thickness of the marine sediments suggests marine OC is sequestered in black sediments, simultaneously with loss of terrestrial OC and DOC from orange sediments.

Temporal variations in Fe fluxes from the seepage face were estimated from 2004 to 2007. During this time, the potential evapotranspiration averaged around 10cm/month, but the estimated effective precipitation (precipitation-evapotranspiration) decreased from about 40 cm/year in 2004 and 2005 to about -10cm/year in 2006 and 2007. This decrease in effective precipitation resulted from a decrease in average rainfall from 13 cm/month to 9 cm/month from

2004 to 2007 and caused the seepage face boundary, as defined by the 300 mM Cl concentration isohaline contour, to shift landward by about 5 m from 2004 to 2007. Because of the smaller seepage face, estimates of Fe flux and OC remineralization from the seepage face decreased from 192 g/year to 153g/year and from 48 g/year to 38g/year, respectively. This study thus showed Fe flux varies temporally with short term changes in over a period of a few years as well as at longer time periods following sealevel rise over the past few hundred years.

Pathways of Fe diagenesis in the subterranean estuarine sediments were identified using δ^{56}Fe values in sediments and porewaters, and a numerically modeled fractionation rate, α. The δ^{56}Fe values in dissolved Fe are enriched in ^{54}Fe compared to the terrestrial orange sediments, but are depleted in ^{54}Fe compared to the black marine sediments. These differences in Fe isotope values reflect the dissimilatory reduction of Fe-oxides in orange sediments, and precipitation of Fe-sulfides in black sediments. Within the terrestrial sediments, δ^{56}Fe values decrease at a constant rate both at the upper and lower part of the Fe maxima. This variation in concentrations and isotope ratios indicates that dissolution of Fe-oxides occurs below the Fe maxima, but a fraction of dissolved Fe is adsorbed onto surface of Fe-oxides within the orange sediments at the upper part of the maxima. Because of this adsorption sink, only a portion of dissolved Fe produced from Fe-oxides flows into the Fe-sulfide precipitation zone. Identification of this Fe sink was possible by comparing dissolved Fe concentrations and isotope values, and could not be identified otherwise just by studying Fe concentrations in sediments and porewaters.

The porewater δ^{56}Fe values allow estimates of α for Fe isotopes in diagenetic settings. This fractionation factor was estimated at a single site, where porewater samples were not collected from the lower part of the dissolved Fe maximum. The estimated fractionation factor, α, is -1.1 $^{o}/_{oo}$ in the dissolved Fe adsorption sink, and is +8.6 $^{o}/_{oo}$ in the Fe-sulfide sink. The α value of -1.1

$^{o}/_{oo}$ agrees well with the previous studies on Fe adsorption onto Fe-oxides, but an α value of +8.6 $^{o}/_{oo}$ is anomalously high compared to previous studies of Fe-sulfide precipitation. This high value of α can result from multiple stages of Fe-sulfide precipitation, and/or relict effect of temporal variations in Fe reactions. Iron-sulfide precipitations in natural sediment may also go through multiple stages including colloidal Fe, and additional fractionations of the Fe isotopes may have resulted from fractionation between each of these phases.

Future Work

In this study only one subterranean estuary was studied for the OC remineralization, and a fraction of OC that gets remineralized in that subterranean estuary was estimated because the study mainly focused on only one electron acceptor, Fe-oxide. In the future, all electron acceptors need to be studied in details so that total OC remineralization in a subterranean estuary can be estimated. Once the estimation of OC remineralization in one subterranean estuary is obtained, the global OC remineralization in all subterranean estuaries and its impact on global C budget need to be determined.

For the present study site, the research needs to be continued further to develop the understanding of Fe distributions in different phases. In future studies, dissolved Fe^{2+} and Fe^{3+} need to be measured separately, because they will provide the information about fractionation factor from the first two steps of Fe-oxide dissolution: transformation between Fe^{3+}solid to Fe^{3+}dissolved, and transformation between Fe^{3+} and Fe^{2+}. These dissolved Fe^{3+}values would need to be measured in the field using ferrozine or similar technique, because longer exposure of samples to the oxic atmosphere will cause oxidation of Fe^{2+} into Fe^{3+}.

Hydrology of the Indian River Lagoon seepage face varies with storms, and it takes several months to return to the previous hydrologic conditions, depending on the distance from shore

(Smith et al., 2008b). The episodic events can cause variations in sources of colloidal and dissolved forms of Fe (Ingri et al., 2006). Consequently, it is important to determine the temporal variations in colloidal and dissolved Fe in subterranean estuaries by measuring the soluble (passes through 0.22μm filter) and colloidal (traps between 0.22 to 0.45 μm filter size) Fe. No Fe concentrations or isotope data were measured during these episodic events. Future studies need to identify the whether these episodic events alter colloidal and dissolved sources of Fe diagenesis in the subterranean estuary.

The present reactive-transport model of dissolved Fe concentrations provides limited information, because of low sampling resolution, and use of truncated porewater Fe profiles in the model. In future studies, sampling resolutions need to be increased and sampling depths should be increased to obtain complete porewater Fe profiles. These complete porewater profiles will improve the model, and high resolution sampling will increase degrees of freedom in the model. Future cores need to penetrate the entire thickness of terrestrial orange sediments, so that total Fe flux from the orange sediments can be obtained.

Non-local exchange is impacted by terrestrial SGD by being allowed to penetrate to progressively greater depths as terrestrial SGD decreases offshore. The modeling technique thus needs to be developed to include non-local exchange in the shallow sediments for transport of dissolved Fe. Having non-local exchange will also allow the quantification of potential Fe-sulfide oxidation, and sulfate reduction. The model developed for this work includes OC remineralization only by Fe-oxides. In the future, similar models need to be developed for all other electron acceptors in the subterranean estuary, so that total OC remineralization can be estimated. This biogeochemical model then needs to be applied to all subterranean estuaries for estimation of OC remineralization.

APPENDIX A
IRON MODELS FROM DIFFERENT SAMPLING TIMES

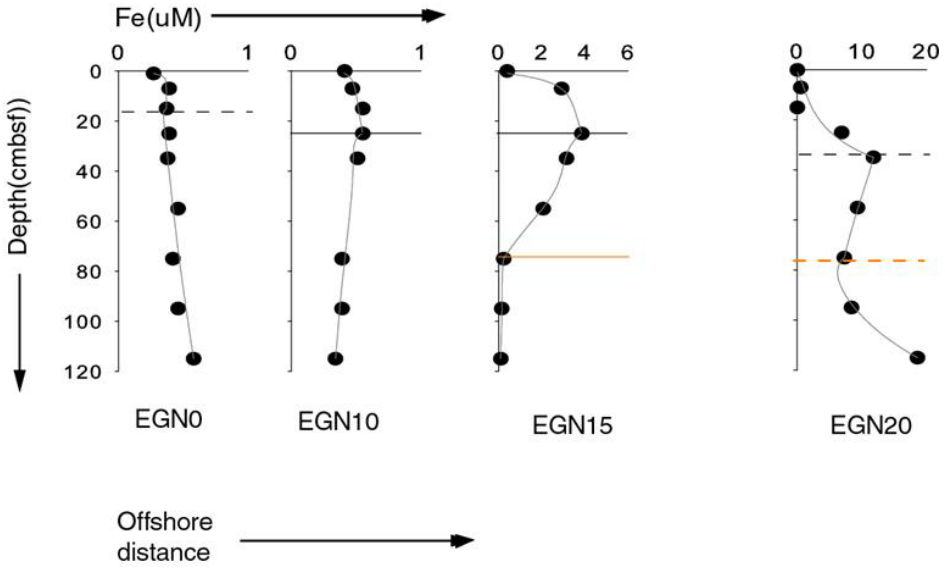

Figure A-1. Dissolved Fe model in November 2004. No multisampler was installed at EGN17.5 and EGN22.5 during this time of sampling.

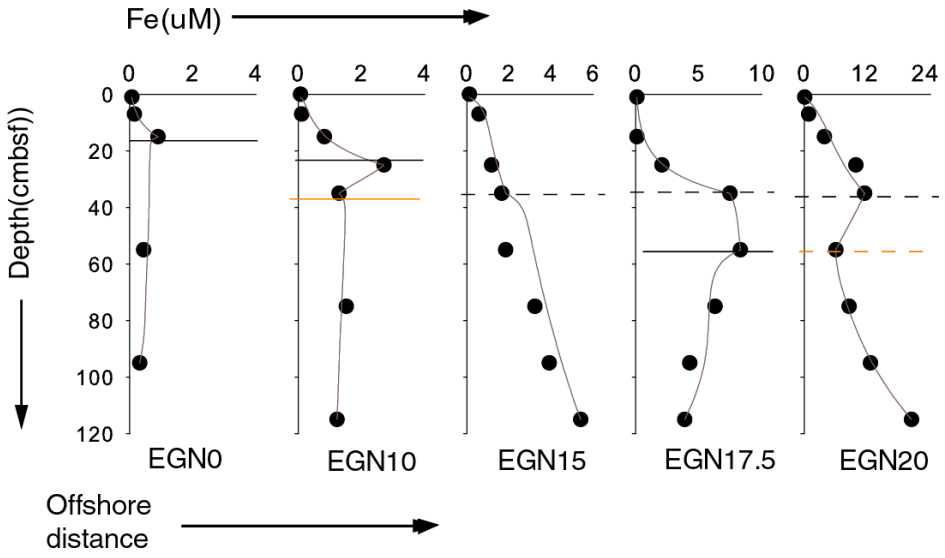

Figure A-2. Dissolved Fe model in February 2005. No multisampler was installed at EGN22.5 during this time of sampling, thus lacking EGN22.5. At sites EGN10, and EGN17.5 the lower Fe-sulfide precipitation zone is missing.

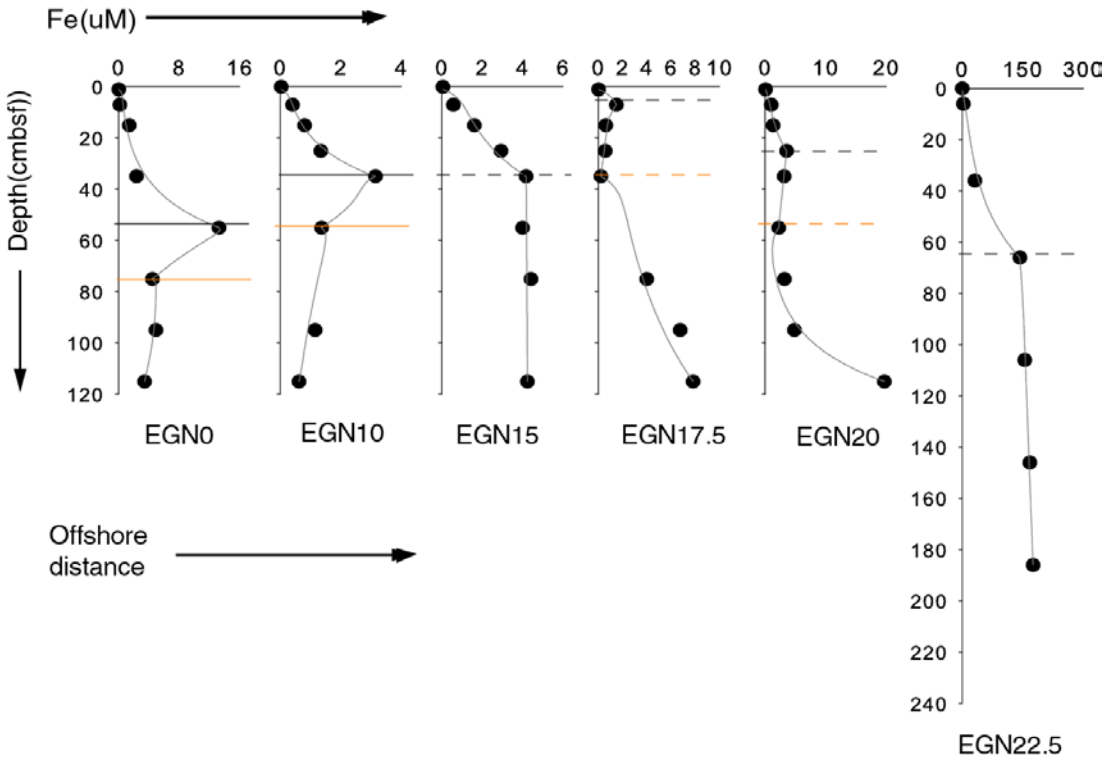

Figure A-3. Dissolved Fe model in May 2005.

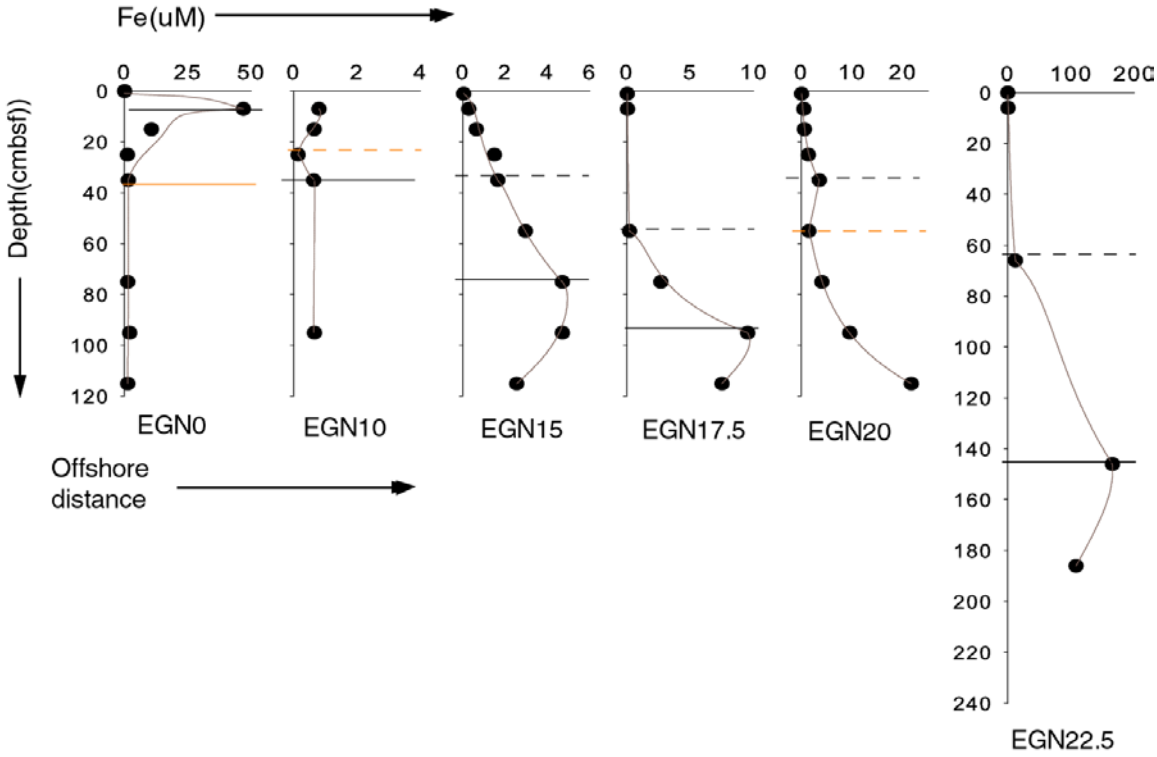

Figure A-4. Dissolved Fe model in September 2005.

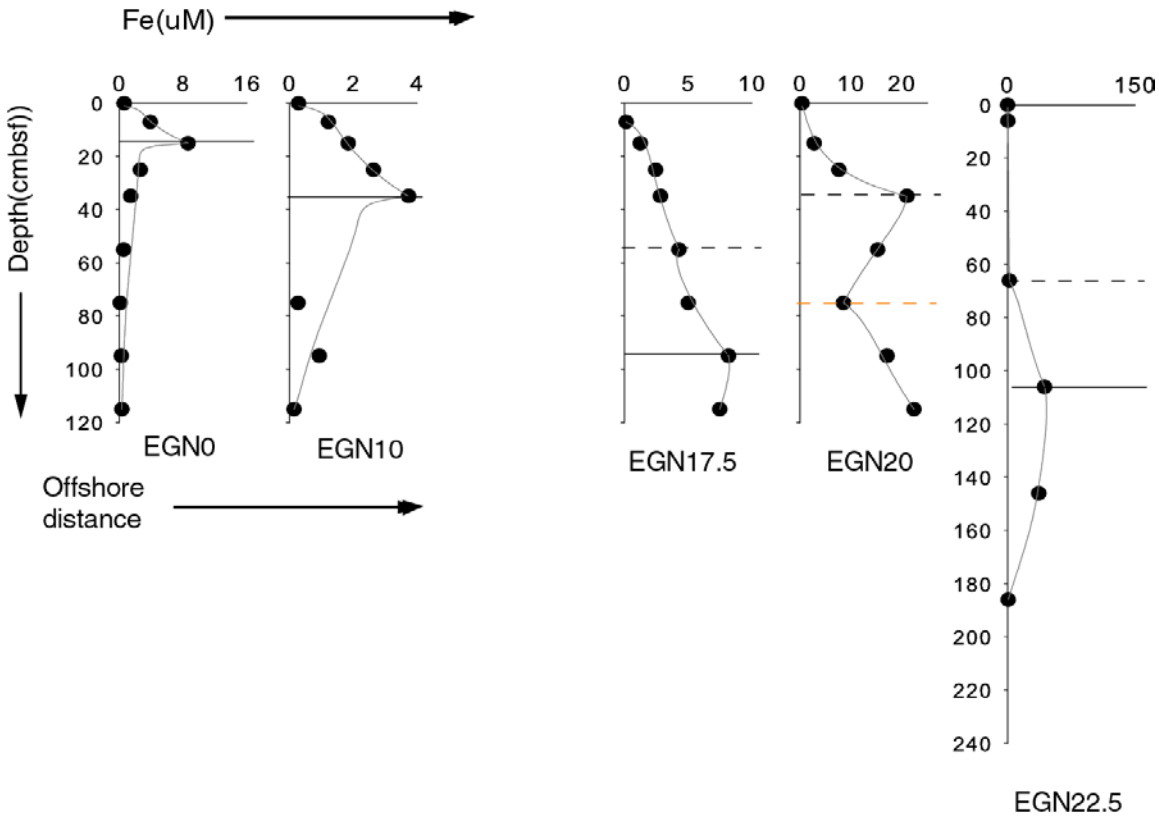

Figure A-5. Dissolved Fe model in May 2006. EGN15 was not sampled.

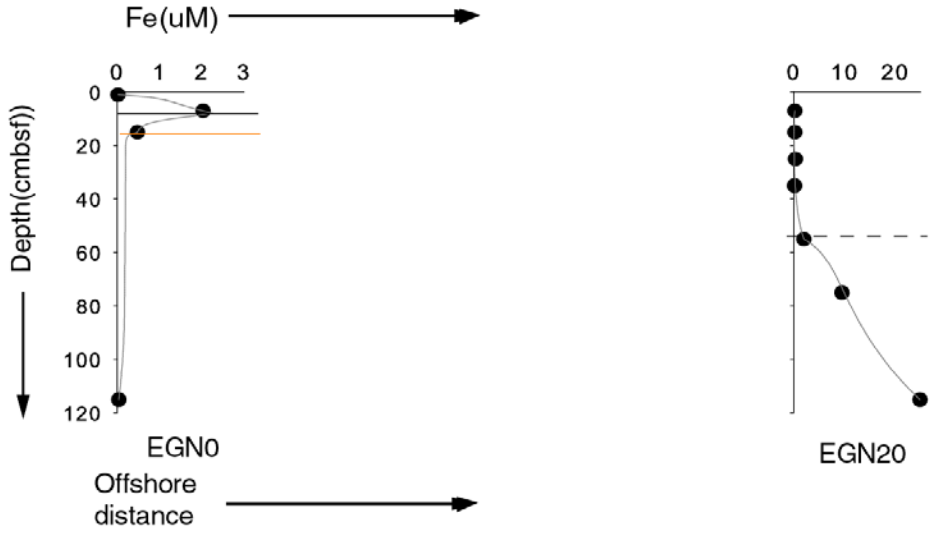

Figure A-6. Dissolved Fe model in October 2006. Only two stations were sampled.

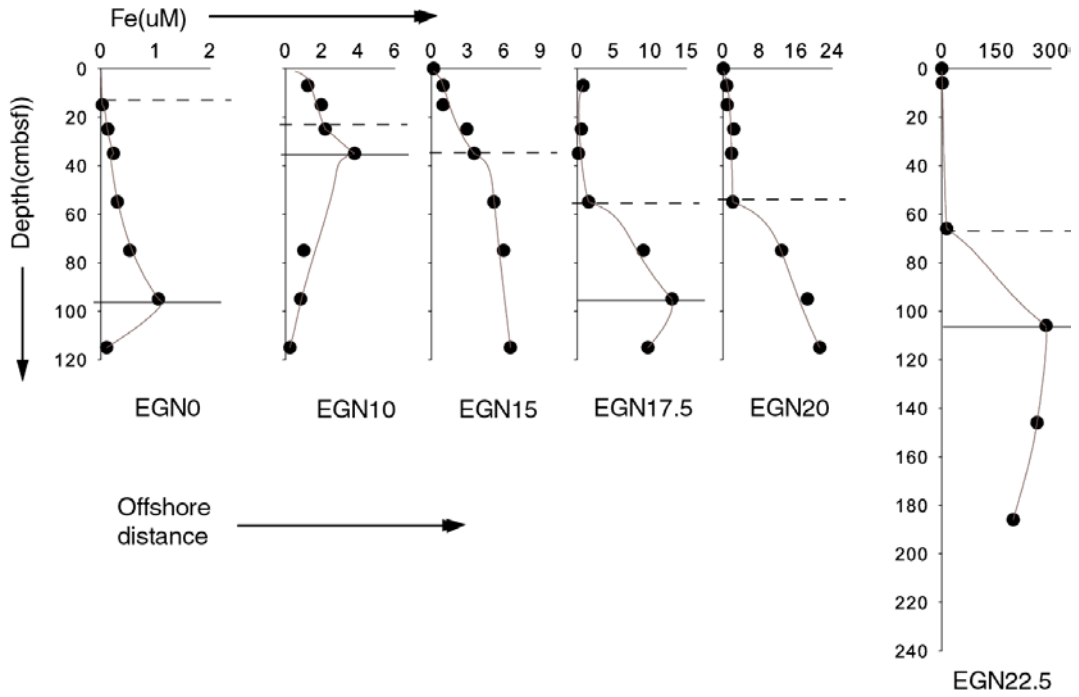

Figure A-7. Dissolved Fe model in April 2007.

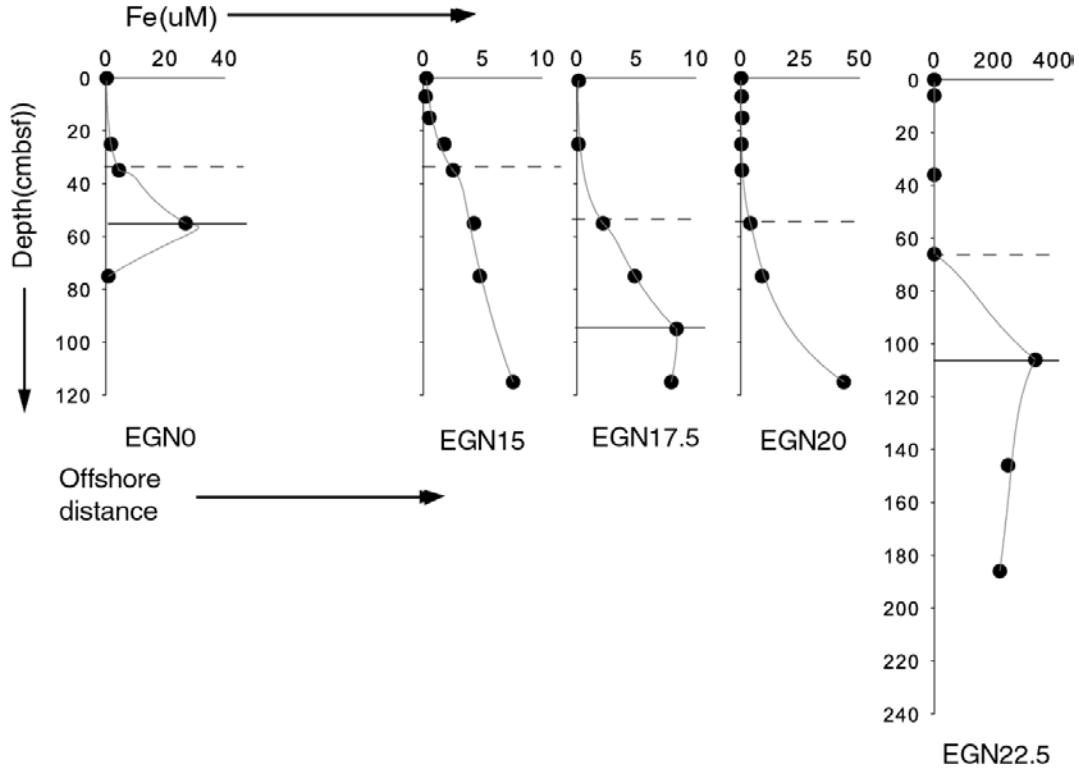

Figure A-8. Dissolved Fe model in September 2007. EGN10 was not sampled.

APPENDIX B
MODEL RESULTS

Table B-1. Model results from November 2004.

Offshore distance (m)	0	10	15	17.5	20	22.5
K_{1a} (1/sec)	-	5.98×10^{-14}	2.31×10^{-11}	-	-	-
K_{1b} (1/sec)	-		8.74×10^{-14}	-	-	-
K_{2a} (1/sec)	5.88×10^{-10}	6.71×10^{-9}	6.67×10^{-9}	-	4.72×10^{-8}	-
K_{2b} (1/sec)	9.97×10^{-9}	-	-	-	1.76×10^{-8}	-
K_3 (1/sec)			-	-	2.28×10^{-12}	-
Fe-sulfide precipitation ($mg/cm^2/year$)	0.0001	0.0025	0.0152	-	0.1869	-
Fe-adsorption ($mg/cm^2/year$)	0.0556	-	-	-	0.3595	-
Total Fe removal ($mg/cm^2/year$)	0.0557	0.0025	0.0152	-	0.5465	-
Fe-sulfide dissolution ($mg/cm^2/year$)	-	-	-	-	0.0844	-
Fe-oxide dissolution ($mg/cm^2/year$)	-	0.0181	45.5024	-	-	-
OC remineralization by Fe-oxides($mg/cm^2/year$)	-	0.0045	11.3756	-	-	-

† dissolved Fe production zones were not sampled and thus not included in the modeled domain.
** missing zones.

Table B-2. Model results from February 2005.

Offshore distance (m)	0	10	15	17.5	20	22.5
K_{1a} (1/sec)	2.30×10^{-12}	4.20×10^{-11}	-	1.84×10^{-12}	-	-
K_{1b} (1/sec)	-	1.17×10^{-13}	-	-	-	-
K_{2a} (1/sec)	3.68×10^{-7}	1.53×10^{-7}	1.96×10^{-8}	1.04×10^{-7}	1.93×10^{-8}	-
K_{2b} (1/sec)	-	-	6.82×10^{-9}	1.24×10^{-9}	9.72×10^{-9}	-
K_3 (1/sec)	-	-	-	-	5.37×10^{-12}	-
Fe-sulfide precipitation ($mg/cm^2/year$)	0.0303	0.1005	0.0340	0.2591	0.1683	-
Fe-adsorption ($mg/cm^2/year$)	-	-	0.2133	0.0050	0.5269	-
Total Fe removal ($mg/cm^2/year$)	0.0303	0.1005	0.2473	0.2641	0.6952	-
Fe-sulfide dissolution ($mg/cm^2/year$)	-	-	-	-	0.0568	-
Fe-oxide dissolution ($mg/cm^2/year$)	0.6832	0.1323	-	0.1101	-	-
OC remineralization by Fe-oxides($mg/cm^2/year$)	0.1709	0.0331	-	0.0276	-	-

Table B-3. Model results from May 2005.

Offshore distance (m)	0	10	15	17.5	20	22.5
K_{1a} (1/sec)	3.20×10^{-10}	3.87×10^{-12}	-	-	-	-
K_{1b} (1/sec)	4.15×10^{-12}	5.11×10^{-13}	-	-	-	-
K_{2a} (1/sec)	1.27×10^{-7}	9.21×10^{-8}	3.98×10^{-8}	3.25×10^{-8}	4.31×10^{-8}	1.24×10^{-8}
K_{2b} (1/sec)	-	-	1.33×10^{-10}	1.13×10^{-8}	3.16×10^{-8}	2.72×10^{-10}
K_3 (1/sec)	-	-	-	1.33×10^{-13}	7.42×10^{-13}	
Fe-sulfide precipitation ($mg/cm^2/year$)	1.6790	0.1518	0.1168	0.0014	0.0470	3.0990
Fe-adsorption ($mg/cm^2/year$)	-	-	0.0046	0.3674	0.8089	0.7948
Total Fe removal ($mg/cm^2/year$)	1.6790	0.1518	0.1214	0.3688	0.8559	3.8939
Fe-sulfide dissolution ($mg/cm^2/year$)	-	-	-	0.0152	0.0194	-
Fe-oxide dissolution ($mg/cm^2/year$)	0.6404	0.1289	-	-	-	-
OC remineralization by Fe-oxides($mg/cm^2/year$)	0.1601	0.0322	-	-	-	-

Table B-4. Model results from Sep 2005.

Offshore distance (m)	0	10	15	17.5	20	22.5
K_{1a} (1/sec)	8.53×10^{-10}	2.14×10^{-14}	3.03×10^{-12}	3.52×10^{-12}	-	1.07×10^{-11}
K_{1b} (1/sec)	6.77×10^{-13}	-	-	-	-	-
K_{2a} (1/sec)	1.49×10^{-7}	-	3.15×10^{-8}	1.57×10^{-8}	4.83×10^{-8}	7.82×10^{-9}
K_{2b} (1/sec)	-	1.39×10^{-7}	1.86×10^{-8}	3.88×10^{-8}	1.97×10^{-8}	3.47×10^{-9}
K_3 (1/sec)		2.89×10^{-12}	-	-	1.93×10^{-12}	-
Fe-sulfide precipitation ($mg/cm^2/year$)	0.2284	-	0.0409	0.0066	0.0800	0.2117
Fe-adsorption ($mg/cm^2/year$)	-	0.2183	0.1128	0.2836	0.7320	2.4619
Total Fe removal ($mg/cm^2/year$)	0.2284	0.2183	0.1537	0.2901	0.8120	2.6737
Fe-sulfide dissolution ($mg/cm^2/year$)	-	0.0072	-	-	0.0204	-
Fe-oxide dissolution ($mg/cm^2/year$)	1.4386	0.1417	0.0002	0.0515	-	0.8984
OC remineralization by Fe-oxides($mg/cm^2/year$)	0.3597	0.0355	0.0000	0.0128	-	0.6684

Table B-5. Model results from May 2006.

Offshore distance (m)	0	10	15	17.5	20	22.5
K_{1a} (1/sec)	1.84×10^{-11}	9.06×10^{-13}	-	1.21×10^{-12}		4.76×10^{-12}
K_{1b} (1/sec)	-	-	-	-		-
K_{2a} (1/sec)	1.96×10^{-7}	4.33×10^{-8}	-	1.31×10^{-8}	5.71×10^{-8}	-
K_{2b} (1/sec)	-	-	-	1.28×10^{-8}	6.50×10^{-9}	3.92×10^{-9}
K_3 (1/sec)	-	-	-	-	7.16×10^{-12}	7.58×10^{-9}
Fe-sulfide precipitation ($mg/cm^2/year$)	0.2245	0.1315	-	0.1089	0.5110	0.0258
Fe-adsorption ($mg/cm^2/year$)	-	-	-	0.1468	0.2154	0.3532
Total Fe removal ($mg/cm^2/year$)	0.2245	0.1315	-	0.2557	0.7789	0.3790
Fe-sulfide dissolution ($mg/cm^2/year$)	-	-	-	-	0.278	-
Fe-oxide dissolution ($mg/cm^2/year$)	5.3749	0.2541	-	0.0178	-	0.1295
OC remineralization by Fe-oxides($mg/cm^2/year$)	1.3437	0.0635	-	0.0044	-	0.0323

Table B-6. Model results from October 2006.

Offshore distance (m)	0	10	15	17.5	20	22.5
K_{1a} (1/sec)	4.32×10^{-12}	-	-	-	-	-
K_{1b} (1/sec)	3.76×10^{-13}	-	-	-	-	-
K_{2a} (1/sec)	2.68×10^{-7}	-	-	-	5.61×10^{-8}	-
K_{2b} (1/sec)	-	-	-	-	9.64×10^{-9}	-
K_3 (1/sec)	-	-	-	-	-	-
Fe-sulfide precipitation ($mg/cm^2/year$)	0.0156	-	-	-	0.0838	-
Fe-adsorption ($mg/cm^2/year$)	-	-	-	-	0.5820	-
Total Fe removal ($mg/cm^2/year$)	0.0156	-		-	0.6658	-
Fe-sulfide dissolution ($mg/cm^2/year$)	-	-	-	-	-	-
Fe-oxide dissolution ($mg/cm^2/year$)		-	-	-	-	-
OC remineralization by Fe-oxides($mg/cm^2/year$)		-	-	-	-	-

Table B-7. Model results from April 2007.

Offshore distance (m)	0	10	15	17.5	20	22.5
K_{1a} (1/sec)	3.78×10^{-12}	1.81×10^{-12}	†	4.99×10^{-12}	†	8.90×10^{-12}
K_{1b} (1/sec)	-	-	-	-	-	-
K_{2a} (1/sec)	21.9×10^{-8}	2.80×10^{-8}	3.63×10^{-8}	3.91×10^{-8}	0.27×10^{-8}	0.64×10^{-8}
K_{2b} (1/sec)	5.74×10^{-8}	5.36×10^{-8}	0.29×10^{-8}	1.39×10^{-8}	0.48×10^{-8}	0.76×10^{-8}
K_3 (1/sec)	-	-	-	-	-	-
Fe-sulfide precipitation (mg/cm^2/year)	0.00076	0.0327	0.094	0.0757	0.0163	0.207
Fe-adsorption (mg/cm^2/year)	0.1796	0.0195	0.128	0.2230	0.3140	2.249
Total Fe removal (mg/cm^2/year)	0.050	0.052	0.222	0.299	0.330	2.456
Fe-sulfide dissolution (mg/cm^2/year)	-	-	-	-	-	-
Fe-oxide dissolution (mg/cm^2/year)	0.054	0.483	†	0.073	†	0.242
OC remineralization by Fe-oxides(mg/cm^2/year)	0.0135	0.121	†	0.018	†	0.061

Table B-8. Model results from September 2007.

Offshore distance (m)	0	10	15	17.5	20	22.5
K_{1a} (1/sec)	1.15×10^{-9}	-	-	7.50×10^{-13}	-	4.75×10^{-12}
K_{1b} (1/sec)	-	-	-	-	-	
K_{2a} (1/sec)	1.86×10^{-7}	-	5.37×10^{-8}	5.20×10^{-8}	4.55×10^{-8}	1.23×10^{-8}
K_{2b} (1/sec)	1.11×10^{-7}	-	8.43×10^{-9}	1.67×10^{-8}	1.72×10^{-8}	8.51×10^{-9}
K_3 (1/sec)	-	-	-	-	-	-
Fe-sulfide precipitation (mg/cm^2/year)	0.3599	-	0.0816	0.1049	0.1552	0.0080
Fe-adsorption (mg/cm^2/year)	0.8465	-	0.3405	0.1660	1.3717	2.8289
Total Fe removal (mg/cm^2/year)	1.2064	-	0.4222	0.2709	1.5269	2.8369
Fe-sulfide dissolution (mg/cm^2/year)	-	-	-	-	-	-
Fe-oxide dissolution (mg/cm^2/year)	5.1227	-	-	0.0108	-	0.1295
OC remineralization by Fe-oxides(mg/cm^2/year)	1.2807	-	-	0.0677	-	0.0324

LIST OF REFERENCES

Archer D. E. and Johnson K. (2000) A model of the iron cycle in the ocean. *Global Biogeochemical Cycles* **14**, 269-279.

Beard B., Johnson C. (2004) Fe isotope variations in the modern and ancient earth and other planetary bodies. *In Reviews in Mineralogy and Geochemistry* **55** *(edited by C. M. Johnson, B. L. Beard, F. Albarede).*The Mineralogical Society of America. Washington D.C., 454p.

Beard B., Johnson C., Skulan J. L., Nealson K. H. Cox L., Sun H. (2003) Application of Fe isotopes to tracing the geochemical and biological cycling of Fe. *Chemical Geology* **195**, 85-117.

Belanger T. V. and Walker R.B. (1990) Ground water seepage in the Indian River Lagoon, Florida. *Tropical Hydrology and Caribbean Water Resources: Proceedings of the International Symposium on Tropical Hydrology and Fourth Caribbean Islands Water Resources Congress*, 367– 375, American Water Resources Association, Middleburg, Virginia.

Berner R. A. (1970) Thermodynamic stability of sedimentary iron sulfides. *American Journal of Science* **265**, 773-785.

Berner R. A. (1980) *Early diagenesis, A theoretical approach*. Princeton University Press. Princeton, New Jersey.

Bokuniewicz H., M., Pollock J., Blum R. Wilson (2004), Submarine ground water discharge and salt penetration across the sea floor, *Ground Water* **42**, 983– 989.

Boyle E.A., Bergquist B.A., Kayser R., Mahowald N. (2005) Iron, manganese, and lead at Hawaii Ocean time series station ALOHA: temporal variability and an intermediate water hydrothermal plume. *Geochimica et Cosmochimica Acta* **69**, 933-952.

Brantley S., Liermann L. (2001) Fractionation of Fe isotopes by soil microbes and organic acids. *Geology* **29**, 535-538.

Brantley S., Liermann L., Guynn R. L., Anbar A., Icopini G. A., Barling J. (2004) Fe isotope fractionation during mineral dissolution with and without bacteria. *Geochimica et Cosmochimica Acta* **68**, 3189-3204.

Burdige D. J. (1991) The kinetics of organic matter mineralization in anoxic marine sediments. *Journal of Marine Research* **49**, 727-761.

Burdige D. J. (2006) *Geochemistry of marine sediments*. Princeton University Press, Princeton, New Jersey.

Burnett W. C., Bokuniewicz H., Huettel M., Moore W. S., Taniguchi M. (2003) Ground water and porewater inputs to coastal zones. *Biogeochemistry* **66**, 3-33.

Butler I. B., Rickard D. (2000) Framboidal pyrite formation via the oxidation of iron (II) monosulfide by hydrogen sulfide. *Geochimica et Cosmochimica Acta* **64**, 2665-2672.

Butler I. B., Archer C., Vance D., Oldroyd A., Rickard D. (2005) Iron isotope fractionation on FeS formation in ambient aqueous solution. *Earth and Planetary Science Letters* **236**, 430-442.

Cable J. E., Martin J. B., Swarzenski P. W., Lindenburg M., Steward J. (2004) Advection within shallow porewaters of a coastal lagoon. *Ground Water* **42**, 1011-1020.

Cable J. E., Martin J.B., Jaeger J. (2006) Exonerating Bernouilli? or evaluating the physics of seepage meter measurements in marine sediments. *Limnology and Oceanography Methods* **4**, 172–183.

Caetano M., Vale C. (2002) Retention of arsenic and phosphorous in iron-rich concretions of Tagus salt marshes. *Marine Chemistry* **79**, 261-271.

Canfield D.E. (1989) Reactive iron in marine sediments. *Geochimica et Cosmochimica Acta* **53**, 619-632.

Canfield D.E. (1993a) Organic matter oxidation in marine sediments. *In Interactions of C, N, P, and S Biogeochemical Cycles and Global change (edited by R. Wollast)* Springer Verlag Publication, 333-363.

Canfield D.E., Thamdrup B., Hansen J.W. (1993b) The anaerobic degradation of organic matter in Danish coastal sediments: Iron reduction, manganese reduction, and sulfate reduction. *Geochimica et Cosmochimica Acta* **57**, 3867-3883.

Canfield D.E., Thamdrup B, Hansen J.W.(1993c) Pathways of organic carbon oxidation in three continental margin sediments. *Marine Geology* **113**, 27-40

Charette M. A. and Sholkovitz E. R. (2002) Oxidative precipitation of groundwater-derived ferrous iron in the subterranean estuary of a coastal bay. *Geophysical Research Letters* **29**, doi10.1029/2001GLO4512.

Charette M. A and Buesseler E. R. (2004) Submarine groundwater discharge of nutrients and copper to an urban subestuary of Chesapeake Bay (Elizabeth River). *Limnology and Oceanography* **49**, 376–385.

Charette M. A., Sholkovitz E. R., Hansel C. M. (2005) Trace element cycling in a subterranean estuary: Part 1. Geochemistry of the Permeable sediments. *Geochimica et Cosmochimica Acta* **69**: 2095-2109.

Charette M. A. and Sholkovitz E. R. (2006) Trace element cycling in a subterranean estuary: Part 2 Geochemistry of the porewater. *Geochimica et Cosmochimica Acta* **70**, 811 - 826.

Charette M. A. (2007) Hydrologic forcing of submarine groundwater discharge: Insight from a seasonal study of radium isotopes in a groundwater-dominated salt marsh estuary. *Limnology and Oceanography* **52**, 230 - 239.

Childers S. E., Ciufo S., Lovley D. R., (2002), Geobacter metallireducens accesses insoluble Fe(II) oxide by chemotaxis. *Nature* **416**, 767-769.

Church T. M., (1996), An underground route for the water cycle. *Nature* **380**, 579-580

Cooper H. H. (1959) A hypothesis concerning the dynamic balance of fresh water and salt water in a coastal aquifer. *Journal of Geophysical Research* **71**, 461-467.

Croal L. R., Johnson C. M., Beard B. L., Newman D. K. (2004) Iron isotope fractionation by Fe(II)-oxidizing photoautotrophic bacteria. *Geochimica et Cosmochimica Acta* **68**, 1227 - 1242.

Crosby H. A., Johnson C. M., Roden E., Beard B. L. (2005) Coupled Fe(II)-Fe(III) electron and atom exchange as a mechanism for Fe isotope fractionation during dissimilator Fe-oxide reduction. *Environmental Science and Technology* **39**, 6698 – 6704.

Crosby H. A., Roden E., Johnson C. M., Beard B. L. (2007) The mechanisms of Fe-isotope fractionation produced during dissimilatory Fe(III) reduction by Shewanella putrefacians and Geocbacter sulfurreducens. *Geobiology* **5**, 169 – 189.

Davison W., Phillips N., Tabner B. J. (1999) Soluble iron sulfide species in natural waters: Reappraisal of their stoichiometry and stability constants. *Aquatic Sciences* **61**, 23-43.

Dauphas N., Pourmand A., Teng F. (2009) Routine isotope analysis of iron by HR-MC-ICPMS: How precise and how accurate? *Chemical Geology* **267** 175-184.

Dorsett A. (2009) Carbon isotopic methods to examine sediment biogeochemistry and groundwater flow from an unconfined aquifer. MS. Thesis. Florida A and M University.

Dos Santos M. A., Stumm W. (1992) Reductive dissolutions of Fe(III) (hydr)oxides by hydrogen sulfide (1992). *Langmuir* **8**, 1671-1675.

Elrod V. A., Berelson W.M., Coale K.H., Johnson K.S. (2004) The flux of iron from continental shelf sediments: A missing source for global budgets. *Geophysical Research Letters* **31** doi:10.1029/2004GL020216.

Escoube R., Rouxel O., Sholkovitz E., Donard O. (2009) Iron isotope systamatics in estuaries: the case of North River, Massachusetts (USA) *Geochimica et Cosmochimica Acta* **73** 4045-4059, doi:10.1016/j.gca.2009.04.026.

Fetter C. W. (2001) *Applied Hydrogeology*. Third Edition, Prentice Hall, Upper Saddle River, New Jersey.

Fontugne M.R., Jouanneau (1987) Modulation of the particulate organic carbon flux to the ocean by a macrotidal estuary: Evidence from measurements of carbon isotopes in organic matter from the Gironde System. *Estuarine, Shelf, and Coastal Science* **24**, 377-387.

Froelich P. N., Klinkhammer G. P., Bender M. L., Luedtke N. A., Heath G. R., Cullen D. P. D., Hammond D., Hartman B., Maynard V. (1979) Early oxidation of organic matter in pelagic sediments of the Eastern equatorial Atlantic: Suboxic diagenesis. Geochimica et Cosmochimica Acta 43, 1075-1090.

Fung I. Y., Meyn S. K.,Tegan I., Doney S. C., John J.G., Bishop K. B. (2000). Iron supply and demand in the upper ocean, Global Biogeochemical Cycles 14, 281– 295.

Furukawa Y. S. and Barnes H.L. (1995) Reactions forming pyrite from precipitated amorphous ferrous sulfate. In *Geochemical Transformations of Sedimentary Sulfur ACS Symposium Series* (edited by M. A. Vairavamurthy and M. A. A. Schoonen) American Chemical Society, Washington, DC **612**, 194–205.

Furukawa, Y., S., Bentley J., Shiller A. M., (2000), The role of biologically enhanced pore water transport in early diagenesis: an example from carbonate sediments in the vicinity of the North Key Harbor, Dry Tortugas National Park, Florida. *Journal of Marine Research* **58**: 493-522.

Garrels R.M. and Christ C.L. (1990) *Solutions, Minerals and Equilibria.* Jones and Bartlett Publishers, Boston and London.

Gieskes J. M., Gamo T., Brumsack H. (1991) Chemical methods for interstitial water analysis on Joides Resolution. Technical Note # 15, Ocean Drilling Program, Texas A 7 M University. *http://www-odp.tamu.edu/publications/tnotes/tn15/f_chem1.htm.*

Hall G.E.M., Vaive J. E., Beer R., Hoashi M. (1996) Selective leaches revisited, with emphasis on the amorphous oxyhydroxide phase extraction. *Journal of Geochemical Exploration* **56**, 59-78.

Hartl K. M. (2006) Facies distribution and hydraulic conductivity of lagoonal sediments in a Holocene transgressive barrier island sequence, Indian River Lagoon, Florida. MS. thesis, University of Florida.

Herzberg A. (1901) Die Wasserversogung eniger Nordseebader. *Journal Gasbeleuchtung und Wasserversogung (Minich)* **44**, 815-19, and 842-44.

Huettel M., Ziebis W., Fortser S., Luther G. W. (1998) Advective transport affecting metal and nutrient distributions and interfacial fluxes in permeable sediments. *Geochimica et Cosmochimica Acta* **62**, 613-631.

Hyacinthe C., BonnevilleS., Van Cappellen P. (2006) Reactive Fe(III) in sediments: Chemical versus microbial extractions. *Geochimica et Cosmochimica Acta* **70**, 4166-4180.

Icopini G. A., Anbar A. D., Ruebash S. S., Tien M., Brantley S. L. (2004) Iron isotope fractionation Turing microbial reduction of iron: the importance of adsorption. *Geology* **32**, 205 – 208.

Ingri J., Malinovsky D., Rodushkin I., Baxter D. C., Widerlund A., Anderson P., Gustafsson O., Forsling W., Ohlander B. (2006) Iron isotope fractionation in river collidal matter. *Earth and Planetary Science Letters* **245**, 792-798.

Jeon B. H., Dempsey B. A., Burgos W. D. (2003) Kinetics and mechanisms for reactions of Fe(II) with Fe(III) oxides. *Environmental Science and Technology* **37**, 3309-3315.

Jevrejeva S., Moore J.C., Grinsted A., Woodworth P. L. (2008) Recent global sea level acceleration started over 200 years ago?. Geophysical Research Letters, 35(15): doi:10.1029/2008GL033611, 2008.

Johnson C. M., Skulan J. L. Beard B. L., Sun H., Nealson K. H., Braterman P.S. (2002) Isotopic fractionation between Fe(III) and Fe(II) in aqueous solutions. *Earth and Planetary Science Letters* **195**, 141-153.

Johnson C. M., Beard B. L., Roden E. E., Newman D. K., Nealson K. H. (2004) Isotopic constraints on Biogeochemical cycling of Fe. *In Reviews in Mineralogy and Geochemistry* **55** *(edited by C. M. Johnson, B. L. Beard, F. Albarede).*The Mineralogical Society of America. Washington D.C., 454p.

Johnson C. M., Beard B. L., Roden E. E. (2008) The iron isotopic fingerprints of redox and biogeochemical cycling in modern and ancient earth. Annual Review, *Earth and Planetary Science Letters* **36**, 457-493.

Jones E. J. P., Nadeau T. L., Voytek M. A., Landa E. R. (2006) Role of microbial iron reduction in the dissolution of hydroxysulfate minerals. *Journal of Geophysical Research* **3**(G0102): doi: 10.1029/2005JG000089, 2006.

Kelly R. P. and Moran S. B. (2002) Seasonal changes in groundwater input to a well-mixed estuary estimated using radium isotopes and implications for coastal nutrient budgets. *Limnology and Oceanography* **47**, 1796-1807.

Langmuir D. (1997) *Aqueous Environmental Geochemistry*. Prentice Hall, Upper Saddle River, New Jersey.

Lee D. R. (1977) A device for measuring seepage flux in lakes and estuaries. Limnology and Oceanography 22, 140-147.

Ler A. and Stanforth R. (2003) Evidence of surface precipitation of phosphate on goethite. Environmental Science and Technology 37, 2694-2700.

Li L., Barry D.A. Stagnitti F., Parlange J.Y., (1999) Submarine groundwater discharge and associated chemical input to a coastal sea. *Water Resources Research* **35**, 3253–3259.

Li Y., Gregory H. S. (1974) Diffusion of ions in seawater and in deep sea sediments. *Geochimica Cosmochimica Acta* **38**, 703-714.

Lion L.W., Altmann R.S., Leckle J. O. (1982) Trace-metal adsorption characteristics of estuarine particulate matter: Evaluations of contributions of Fe/Mn oxide and organic surface coatings. *Environmental Science and Technology* **16**, 660-666.

Lovely D. R., Phillips E. J. P.(1987) Anaerobic production of magnetite by a dissimilatory iron-reducing microorganism. *Nature* **330**, 252-254.

Luther G. W., Wu J. (1997) What controls dissolved Fe concentration in the world ocean? A comment. *Marine Chemistry* **57**, 173-179.

Martin J. B., Hartl K. M., Corbett D. R., Swarzenski P. W., Cable J. E. (2003) A multilevel porewater sampler for permeable sediments. *Journal of Sedimentary Research* **73**, 128–132.

Martin J. B., Cable J. E., Swarzenski P. W., Lindenberg M. K. (2004) Enhanced submarine ground water discharge from mixing of porewater and estuarine water. *Ground Water* **42**, 1000-1010.

Martin J. B., Cable J. E., Jaeger J., Hartl. K., Smith C.G. (2006) Thermal and chemical evidence for rapid water exchange across the sediment-water interface by bioirrigation in the Indian River Lagoon, Florida. *Limnology and Oceanography* **51**, 1332-1341.

Martin J. B., Cable J. E., Smith C. G., Roy M., Cherrier J. (2007) Magnitudes of submarine groundwater discharge from marine and terrestrial sources: Indian River Lagoon, Florida. *Water Resources Research* **43**, doi:10.1029/2006WR005266.

Martin, J. B., Cable J. E., and Jaeger J. (2005) Quantification of advective benthic processes contributing nitrogen and phosphorus to surface waters of the Indian River Lagoon, 244 pp., *Report for St. Johns River Watershed Management District, Palatka, Florida*.

Martin J. H., Fitzwater S.E. (1988) Iron deficiency limits phytoplankton growth in the north-east Pacific subarctic. *Nature* **331**, 341-343.

Martin, J. H. (1990a) Glacial-interglacial CO2 change: The iron hypothesis. *Paleoceanography* **5**, 1–13.

Martin J. H., Fitzwater S. E., Gordon R.M. (1990b) Iron deficiency limits phytoplankton growth in Antarctic waters. *Global Biogeochemical Cycles* **4**, 5-12.

Martin, J. H., Coale K. H., Johnson K.S., Fitzwater S. E., Grodon R. M., Tanner S. J., Hunter C. N., Elrod V.A., Nowicki J. L., Coley T.L., Barber R.T., Lindley S., Watson A.J., Scoy K. V., Law C. S., Liddicoat M. I., Ling R., Stanton T., Stockel J., Collins C., Anderson A., Bidigare R., Ondrusek M., Latsa M., Millero F.J., Lee K., Yao W., Zhang J .Z., Friederich G., Sakamoto C., Chavez F., Buck K., Kolber Z., Greene R., Falkowski P., Chisholm S.W, Hoge F., Swift R., Yungel J., Turner S., Nightingale P., Hatton A., Liss P., Tindale N. W. (1994) Testing the iron hypothesis in ecosystems of the equatorial Pacific Ocean. *Nature* **371**, 123–129.

Meile C., Koretsky C. M., Van Cappellen P. (2001) Quantifying bioirrigation in aquatic sediments: An inverse modeling approach. *Limnology and Oceanography* **46**, 164-177.

Michael H. A., Mulligan A. E., Harvey C. F. (2005) Seasonal oscillations in water exchange between aquifers and the coastal ocean. *Nature* **436**, doi:10.1038/nature 03935.

Middelburg J. J., Herman P M. J.(2007) Organic matter processing in tidal estuaries. *Marine Chemistry* **106**, 127-147.

Mikutta C., Wiederhold J. G., Cirpka O. A., Hofstetter T. B., Bourdon B., Von Gunten U. (2009) Iron isotope fractionation and atom exchangeduring sorption of ferrous iron to mineral surfaces. *Geochimica Cosmochimica Acta*. doi:10.1016/j.gca.2009.01.014

Moore W. S (1996) Large groundwater inputs to coastal waters revealed by Ra-226 enrichments. *Nature* **380**, 612-614.

Moore W. S. and Church T. M. (1996) Submarine groundwater discharge. *Nature* **382**, 121–122.

Moore W. S. (1997) High fluxes of radium and barium from the mouth of the Ganges-Brahmaputra during low river discharge suggest a large groundwater source. *Earth and Planetary Science Letters* **150**, 141-150.

Moore W. S. (1999) The subterranean estuary: A reaction zone of ground water and sea water. *Marine Chemistry* **65**, 111–125.

Morse J.W., Millero F. J., Cornwell J.C., Rickard D. (1987) The chemistry of the hydrogen sulfide and iron sulfide systems in natural waters. *Earth Science Reviews* **24**, 1-42.

Nelder J. A. and Mead R.. (1965) A simplex method for function minimization. *The Computer Journal* **7**, 308-313.

Pandit A., El-Khazen C. C. (1990) Groundwater seepage into the Indian River Lagoon at Port St. Lucie, Fla. *Science* **53**, 169–179.

Penland S., Ramsey K.E. (1990) Relative sea level rise in Louisiana and the Gulf of Mexico: 1908-1988. *Journal of Coastal Research* **6**, 323-342.

Pham A. N., Rose A. L. Feitz A.J., Waite T. D. (2006) Kinetics of Fe(III) precipitation in aqueous solutions at pH 6.0-9.5 and 25^{o}C. *Geochimica Cosmochimica et Acta* **70**, 640-650.

Pollard R.T., Salter I., Sanders R.J., Lucas M.I., Moore C.M., Mills R.A., Statham P.J. Allen J. T., Bakker A. R., Charette M. A., Fielding S., Fones G. R., French M., Hickman A. E., Holland R.J., Hughes J. A., Jickells T.D., Lampitt R.S., Morris P.J., Nedelec F.H., Nielsdottir M., Planquette H., Popova E.E., Poulton A. J., Read J.F., Seeyave S., Smith T., Stinchcombe M., Taylor S., Thomalla S., Venables H.J, Williamson R., Zubkov M.V. (2009) Southern Ocean deep-water carbon export enhanced by natural iron fertilization. *Nature* **457**, 577-581.

Postma D. (1985) Concentration of Mn and separation from Fe in sediments—I. Kinetics and stoichiometry of the reaction between birnessite and dissolved Fe(II) at 10°C. *Geochimica et Cosmochimica Acta* **49**(4), 1023-1033.

Poulton S.W., Krom M. D.E., Raiswell R. (2004) A revised scheme for the reactivity of the iron (oxyhydr)oxide minerals toward dissolved sulfides. *Geochimica et Cosmochimica Acta* **68**, 3703-3715.

Poulton S.W., Canfield D.E. (2006) Co-diagenesis of iron and phosphorous in hydrothermal sediments from the southern East Pacific Rise: Implications for the evaluations of paleoseawater phosphate concentrations. *Geochimica et Cosmochimica Acta* **70**, 5883-5898.

Press W. H., Teukolsky S. A., Vetterling W.T., Flannery B. P. (1992) *Numerical Recipes in C: The art of scientific computing*. Second Edition. Cambridge University Press, New York. http://www.nrbook.com/nr3.

Riedl, R. J., Huang N., Machan R. (1972) The subtidal pump: A mechanism of interstitial water exchange by wave action. *Marine Biology* **13**, 210– 221.

Rickard D. (2006) The solubility of FeS. *Geochimica et Cosmochimica Acta* **70**, 5779-5889.

Rouxel O., Sholkovitz E., Charette M., Edwards K. J. (2008) Iron isotope fractionation in subterranean estuaries. *Geochimica et Cosmochimica Acta* **72**, 3413-3430.

Rudnicki M., Elderfield H., Spiro B. (2001) Fractionation of sulfur isotopes during bacterial sulfate reduction in deep ocean sediments at elevated temperatures. *Geochimica et Cosmochimica Acta* **65**, 777-789.

Schippers A., Jorgensen B.B. (2002) Biogeochemistry of pyrite and iron sulfide oxidation in marine sediments. *Geochimica et Cosmochimica Acta* **66**, 85-92.

Schauble E. A., Rossman G. R., and Taylor H. P. (2001) Theoretical estimates of equilibrium Fe-isotope fractionations from vibrational spectroscopy. *Geochimica et Cosmochimica Acta* **65**, 2487-2497.

Schwertmann U., Fitzpatrick R.W. (1992) Iron minerals in surface environments. In Biomineralization processes of iron and manganese (edited by H. C. W. Skinner and R.W. Fitzpatrick), Catena, Cremlingen, 7-13.

Schwertmann U., Murad E. (1983) Effect of pH on the formation of goethite and hematite from ferrihydrite clays. *Clay Minerals* **31**, 277–284.

Scott T. M. (1992) A geological overview of Florida. Florida Geological Survey, Tallahassee.

Severmann S., Johnson C. S., Beard B. L., McMmanus J. (2006) The effect of early diagenesis on the Fe isotope compositions of porewaters and authigenic minerals in continental margin sediments. *Geochimica et Cosmochimica Acta* **70**, 2006-2022.

Sholkovitz E. R., Boyle E. A., Price N. B (1978) Removal of dissolved humic acids and iron during estuarine mixing. *Earth and Planetary Science Letters* **4**, 130-136.

Shum, K. T. (1992) Wave-induced advective transport below a rippled water-sediment interface. *Journal of Geophysical Research* **97**, 789–808.

Simmons G.M. (1992) Importance of submarine groundwater discharge (SGWD) and seawater cycling to material flux across sediment water interfaces in marine environments. *Marine Ecology Progress Series* **84**, 173-184.

Skolasinska, K. (2006) Clogging microstructures in the vadose zone-laboratory and field studies. *Journal of Hydrogeology* **14,** 1005-10017.

Slomp C.P., Malschaert J. F. .P., Lohse L., Van Raaphorst W. (1997) Iron and manganese cycling in different sedimentary environments on the North Sea continental margin. *Continental Shelf Research* **17**: 1083-1117

Smith C. G., Cable J. E., Martin J. B., Cherrier J., Roy M. (2006) Mixing in the subterranean estuary: A comparison of Radon-222 porewater models. *Coastal Hydrology and Processes*, 355-368.

Smith C. G., Cable J. E. (2008a) Episodic high intensity mixing events in a subterranean estuary: Effects of tropical cyclones. *Limnology and Oceanography* **53,** 666-674.

Smith C. G., Cable J. E., Martin J. B., Roy M. (2008b) Evaluating the source and seasonality of submarine groundwater discharge using a radon-222 porewater transport model. *Earth and Planetary Science Letters* **273**, 312-322.

Smith C. G., Cable J. E., Martin J. B., Roy M., Cherrier J., Dorsett A. (2008b) Cycling of ^{238}U-series radionuclides in a subterranean estuary and impacts on their application as groundwater tracers (in review).

Smith N. P. (1987) An introduction to the tides of Florida's Indian River Lagoon. I. Water Levels. *Oceanographic Sciences* **50**, 49-61.

Snyder M., Taillefert M., Ruppel C. (2004) Redox zonation at the saline-influenced boundaries of a permeable surficial aquifer: effects of physical forcing on the biogeochemical cycling of iron and manganese. *Journal of Hydrology* **296**, 164-178.

Spiteri C., Regnier P., Slomp C. P., Charette M. A. (2006) pH-Dependent Iron-oxide precipitation in a subterranean estuary. *Journal of Geochemical Exploration* **88**, 399-403.

Spiteri C., Slomp C.P., Charette M.A., Tuncay K., Meile C. (2008) Flow and nutrient dynamics in a subterranean estuary (Waquoit Bay, MA, USA): Field data and reactive transport modeling. *Geochimica et Cosmochimica Acta* **72**, 3398-3412.

Soto-Jimenez M.F., Paez-Osuna F. (2008) Diagenetic processes on metals in hypersaline mudflat sediments from a sub-tropical saltmarsh (SE Gulf of Califorinia): Postdepositional mobility and geochemical fractions. *Applied Geochemistry* **23**, 1207-1217.

Starube K. L., Benz M., Schink B. (2001) Iron metabolism in anoxic environments at near neutral pH. *Federation of European Microbiological Societie*s **34**, 181-186.

Stumm W. and Sulzberger B. (1992) The cycling of iron in natural environments: considerations based on laboratory studies of heterogeneous redox processes, *Geochimica et Cosmochimica Acta* **56**, 3233–3257

Stumm W., Morgan J.J. (1996) Aquatic Chemistry, chemical equilibria and rates in natural waters. Third Edition, Jon W*iley and Sons, Inc. New York. 1022p.*

Suess E. (1980) Particulate organic carbon flux in the oceans, surface productivity and oxygen utilization. *Nature* **288**, 260-267.

Sweeney R. E., and Kaplan I.R. (1973) Pyrite framboid formation; laboratory synthesis and marine sediments. *Economic Geology* **68**, 618-634.

Taniguchi M., Ishitobi T., Saeki K. (2003) Evaluations of time-space distributions of submarine groundwater discharge. Groundwater **43**, 336-342.

Tebo B. M., Bargar J. R., Clement B. J., Dick G. J., Murray K. J., Parker D., Verity R., Webb S. M. (2004), Biogenic manganese oxides: properties and mechanisms of formation; Annual Review *Earth and Planetary Science Letters*, **32**, 287-328

Testa J. M., Charette M. A., Sholkovitz E. R., Allen M. C., Rago A., Herbold C. W. (2002) Dissolved iron cycling in the subterranean estuary of a coastal bay: Waquoit Bay, Massachusetts. *Estuarine and Freshwater Biogeochemistry* **203**, 255-256.

Teutsch N., Von Gunten U., Porcelli D., Cirpka O. A., Halliday A. N. (2005) Adsorption as a cause for isron isotope fractionation in reduced groundwater. *Geochimica et Cosmochimica Acta* **66**, 4175 - 4185.

Teutsch N., Schmid M., Muller B., HAlliday A. N., Burgmann H., Wehrli B. (2009) Large iron isotope fractionation at the oxic-anoxic boundary in Lake Nyos. *Earth and Planetary Science Letters* **285**, 52-60.

Thamdrup B. (2000) Bacterial manganese and iron reduction in aquatic sediments. In: Advances in. *Microbial Ecology*, **16**, 41-84

Thornthwaite C.W. (1944) Report of the committee on transpiration and evaporation 1943-1944. *Transactions, American Geophysical Union* **25**:687 p.

Toth D. J. (1988) Salt water intrusion in coastal areas of Volusia, Brevard, and Indian River counties, Palatka, Fl. Technical Publication # SJ 88-1, St. Johns River Water Management District, Florida.

Van Cappellen P., Wang Y. (1995) Metal cycling in surface sediments: modeling the interplay of transport and reaction. *In Metal contaminated aquatic sediments (edited by H. E. Allen).*Ann Arbor Press. Chelsea, Michigan, 292p

Van Cappellen P., Wang Y. (1996) Cycling of iron and manganese in surface sediments: A general theory for the coupled transport and reaction of carbon, oxygen, nitrogen, sulfur, iron and manganese. *American Journal of Science*. **296**, 197-243.

Van Cappellen P., Viollier E., Roychoudhury A. (1998) Biogeochemical cycles of Mn and Fe at the oxic-anoxic transition of a stratified marine basin (Orca Basin, Gulf of Mexico). *Environmental Science and Technology* **32**, 2931-2939.

Wang Y., Van Cappellen P. (1996) A multicomponent reactive transport model of early diagnesis: Application to redox cycling in coastal marine sediments *Geochimica et Cosmochimica Acta* **60**(16), 2993-3014.

Younger P. L. (1996) Submarine groundwater discharge. *Nature* **382**, 121–122.

Zhang H., Davison W., Mortimer R. J. G., Krom M. D., Hayes P. J., Davies I. M. (2002) Localised remobilization of metals in a marine sediment. *The Science of the Total Environment* **296**, 175-187.

BIOGRAPHICAL SKETCH

Moutusi Roy was born in Calcutta, India. She finished her first Master of Science (M.Sc) degree in 2001 from the University of Calcutta. Her thesis title was '*Coastal Zone Management Plan in and around Digha, West Bengal, India*'. Moutusi finished her second masters in Hydrogeology from Wright State University, in Dayton, Ohio. At Wright state, Moutusi worked on '*Spatial Distribution of Permeability in Heterogeneous Sedimentary Structures*'. Moutusi joined University of Florida, in fall 2004, and started working with Professor Jonathon B. Martin as an Alumni Fellow. She conducted her present research on submarine groundwater discharge in Indian River Lagoon, Florida.